REPUBLIC OF TÜRKİYE

ALTINBAŞ UNIVERSITY

Institute of Graduate Studies

Mechanical Engineering

TURBULENCE GENERATION TECHNIQUES IN FLUID MECHANICS

Mohammed Khudhair Alwan AL-JUBOORI

Master's Thesis

Supervisor

Prof. Dr. Aydın ŞALCI

Istanbul, 2023

TURBULENCE GENERATION TECHNIQUES IN FLUID EXPERIMENTS

Mohammed Khudhair Alwan AL-JUBOORI

Mechanical Engineering

Master’s Thesis

ALTINBAŞ UNIVERSITY

2023

The thesis titled TURBULENCE GENERATION TECHNIQUES IN FLUID MECHANICS prepared by MOHAMMED KHUDHAIR ALWAN AL-JUBOORI and submitted on 14/03/2023 has been **accepted unanimously** for the degree of Master of Science in Mechanical Engineering.

____

Prof. Dr. Aydın ŞALCI

Supervisor

Thesis Defense Jury Members:

Prof. Dr. Aydın ŞALCI	Department of Mechanical Engineering, Altınbaş University	_________________
Asst. Prof. Dr. İbrahim KOÇ	Department of Mechanical Engineering, Altınbaş University	_________________
Prof. Dr. Gökhan BULUT	Department of Mechanical Engineering, Haliç University	_________________

I hereby declare that this thesis meets all format and submission requirements of a Master's thesis.

Submission date of the thesis to Institute of Graduate Studies: ___/___/___

I hereby declare that all information in this graduation project has been obtained in full accordance with academic rules and ethical conduct. I also declare all unoriginal materials and conclusions have been cited in the text and all references mentioned in the Reference List have been cited in the text, and vice versa as required by the abovementioned rules and conduct.

Mohammed Khudhair Alwan AL-JUBOORI

Signature

DEDICATION

I would like to dedicate my study to my great father and beloved mother, who both supported me and provided significant aid and energy to carry out this research. Moreover, I would like to dedicate this thesis to my friends. Without their care and support, while I was conducting this study, I would not reach this milestone. In addition, I would like to dedicate my research to my supervisor, as he offered a valuable amount of his worth time to help and advise me to contribute to the improvement of my research results. Furthermore, I would like to dedicate this study to the academic staff and defending committee due to their valuable advice, comments, and consultations to promote my work. Their experience and knowledge help enhance my research outputs.

ACKNOWLEDGEMENTS

Firstly, I would like to thank our God Allah as he gave me the power and patience to conduct my research. Also, I would like to acknowledge the academic staff and doctors at the Mechanical Engineering Department as they offered me the potential and information to write and conduct this research. Additionally, my deepest thanks and gratitude is to my thesis supervisor, Prof. Dr. Aydın ŞALCI. He gave me patience, encouragement, and support. Thus, I was able to complete this study. I hope my supervisor will have the potential to reflect upon this study with considerable satisfaction. Besides, I would like to acknowledge all the members of the defending and examination committee as they provided valuable assessment and evaluation of my research. In the end, I would like to extend my deepest acknowledgment to all the academic and non-academic employees at Altınbaş University for their aid and help.

ABSTRACT

TURBULENCE GENERATION TECHNIQUES IN FLUID MECHANICS

Al-Juboori, Mohammed Khudhair Alwan

M.Sc, Mechanical Engineering, Altınbaş University

Supervisor: Prof. Dr. Aydın ŞALCI

Date: March / 2023

Pages: 126

This work is conducted to investigate the turbulence characteristics of a jet engine and investigate the synthetic turbulence generation techniques. The research depends on a systematic literature review by which synthetic turbulence generation techniques are addressed. Also, primary data are collected from a case study of the Rolls-Royce RB211 jet engine depending on some turbulence parameters and using nano-ceramic coating layer. The STAR-CCM+ 2022.1 software package is employed. The results revealed that using a nano-ceramic coating layer would reduce turbulent viscosity after this coating layer is implemented. Furthermore, the nano-ceramic coating layer would reduce turbulent kinetic energy after coating layer is applied. The findings also indicated that employing a nano-ceramic coating layer could minimize the values related to the static and total pressure, turbulence velocity, and Reynolds number values after the coating layer is implemented. Moreover, it was found that Mach number would increase after applying the coating layer due to the reduction in turbulence. It is recommended to use another software tool that can handle the jet engine inner and outer temperature simulation flexibly with less time and computation effort.

Keywords: Turbulence, Jet Engine, Synthetic Turbulence Generation, Nano-Ceramic Coating, Computational Fluid Dynamics

TABLE OF CONTENTS

Pages

ABSTRACT .... **vii**

LIST OF TABLES .... **xi**

LIST OF FIGURES .... **xii**

ABBREVIATIONS .... **xvi**

1. INTRODUCTION **1**

1.1 RESEARCH BACKGROUND 1

1.2 PROBLEM STATEMENT 1

1.3 RESEARCH SIGNIFICANCE 2

1.4 RESEARCH MAJOR AIM AND MINOR OBJECTIVES 4

1.5 RESEARCH QUESTIONS 4

1.6 RESEARCH HYPOTHESES 5

1.7 THESIS STATEMENT 6

1.8 THESIS ORGANIZATION 6

2. LITERATURE REVIEW **8**

2.1 INTRODUCTION 8

2.2 SYNTHETIC TURBULENCE GENERATOR CRITICAL CHARACTERISTICS AND CONTRIBUTIONS FOR JET ENGINES 8

2.3 CRITICAL TURBULENCE GENERATION APPROACHES 15

2.4 COMPUTATIONAL FLUID DYNAMICS ANALYSIS OF JET ENGINES 25

2.5 VITAL EXAMPLES OF TURBULENCE GENERATION MODELS AND TRIP WIRE PRINCIPLES EMPLOYMENT 38

2.6 LITERATURE REVIEW CONTRIBUTIONS SUMMARY 50

2.6 CHAPTER SUMMARY 64

3. RESEARCH METHODOLOGY **66**

3.1 INTRODUCTION 66

3.2 RESEARCH METHODOLOGY 66
3.3 CASE STUDY DESCRIPTION 69
3.3 THEORY AND MATHEMATICAL MODEL 72
3.3.1 Turbulent Kinetic Energy 72
3.3.2 Turbulent Velocity 73
3.3.3 Reynold and Mach Number 75
3.3.4 Engine Pressure Ratio 78
3.3.5 Turbulent Viscosity 79
3.4 NUMERICAL MODELING AND SIMULATION 79
3.4.1 Computational Fluid Dynamics 80
3.4.2 Modeling and Simulation 81
3.4.3 Software Package 81
3.5 RESULTS VALIDATION 82
4. RESULTS AND DISCUSSIONS 84
4.1 GENERAL 84
4.2 CAD DESIGN OF THE JET ENGINE 84
4.3 MESHING ANALYSIS OF THE JET ENGINE 87
4.4 CFD ANALYSIS OF TURBULENT VISCOSITY 89
4.5 CFD ANALYSIS OF TURBULENT KINETIC ENERGY 90
4.6 CFD ANALYSIS OF THE STATIC PRESSURE 91
4.7 CFD ANALYSIS OF THE TOTAL PRESSURE 95
4.8 CFD ANALYSIS OF THE TURBULENT VELOCITY 96
4.9 CFD ANALYSIS OF THE MACH NUMBER 97
4.10 CFD ANALYSIS OF THE REYNOLDS NUMBER 98
4.11 PERCENTAGES OF IMPROVEMENTS DUE TO COATING 99
4.12 DISCUSSIONS 100
5. CONCLUSIONS AND RECOMMENDATIONS 102
5.1 INTRODUCTION 102
5.2 CONCLUSIONS 102

5.3 RECOMMENDATIONS 103
5.4 RESEARCH LIMITATIONS 104
REFERENCES 105
APPENDIX A.. 115

LIST OF TABLES

Pages

Table 2.1: The area-mean overall pressure loss coefficient and loss reduction percent based on the four coating configurations DRC-1, DRC-2, DRC-3, and DRC-4. 36

Table 2.2: Literature review publications reviewed in this work. 50

Table 3.1: Some mechanical and thermophysical properties of the nanomaterial ceramic coating - SiO_2 68

Table 4.2: The calculation results of the coating contribution in the jet engine........................ 99

LIST OF FIGURES

Pages

Figure 2.1: An architecture of Kaltenbach as well as Spill and Kohoff approach to handle major challenges related to the STG process..10

Figure 2.2: The investigated jet engine in. 13

Figure 2.3: The 2D and realistic jet engine model built by NASA in the. 14

Figure 2.4: A short period of a shadowgraph illustrating the turbulence creation and disturbance of the laminar boundary layer related to a bullet projectile. 17

Figure 2.5: Turbulence generation via a grid, making a disturbance in the uniform and stable motion of smoke streamlines to cause turbidity features. 18

Figure 2.6: An airfoil with symmetric plane fluid motion related to the profile NACA/ 64A015 19

Figure 2.7: Subsonic jet fluid flow transforming to the turbulent motion of a 5-cm-diameter nozzle flowing in atmospheric air with a speed of twelve m/s...19

Figure 2.8: The turbulence generation of the air flow from a supersonic jet with a Mach number reaching around 1.80. 20

Figure 2.9: Impact of Reynolds number on the vortex breakdown. 21

Figure 2.10: Turbulence generation scenario linked to buoyancy-based convection rolls. 21

Figure 2.11: Turbulence generation scenario linked to buoyancy-based convection rolls. 22

Figure 2.12: Turbulence generation scenario linked to buoyancy-based convection rolls. 22

Figure 2.13: Turbulence generation scenario linked to buoyancy-based convection................23

Figure 2.14: Control of pressure gradient and turbulence by (a) trailing-edge flaps and (b) multiple slots that minimize separation levels...24

Figure 2.15: The tea leaf paradox occurrence. 24

Figure 2.16: Control of pressure gradient and turbulence by (a) trailing-edge flaps and (b) multiple slots that minimize separation levels...25

Figure 2.17: The performance improvements and turbulence control of the compressor using a micro-groove polyurethane coating layer. 29

Figure 2.18: The testing results linked to turbulence intensity and overall pressure profiles closer to the section surface, including (a) values of turbulence intensity and (b) contours of overall pressure. 29

Figure 2.19: The research results related to the micro-groove polyurethane coating layer on the compressor. 30

Figure 2.20: 3D configurations related to the micro-groove polyurethane coating layer structure 31

Figure 2.21: The turbulence testing apparatus of the coating. 32

Figure 2.22: A physical architecture of the testing apparatus. 33

Figure 2.23: The total pressure loss coefficient distribution using the coating configurations DRC-1, DRC-2, DRC-3, and DRC-4. 35

Figure 2.24: Maximum overall pressure loss coefficient. 37

Figure 2.25: The wake area width. 38

Figure 2.26: The ice-shape aeroplane model investigated under vortex-turbulence generation conditions. 43

Figure 2.27: The turbulence vorticity investigations and generation related to the four-screw ship. In addition, Figure 2.28 illustrates the employment of the towing test applied for ships. 44

Figure 2.28: A towing test conducted for ships, including (a) a general configuration of the ship's body and (b) modeling of the ship developed for turbulence experimental analysis. 44

Figure 2.29: Different configurations and layouts of towing tests carried out to assess turbulence for typical ship models. 45

Figure 2.30: The variation of the drag coefficient of the heavy-duty vehicle with the Reynolds number. 47

Figure 2.31: The tractor-trailer model investigated in the Canadian Wind Tunnel with a total length of 9 m....48

Figure 2.32: The turbulence generation techniques adopted to test the aerodynamic properties of the vehicle in a 9 m pilot Canadian wind tunnel....49

Figure 3.1: Configuration of (a) Rolls-Royce RB211 jet engine, and (b) Boeing 757. 67

Figure 3.2: The research methodology flowchart....70

Figure 3.3: The major components of the aircraft jet engine and the horsepower profile. 71

Figure 3.4: Variation of turbulent and laminar flow presenting the Reynolds number....76

Figure 3.5: Mach number of a jet engine in aircraft....77

Figure 3.6: Jet engine major zones....79

Figure 4.1: A 3D design of the jet engine investigated in this research....85

Figure 4.2: The 3D design of the jet engine without the protective shields....85

Figure 4.3: The jet engine shielding the whole components....86

Figure 4.4: The actual dimensions of the jet engine....87

Table 4.1: The meshing process specifications and boundary conditions....87

Figure 4.5: The meshing procedure implemented to the whole jet engine....87

Figure 4.6: Meshing process applied to the inner parts of the jet engine....88

Figure 4.7: Meshing of the jet engine: (a) inlet compressors, (b) outlet turbines. 89

Figure 4.8: The jet engine's turbulent viscosity, (a) before and (b) after using a thin layer of nano-ceramic coating....90

Figure 4.9: The jet engine's turbulent kinetic energy, (a) before and (b) after using a thin layer of nano-ceramic coating. 91

Figure 4.10: The jet engine's static pressure, (a) before and (b) after using a thin layer of nano-ceramic coating....92

Figure 4.11: The jet engine's static pressure, (a) before and (b) after using a thin layer of nano-ceramic coating. (A second view). 93

Figure 4.12: The jet engine's static pressure, (a) before and (b) after using a thin layer of nano-ceramic coating. (A third view). 94

Figure 4.13: The jet engine's total pressure, (a) before and (b) after using a thin layer of nano-ceramic coating. 95

Figure 4.14: The jet engine's 2D turbulent velocity, (a) before and (b) after using a thin layer of nano-ceramic coating. 96

Figure 4.15: The jet engine's 3D turbulent velocity, (a) before and (b) after using a thin layer of nano-ceramic coating. 97

Figure 4.16: The jet engine's Mach number, (a) before and (b) after using a thin layer of nano-ceramic coating. 98

ABBREVIATIONS

CFD	:	Computational Fluid Dynamics
DNS	:	Direct Numerical Simulations
DDES	:	Delayed Detached Eddy Simulation
EPR	:	Engine Pressure Ratio
LES	:	Large Eddy Simulations
NASA	:	National Aeronautics and Space Administration
RANS	:	Reynolds-Averaged Navier-Stokes
R&D	:	Research and Development
STG	:	Synthetic Turbulence Generation
TKE	:	Turbulent Kinetic Energy

1. INTRODUCTION

1.1 RESEARCH BACKGROUND

Resource conservative and remarkably efficient jet engines that have a functional design with less noise and vibration require an investigation of their turbulent flow structure via Computational Fluid Dynamics (CFD) analysis [1]–[4]. Some critical mechanical and industrial applications associated with high turbulence include jet engines, airplanes, automobiles, and space crafts.

Generally, when the air or liquid flow at low-velocity rates, the flow profile can be recognized as laminar. Nevertheless, with the increase in fluid momentum and speed, the fluid profile becomes turbulent [5], [6]. The terminology ‘turbulent’ fluid profile can indicate a significant rate of kinetic energy, which can overcome the damping impact of the fluid’s viscosity in some zones in the fluid. Therefore, the turbulence phenomenon can be broadly noted in fluids with lower viscosity rates. Most of the fluids in nature are turbulent.

Therefore, it is essential to understand the turbulence concept and its associated parameters, including inertia, momentum, velocity, gravity, viscosity, and pressure [7], [8]. To achieve this goal, several scholars developed a novel approach, known as Synthetic Turbulence Generator (STG) method, to analyze turbulent fluids. STG can be described as a process by which synthetical production of velocity variations and fluctuations can be applied according to the valid presentation of several integral quantities, such as time and length scales [9], [10].

Mapping and modeling related to mechanical devices, engines, and systems with high turbulence characteristics are greatly essential to explore and judge the fluid mechanical properties and behavior under turbulence conditions [11]. Researchers reported that the synthetically produced velocity variations that are generally based on the Gaussian distribution lacked active fluid dynamic principles.

Also, they are not capable of generating the required turbulent profile. Hence, the provision of valid temporal and spatial relations associated with the STG is remarkably crucial to developing accurate and realistic turbulent models and structures [12].

1.2 PROBLEM STATEMENT

Over the last decades, several industrial and mechanical engineering applications and innovations have been developed and designed, contributing to more complex structures and resulting in some challenges and difficulties in modeling the turbulent flow profile with higher accuracy.

For instance, Reynolds-averaged Navier-Stokes (RANS) modeling faces some challenges and key obstacles in CFD mirrored by less accuracy in zones where significant turbulence, flow transition, re-laminarization, separation, and streamline curvature exist [12], [13].

Regardless of the availability of scale-solving simulations, including Large Eddy Simulations (LES) and Direct Numerical Simulations (DNS), these techniques will not be a leading contribution to industrial design in the future due to their lower accuracy compared with other advanced simulation methods [14], [15].

In contrast, RANS are considered a practical approach to analyzing the turbulent flow because of their compromise between calculation costs and precision. Thus, RANS will witness a continuous enhancement in their functionality.

Nonetheless, because RANS, LES, and DNS methods cannot handle complex turbulence profiles in several industrial applications that need considerable accuracy, scholars developed novel approaches through which accurate analysis of turbulent flow and complicated turbulence circumstances can be flexibly implemented.

One example of these innovative methods is the STG. In this work, the STG approach is used for a jet engine to investigate and assess the turbulent flow depending on the CFD software package, aiming to predict zones with key turbulence weaknesses that can be improved.

1.3 RESEARCH SIGNIFICANCE

The significance of this work stems from some distinct relevance's. Firstly, this research sheds light on the critical concept of 'turbulence' flow and its importance in different mechanical and industrial engineering applications.

Furthermore, the first relevance addresses fundamental approaches and novel methods used to model, analyze, and examine turbulence generation through fluid experiments. The main characteristics and key strengths of these approaches are identified in terms of their accuracy and performance in describing the turbulent flow profile of numerous applications.

To achieve the first relevance, this thesis depends on a comprehensive literature review through which a secondary data collection associated with these aspects is implemented. The secondary data collection relies on information and databases that exist in web journals, such as Academia, ResearchGate, ScienceDirect, SCOPUS, Semantic-Scholar, and MDPI.

In addition, secondary data are collected from conference proceedings and master and Ph.D. dissertations. The second relevance of this study is based on selecting a case study of a jet engine in which the turbulent flow is analyzed.

Also, one turbulence generation technique, including the STG method, is applied via a CFD software package to investigate the turbulence profile and areas with higher weaknesses due to significant turbulence. Then, key improvements and design modifications are applied to resolve these weaknesses and enhance the overall profile characteristics and performance by addressing the turbulence problem.

Further, the theoretical research relevances lie in the following:

a. To enrich the literature review with the major definition of ‘turbulence’ flow and highlight its significance in several industrial and mechanical engineering applications.
b. To validate and examine several approaches and novel methods used to model, analyze, and examine turbulence generation through fluid experiments.
c. To employ numerical analysis and simulations using STAR-CCM+ 2022.1 software package that can implement CFD principles to investigate the turbulence problem in a jet engine.
d. To conduct further research and development (R&D) work on turbulent flow and STG approach to improve its contribution in modeling and analyzing turbulent profiles.

The practical significance of this research can be classified into the following articles:

a. The need for intelligent methods and innovative approaches that can analyze and examine the turbulent flow in several applications with higher degrees of accuracy and performance.

b. The requirement for higher CFD software package tools that can handle the analysis of turbulent flow applications with higher reliability and effectiveness and better results.
c. The necessity to help scholars and engineers depends on a reliable turbulence generation method to investigate and analyze the turbulent flow of several engineering applications flexibly.

1.4 RESEARCH MAJOR AIM AND MINOR OBJECTIVES

The research's major aim is to investigate and examine the critical role of the STG approach in analyzing and modeling turbulent flow with higher accuracy.
It is vital to implement a group of minor objectives that can guarantee the successful execution of this research. These minor objectives include:

a. To conduct a comprehensive literature review classifying the CFD analysis of jet engines and describing the turbulence flow features.

b. To highlight critical significances and beneficial impacts related to the turbulence generation methods through fluid experiments in providing higher accuracy and performance in modeling turbulent fluids.

c. To select a case study that focuses on analyzing the turbulent flow and turbulence profile of a jet engine.

d. To implement numerical analysis, simulations, and CFD modeling of the jet engine using the STAR-CCM+ 2022.1 software package.

e. To validate and modify the results according to the points of view of a panel of CFD experts and turbulence flow professionals.

1.5 RESEARCH QUESTIONS

This research is executed to offer some answers to the research questions, which are illustrated in the following articles:

a. What are the key obstacles and substantial difficulties related to the modeling and analysis of turbulent flow?

b. What are the significant contributions and critical relevances of turbulence generation methods in analyzing and modeling turbulent flow problems?

c. Could the use of STG provide higher accuracy, effectiveness, and reliability in modeling and analyzing the turbulent flow profile of the jet engine?

d. Does the STG approach have limitations or difficulties in modeling and analyzing the turbulent flow of jet engines?

e. Could the implementation of CFD and STG along with numerical analysis via the STAR-CCM+ 2022.1 software package tool provide better analysis of turbulent flow in a jet engine with a higher accuracy level?

1.6 RESEARCH HYPOTHESES

This research is conducted to examine the STG's critical role in improving the modeling and analysis process of a jet engine. The research hypothesis will be validated or invalidated based on the CFD simulation outputs of this study. These hypotheses are presented in the following paragraphs:

a. Null Hypothesis, H_o – which assumes that: "The use of STG principles and modern CFD analysis and modeling would not provide an accurate analysis and investigation of the turbulence flow profile of a jet engine."

b. Alternative Hypothesis, H_a – which assumes that "Utilizing STG principles and modern CFD analysis and modeling plays a significant role in modeling and analyzing the turbulence issue of the jet engine with higher accuracy."

c. Sub Hypothesis, $H_{a,1}$ – which assumes that: "The STG turbulence analysis approach has no limitations or key obstacles in analyzing and modeling the jet engine."

d. Sub Hypothesis, $H_{a,2}$ – which assumes that: "Employing CFD analysis along with the STG method is greatly beneficial in predicting areas with higher turbulence, drag, and friction."

e. Sub Hypothesis, $H_{a,3}$ – which assumes that "Applying CFD analysis and the STG technique helps engineers and scholars conduct further improvements to reduce drag, friction, and other turbulence issues in the jet engine."

1.7 THESIS STATEMENT

The title of this study is "*Turbulence Generation Techniques in Fluid Experiments*." This research is executed to investigate the significant role of the STG with CFD in modeling and to analyze the turbulence problem in jet engines with higher effectiveness and accuracy.

1.8 THESIS ORGANIZATION

The layout of this thesis includes five chapters. These chapters cover several topics and key ideas associated with CFD and STG implementation in jet engines and its critical role and benefits in providing higher accuracy and performance in predicting weak and robust zones in a jet engine characterized by a significant turbulence flow.

The thesis layout can be summarized in the following articles:

i. Chapter One, which has the title INTRODUCTION, describes essential information on the study background, problem statement, study significance, research questions, hypotheses, and research goal and objectives.

ii. Chapter Two, which has the title of LITERATURE REVIEW. It discusses major aspects related to the 'turbulence' concept and sheds light on major characteristics and critical contributions of turbulence generation techniques. Also, this chapter identifies the relevance of the STG approach in providing higher accuracy in modeling and analyzing the turbulent flow of several mechanical and industrial applications. Chapter two will collect the data from publications found in Ph.D. and master dissertations and web research engines, including ScienceDirect, ResearchGate, Google Scholar, and Academia. Additionally, several conference proceedings will gather a database on the significance and critical contributions of turbulence, the STG approach, and CFD analysis.

iii. Chapter Three, which has the title of RESEARCH METHODOLOGY, illustrates the major approach and methodology followed in executing this research. It also describes major study variables and parameters that will be investigated using CFD - STAR-CCM+ 2022.1 software package to assess the critical role of the STG in analyzing the jet engine and modeling the turbulence profile with higher performance and accuracy.

iv. Chapter Four has the title of RESULTS AND DISCUSSIONS. This chapter presents major thesis findings associated with the numerical analysis and simulation work conducted via STAR-CCM+ 2022.1 software package to validate the contribution of STG approach. Moreover, chapter four shows the research discussions that relate the research outputs to other scientists' results.

v. Chapter Five, which has the title CONCLUSIONS AND RECOMMENDATIONS, indicates the main study's conclusions summarizing the case study's critical numerical STAR-CCM+ 2022.1 software package findings. Furthermore, chapter five explains some recommendations and essential suggestions associated with future work to help scientists and engineers carry out further work by which STG contribution and critical role can be maximized in achieving higher accuracy and performance of turbulence flow analysis and modeling.

2. LITERATURE REVIEW

2.1 INTRODUCTION

The previous chapter provided an illustration of the study background, problem statement, study significance, research questions, hypotheses, and research goal and objectives associated with turbulence generation techniques and STG mechanism.

Following this chapter, chapter two provides detailed information and further discussions on the critical contributions and beneficial impacts of employing turbulence generation techniques and STG mechanisms in the jet engine. Also, data related to the CFD analysis of turbulence in jet engines are described.

2.2 SYNTHETIC TURBULENCE GENERATOR CRITICAL CHARACTERISTICS AND CONTRIBUTIONS FOR JET ENGINES

In [16] carried out research examining the performance of a hydrokinetic vertical-axis turbine subjected to turbulence working conditions. The researchers implemented turbulent inflow and uniform inflow corresponding to 10% and 5% turbulence intensity, respectively.

In addition, the researchers applied some governing equations to describe the turbulent flow field depending on Navier-Stokes formulas, which considered the arbitrary Lagrangian-Eulerian approach. They described the turbulent flow characteristics through the STG mechanism associated with Smironov's random flow production.

Also, they used a multi-domain approach to investigate the turbulence flow features. Their analysis results revealed that the performance of the turbine slightly declined when the turbulent flow existed. Moreover, the findings confirmed that the turbulent inflow contributed to significant fluctuations in the instantaneous power coefficient, affecting the fatigue life of some parts in the hydrokinetic vertical-axis turbine. Besides, it was noted that the wake recovery has significantly enhanced with the presence of turbulent inflow.

In [17] conducted a study exploring the critical role of the STG approach in identifying the performance of synthetic piston-driven jet actuators. The researchers depended on an STG method through which the turbulence parameters were analyzed, considering thirty-two supersonic jets which generate turbulence. Every actuator produces intermittently supersonic jets having four orifice holes. The velocity of the actuators was assessed using velocimetry images with an oil mist to trace flow molecules. The research analysis revealed that the highly intermittence nature related to supersonic synthetic jets caused large-scale turbulence intermittency.

In addition, the research results indicated that the turbulent flow's Mach and Reynold numbers at the chamber center region reached 0.01 and 1,000, respectively. Furthermore, it was observed that despite that the turbulent Mach number was not high at the center of the chamber, the turbulence generation process was significantly affected by compressibility because of supersonic jet flow. For this reason, the density variation is present in turbulence conditions.

In [18] executed an analysis identifying critical STG in studying and examining the turbulent inflow characteristics for real problems. The researchers implemented a comprehensive literature review by which several inflow turbulence analysis approaches, including recycling–rescaling-based methods, turbulence library-based methods, and the STG. Their literature analysis revealed that STG is better than other methods to analyze the turbulent inflow characteristics due to its effectiveness and remarkable practicality in various industrial applications associated with turbulence. Furthermore, they found that the STG approach plays a critical role in predicting the inflow turbulence features of several engineering problems.

Nonetheless, the lack of knowledge and experience regarding the turbulence and its quantitative aspects formulate a limiting factor facing practical and effective implementation of the STG approach. Moreover, the researchers reported that engineers face several difficulties in generating realistic turbulent inflow fluctuations for problems that analyze inflow turbulence aspects. Also, they stated that some scholars (including Kaltenbach as well as Spill and Kohoff) investigated critical approaches to handle critical challenges associated with the STG process, which is expressed in Figure (2.1).

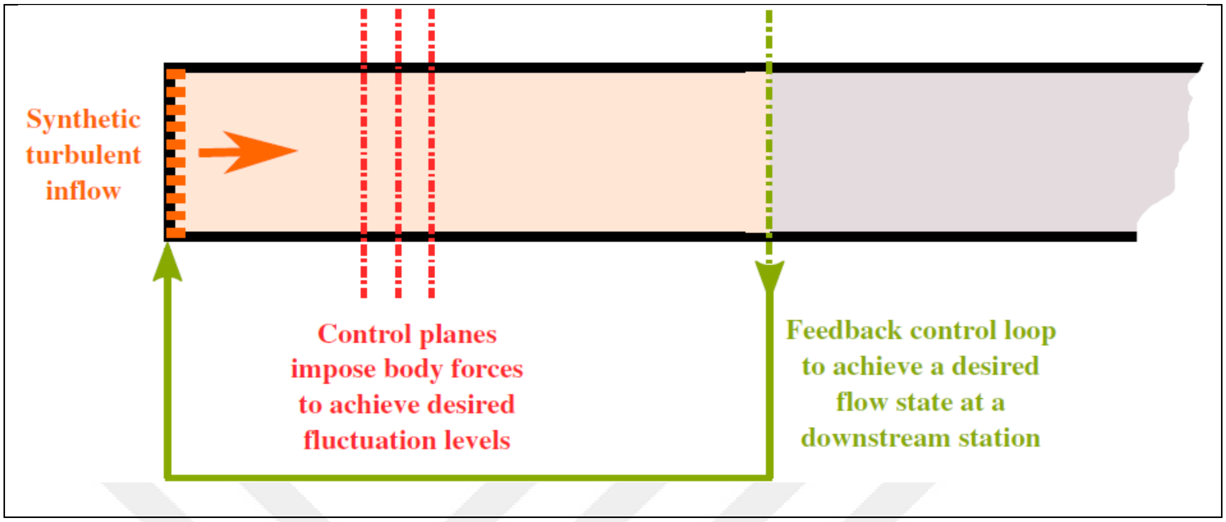

Figure 2.1: An architecture of Kaltenbach as well as Spill and Kohoff approach to handle major challenges related to the STG process [18].

It can be inferred from Figure (2.1) that control planes are employed to help impose body forcing contributing to the achievement of the required fluctuations level. In addition, feedback control loop is employed for the synthetic turbulent inflow to help accomplish the needed flow state at a downstream station.

Additionally, [18] reported that using the STG approach and producing realistic turbulence circumstances is considerably significant and practical to comprehensively analyze and investigate inflow turbulence behavior using the large-eddy simulations and further large-scale turbulence analysis methods. Also, [18] investigated a formula that can describe the filtered velocity fluctuation related to STG process, $\acute{u}_k$, which is expressed in the relationship:

$$\acute{u}_k = \sum_{a=-W}^{W} b_a r_{k+a} \tag{2.1}$$

Where:

W	The filter stencil halfwidth
b_a	The filter coefficient

k Location index

r Random value

In [19] performed a study assessing the critical relevance and role of the STG analysis in analyzing the inflow turbulence of a supersonic boundary layer with higher turbulence. The researcher depended on numerical modeling and direct simulations juxtaposed with an enhanced synthetic eddy approach to analyze and investigate the inflow turbulence characteristics. Based on their numerical analysis, the results revealed that their enhanced synthetic eddy approach generated turbulent fluctuations with higher accuracy and the findings were greatly closer to the direct numerical simulation outputs in their experiment.

Moreover, they found that the skin friction coefficient of their enhanced synthetic eddy approach for turbulence generation recovered faster and had low dimensionless speed at the outer region of the boundary layer compared with the conventional synthetic eddy approach employed for turbulence generation.

In [20] conducted research investigating the beneficial role and contributions of the STG approach to explore the inflow turbulence characteristics of air depending on the three-dimensional modeling of a jet nozzle for the reproduction of experimental circumstances. The authors relied on the lower noise STG technique and roughness elements considering immersed boundary conditions.

Their numerical simulation results revealed that the Mach and Reynolds numbers reached 0.9 and 1,000,000, respectively. In addition, the findings confirmed that there was a small area at the jet nozzle that had robust shear layer fluctuations and uncertainties, which led to the rapid development of three-dimensional turbulent flow at the mixing boundary layer.

The researchers reported that their results are vital for scholars and engineers to fully understand the turbulent modeling of the nozzle boundary layer relying on jet flow modeling and simulation.

[21] published a manuscript examining the turbulence characteristics, noise, and performance of an engine's turbofan. The researchers made a comparative analysis between numerical CFD

analysis and experimental work to validate the confidence and effectiveness of the CFD process of the engine fan using modeling and simulations.

Additionally, the researchers depended on the STG approach besides zonal technique and Reynolds-averaged Navier–Stokes formulas to analyze the engine's fan in terms of noise, performance, and turbulence features. Their comparative analysis revealed that using the STG method provided a low-cost analytical technique to understand and investigate these three aspects.

Moreover, the findings confirmed that using the STG method, zonal technique, and (RANS) Reynolds-averaged Navier–Stokes formulas provided higher reliability, cost-effectiveness, and performance to investigate and understand the turbulence behavior, noise, and performance of the engine's fan. The jet engine investigated in their work can be expressed in Figure (2.2). [22] conducted a study exploring the critical benefits and substantial role of the STG approach in predicting the noise, performance, and turbulence properties of a jet engine. The author implemented the STG method using large eddy simulations and coupled synthetic turbulent approach to assess the noise, performance, and turbulence properties of the jet engine, which are associated with environmental concerns and need to be addressed and taken into account.

In addition, the author used Fourier mode-based stochastic turbulence model to predict the noise field in the jet engine. They found that using the STG technique provides higher accuracy and significant effectiveness in controlling and reducing the noise and turbulence aspects in the jet engine. Furthermore, their simulation and modeling affirmed that using Fourier mode-based stochastic turbulence approach offered higher cost-effectiveness in analyzing the jet engine noise and turbulence compared with other synthetic eddy techniques for small-scale analysis.

Nevertheless, the synthetic eddy turbulent approach provided higher effectiveness in analyzing and understanding turbulence for high-scale turbulence applications.

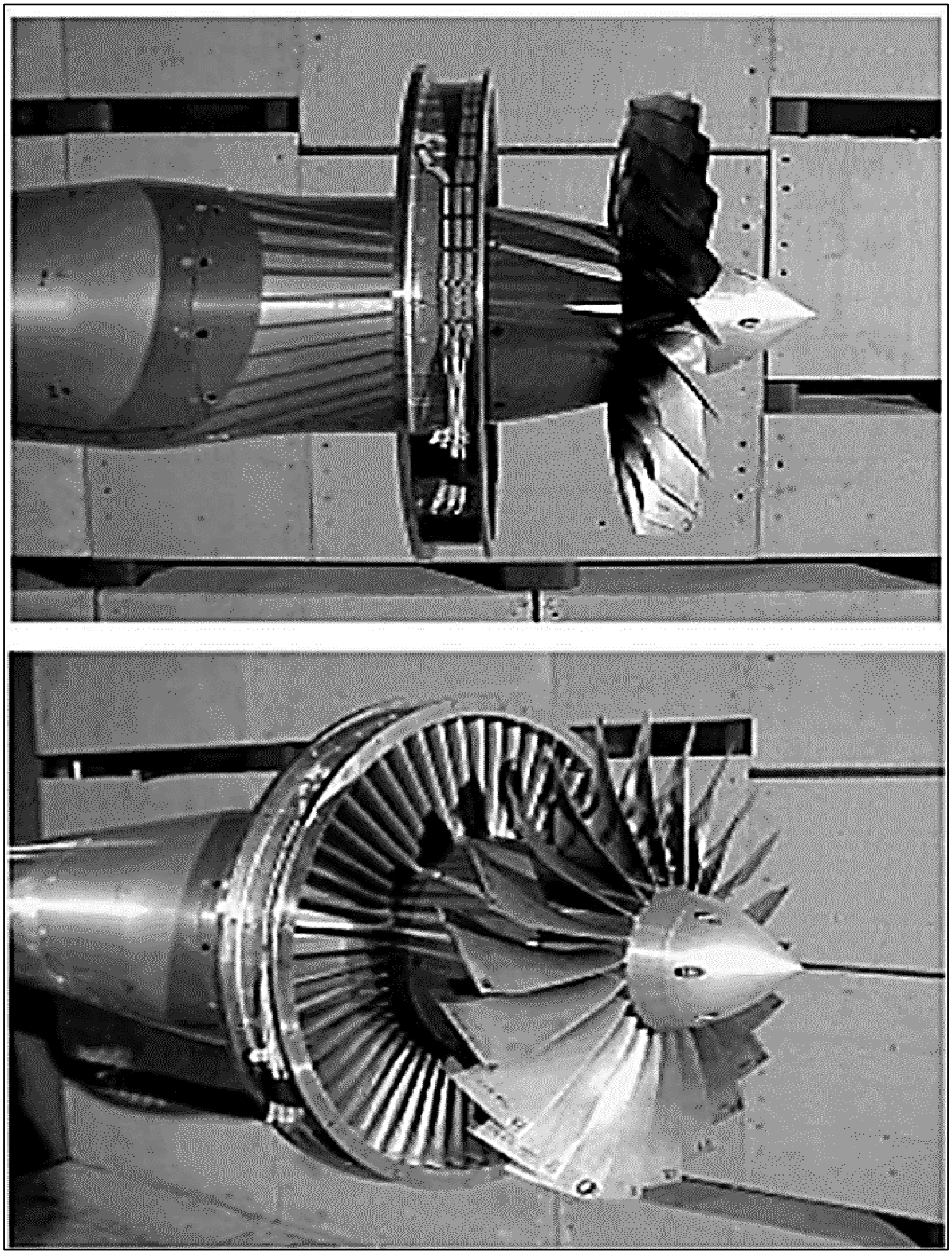

Figure 2.2: The investigated jet engine in [21].

Also, the 2D and realistic jet engine model built by NASA in [21] study is shown in Figure (2.3).

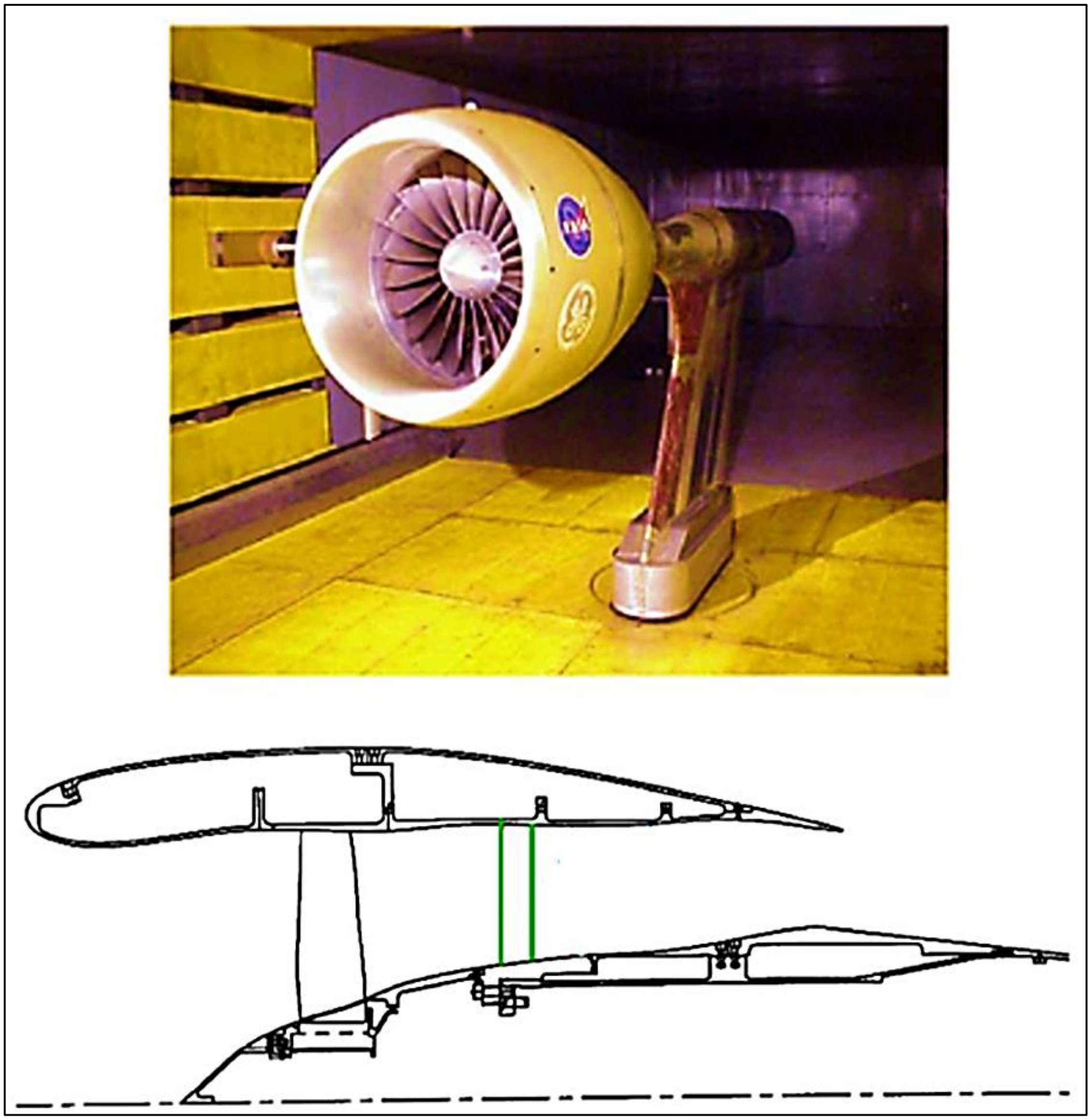

Figure 2.3: The 2D and realistic jet engine model built by NASA in the [21].

2.3 CRITICAL TURBULENCE GENERATION APPROACHES

In [23] conducted an analysis investigating the turbulence properties of periodic configurations. The type of turbulence approach used in their work is the STG approach.

In addition, the researchers employed a large-eddy simulation process to study the Reynolds stresses, energy spectra, and two-point correlations. Their numerical simulation and research analysis indicated that using the STG process contributed to significant effectiveness and performance compared with other conventional turbulence analysis approaches. Furthermore, their research findings confirmed that employing the STG process is greatly practical for several industrial turbomachinery and aerogenic applications.

For [24] performed research exploring the turbulence properties of a rocket engine. The type of turbulence generation methods used in their study includes the STG and Fourier synthetic turbulence analysis, considering Navier–Stokes formulas. Additionally, they used direct numerical simulations to validate the approaches they used. Their analysis revealed that using the STG approach and Fourier synthetic turbulence technique helped provide effective neutralizing at the injection area of the engine.

Moreover, they found that these two methods offered higher cost-effective techniques for analyzing the turbulence and noise of the engine compared with traditional turbulence analysis methods.

In [25] performed research examining the turbulence properties and studying the velocity fluctuation profile. The methods of turbulence analysis they used in their research are the STG approach, targeted forcing technique, and large eddy turbulence mechanism. Furthermore, they used hybrid large-eddy Reynolds-averaged Navier-Stokes CFD modeling and simulation to analyze the velocity and turbulence profile. Their simulations and research analysis confirmed that the STG method, targeted forcing technique, and hybrid large-eddy Reynolds-averaged Navier-Stokes CFD modeling and simulation offered higher flexibility in analyzing the velocity and turbulence profiles.

Also, using these turbulence generations approaches contributed to the successful reproduction of the required statistical distributions for homogenous turbulent flow.

In [26] carried out a study identifying the critical role of some turbulence generation techniques in investigating the inflow turbulence conditions for CFD modeling and simulations. They used the STG approach and proposed a new turbulence analysis approach with spectral approaches, considering Taylor's assumption and divergence-free conditions.

Their research analysis revealed that their proposed method provided several critical strengths in studying and analyzing the turbulence characteristics, mirrored by its simplicity and generality. Furthermore, their proposed method offered effective and direct control over several turbulence scales. Also, the new approach was capable of targeting anisotropic fields with higher robustness.

In [27] executed research classifying the critical role of synthetic turbulence production methods in studying the turbulence characteristics and exploring the neutrally stratified atmospheric flow. The researchers depended on the STG method through which spatially distributed turbulent zones (spots) were employed to produce the flow profile related to the boundary layer conditions of the neutrally stratified atmospheric flow.

Their research analysis confirmed that the STG technique had a higher potential to provide perfect continuity conditions and generate turbulence with the desired statistics. In addition, their findings indicated that using the STG approach allows researchers to obtain valuable results related to Computational Wind Engineering (CWE) applications.

In addition, in a book written and edited by [28], the authors investigated difference concepts and aspects associated with dynamic fluid mechanics and turbulence characteristics related to fluid flow. They reported that turbulence could be created when there is considerable variation and divergence in the fluid speed. For instance, a bullet/ projectile can develop a turbulent region around the line/ path it passes through, resulting in a disturbance and irregular boundary profile, as indicated in Figure 2.4.

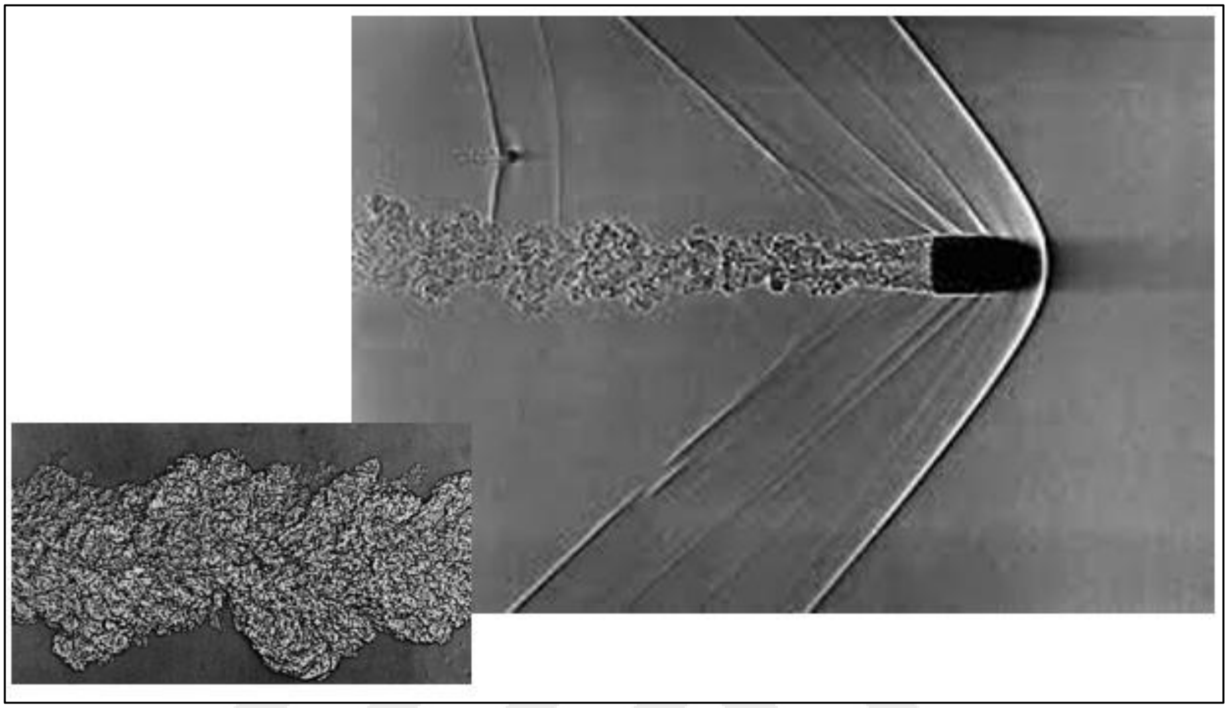

Figure 2.4: A short period of a shadowgraph illustrating the turbulence creation and disturbance of the laminar boundary layer related to a bullet projectile [28].

Additionally, the scholars mentioned that turbulence characteristics could be clearly identified and distinguished through a smoke test in which multiple threads of smoke lines are initiated in the fluid. When there is a disturbing process reflected in a change of the fluid speed, particularly high speed (quick motion), the laminar smoke stream will change its profile from straight streamlines into unstable lines and inhomogeneous fluid profile that can represent a disturbance and turbulence situation, as explained in Figure 2.5.

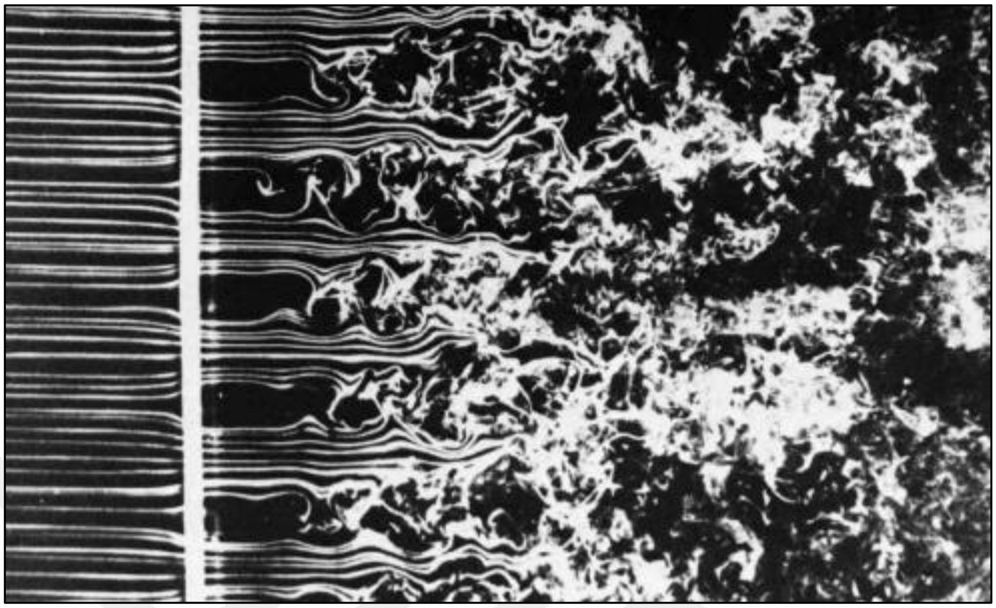

Figure 2.5: Turbulence generation via a grid, making a disturbance in the uniform and stable motion of smoke streamlines to cause turbidity features [28].

In contrast, laminar flow is characterized by its stability, uniform fluid motion profile, smooth streamlines, homogenous path, and steady lines that have approximately the same velocity without the existence of vortices or mixing between laminar lines, as indicated in Figure 2.6, which expresses an airfoil with symmetric plane fluid motion related to the profile NACA/ 64A015. The Reynolds number of this case reaches roughly 7,000, depending on the dimensions of the chord length.

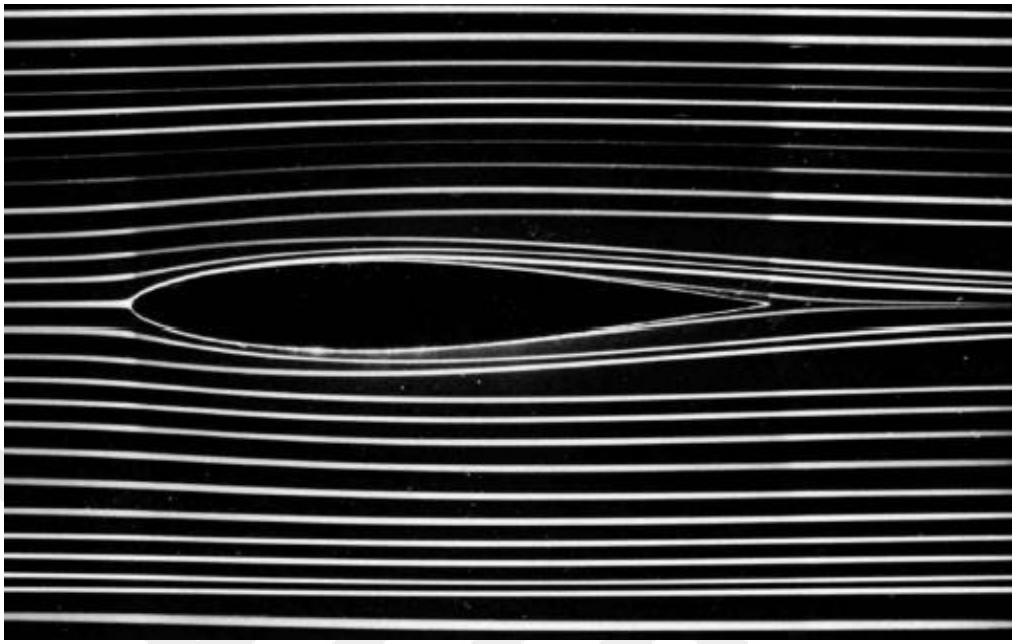

Figure 2.6: An airfoil with symmetric plane fluid motion related to the profile NACA/ 64A015 [28].

Regarding the turbulence generation and dynamic turbulence behavior in jet engines and aircraft, [28] referenced an image related to a jet engine travelling in the ambient air with a velocity magnitude of 12 m/s, as illustrated in Figure 2.7.

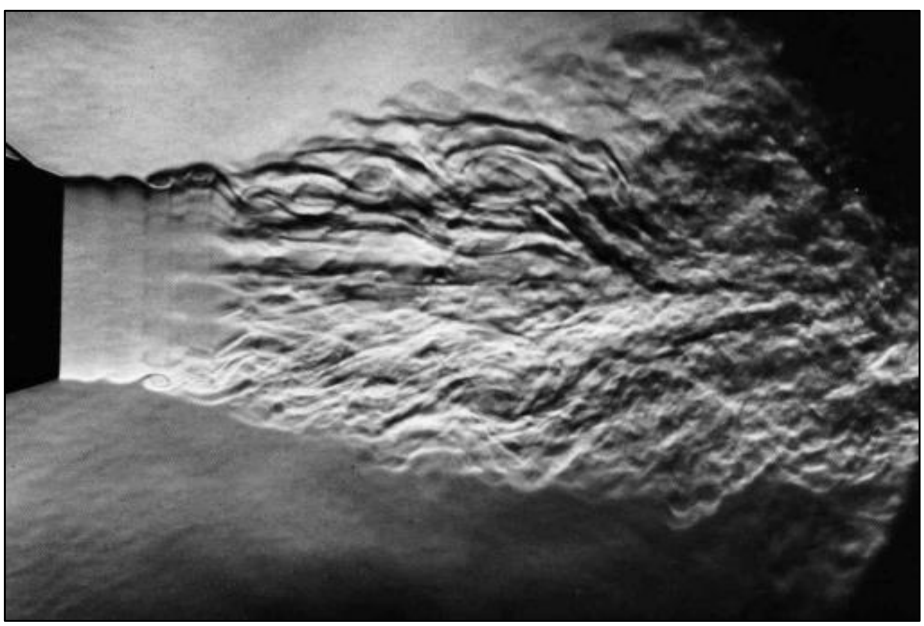

Figure 2.7: Subsonic jet fluid flow transforming to the turbulent motion of a 5-cm-diameter nozzle flowing in atmospheric air with a speed of twelve m/s [28].

Also, the authors reported a photo associated with the turbulence generation of the air flow from a supersonic jet with a Mach number reaching around 1.80. This value is relatively over-disturbed and expanded around the jet of air stream depending on the succession of normal and oblique shock waves, as explained in Figure 2.8.

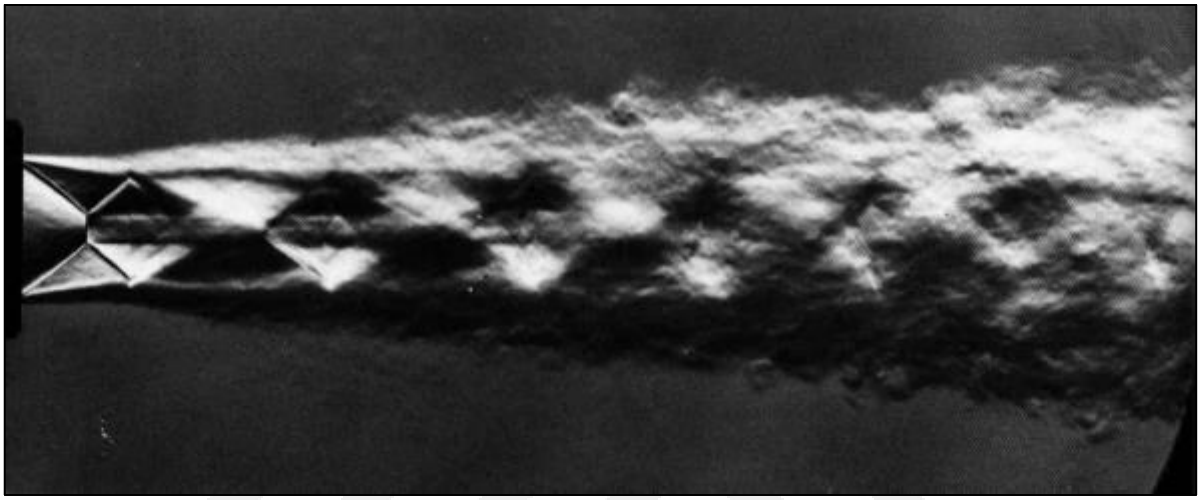

Figure 2.8: The turbulence generation of the air flow from a supersonic jet with a Mach number reaching around 1.80 [28].

Regarding the assessment of vortex breakdown, the scholars in the same textbook studied and inspected the effect of the Reynolds number variation in making vortex breakdown. They detected a photo, as seen in Figure 2.9, which illustrates the transformation of vortex motion to be upstream when the Reynolds number changes from 5,000 to 10,000, indicating more turbulence merits. The further divergence and continuous vortex motion into the upstream direction are linked to a Reynolds number of 20,000.

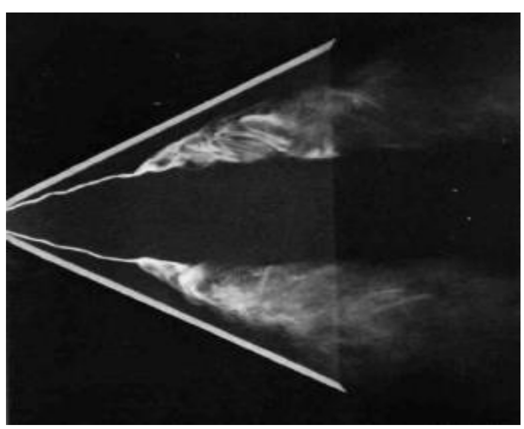

Figure 2.9: Impact of Reynolds number on the vortex breakdown [28].

The scholars also investigated the buoyancy effects related to the convection rolls, as described in Figure 2.10. They clarified that differential interferograms revealed some side layouts of turbulence generation scenarios in which convective instability related to silicon oil is heated from below in a rectangular box having relative dimensions of 10:4:1. The top image of the three indicates classical Rayleigh-Benard case, which consists of uniform heating that generates rolls that are parallel to the shorter part. Meanwhile, the second middle photo shows more temperature variation, thus increasing the motion from right to left. The bottom/ third image expresses the box is rotating around a vertical axis. Therefore, the generated turbulent profiles have relatively different shapes.

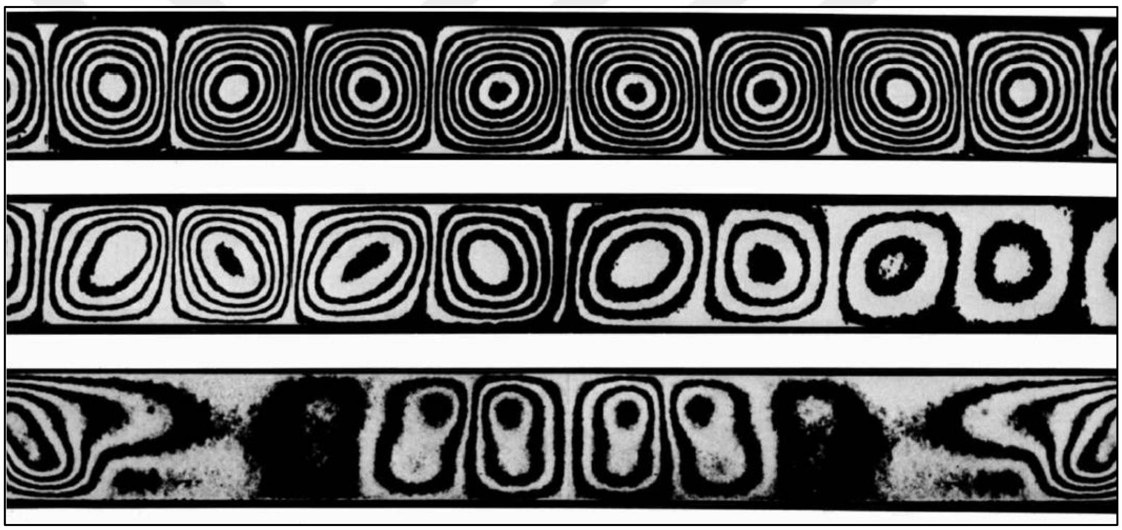

Figure 2.10: Turbulence generation scenario linked to buoyancy-based convection rolls [28].

Similarly, the authors stated that turbulence generation case would be achieved taking into account circular buoyancy-based convection rings/ cells, as shown in Figure 2.11. Here, silicon oil comprising aluminum powder is covered using a glass plate that is cooled according to a uniform cooling process. In the left image, the bottom of the copper is heated steadily based on 2.9 folds, the critical Rayleigh number, contributing to uniform rings/ cells configuration. On the other hand, the image on the right includes larger rings/ loops formulated by more significant heating at the rim compared with the central region,

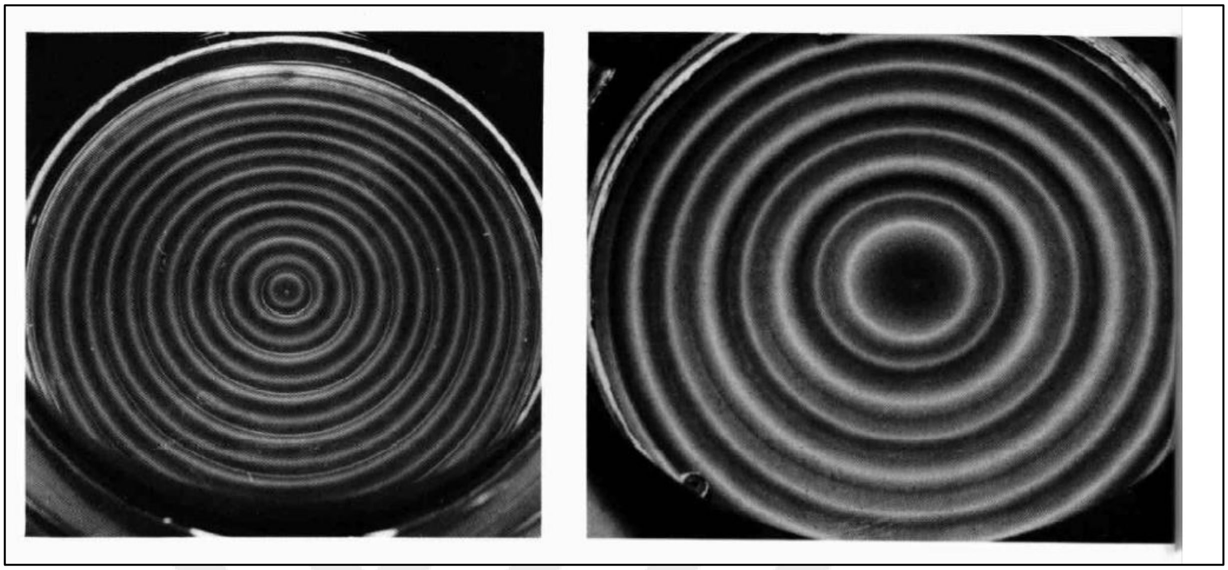

Figure 2.11: Turbulence generation scenario linked to buoyancy-based convection rolls [28].

In respect of the turbulence separation situation, the authors indicated an example of a turbulence generation process in which the turbulent flow over a rectangular block is separated on a plate. They reported that the step height is relatively more prominent than the thickness of the oncoming laminar boundary layer. This aspect, in turn, would cause the flow to create circulations after it passes over the block due to the variation in the thickness, resulting in vortices.

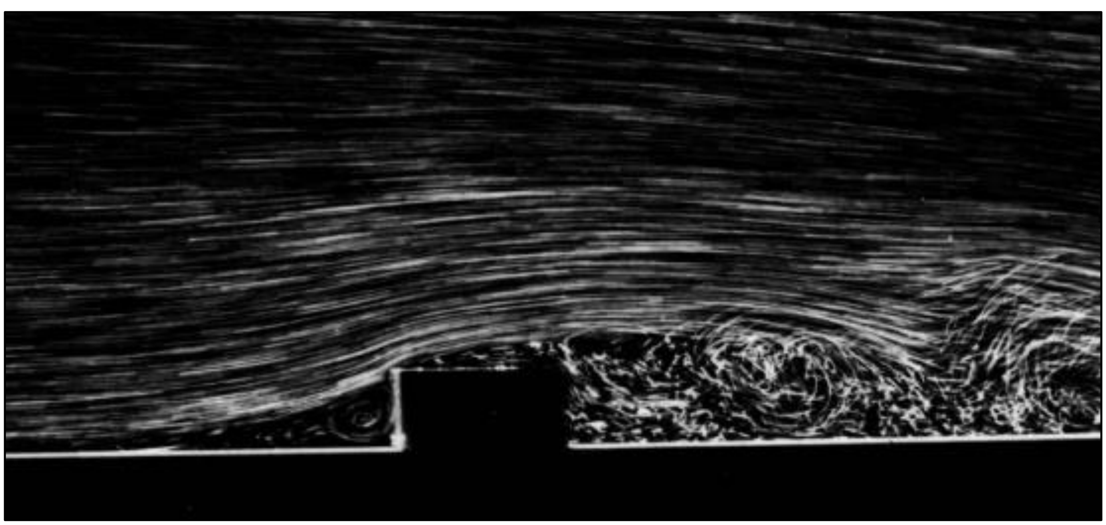

Figure 2.12: Turbulence generation scenario linked to buoyancy-based convection rolls [28].

Furthermore, in a textbook on material films in fluid mechanics published and written by [29], the authors classified some critical characteristics and substantial images taken based on experimental procedures of dynamic fluid mechanics. They described that the ‘turbulence concept’ cannot be easily defined and depicted. However, observations in fluid mechanics can clearly indicate the turbulence properties of the fluid. For example, mixing milk into tea, industrial emissions, and tobacco smoke can express clear turbidity behavior of fluids (which is the air in these examples). In addition, turbulence has some properties translated by the ‘disorder’ aspects in the air/ water motion.

Also, the authors touched on some boundary layer controlling techniques through which the degree of turbulence can be controlled (by generating or minimizing turbulence characteristics of the fluid). They mentioned that some devices (like the one shown in Figure 2.13) could be used to make vortices and create turbulence features on the wing surface of the airplane. This device, illustrated in Figure 2.13, is known as a vortex generator, which is fixed at the transport-airplane wing.

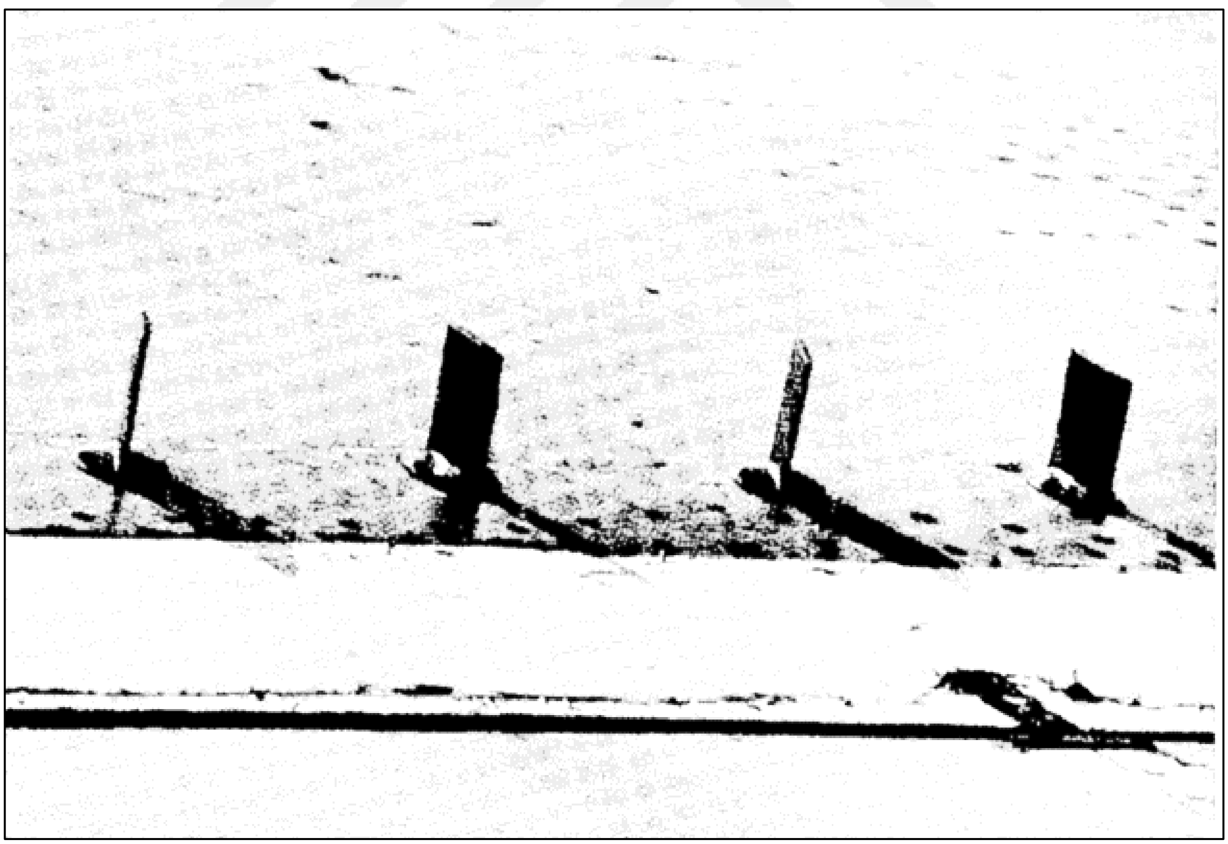

Figure 2.13: Turbulence generation scenario linked to buoyancy-based convection [29].

Other examples in which the boundary layers and turbulence generation are controlled include the implementation of a deflected trailing edge flap that can reduce vortices and turbulence characteristics by lowering separation rates, expressed in Figure 2.14 (a). Also, Figure 2.14 (b) shows the generation of vortices by virtue of multiple slots that can minimize the level of separation. Those two techniques, in turn, could help overcome the high values of a pressure gradient that may cause large variations in the fluid velocity and motion profile. Hence, turbulence aspects can be controlled effectively.

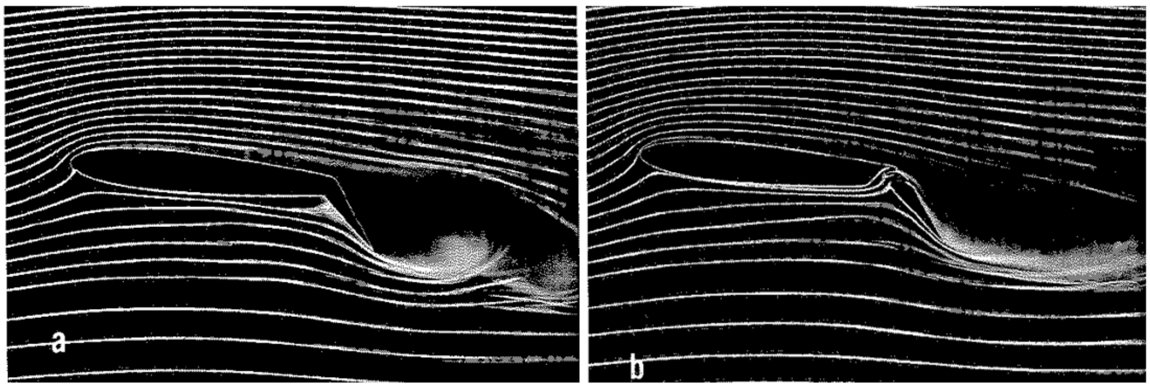

Figure 2.14: Control of pressure gradient and turbulence by (a) trailing-edge flaps and (b) multiple slots that minimize separation levels [29].

The authors also described a term recognized as ‘The Secondary Flow.’ This notation can be defined as a part of a fluid that is affected by the primary flow with higher velocity and pressure. This term can also be expressed with the help of the ‘tea leaf paradox.’ This concept explains that after stirring the tea leaves in a cup of tea, it would be expected that tea may spread to the sides of the cup due to the centrifugal force action. However, the observation is that the tea would migrate into the bottom and the center instead of moving to the sides, creating secondary flow principles, as shown in Figure 2.15.

Figure 2.15: The tea leaf paradox occurrence [30].

Furthermore, the authors explained that the radial motion of the secondary flow would follow the Euler formula of motion, as indicated in Figure 2.16. Secondary flow principles in fluid mechanics are substantial as they could act to change the slow-moving fluid closer to the sides (walls) to move faster and engage with streamlines having more significant velocity. As a result, the viscosity action and viscous friction could be enhanced at the sides/ walls of the path [29].

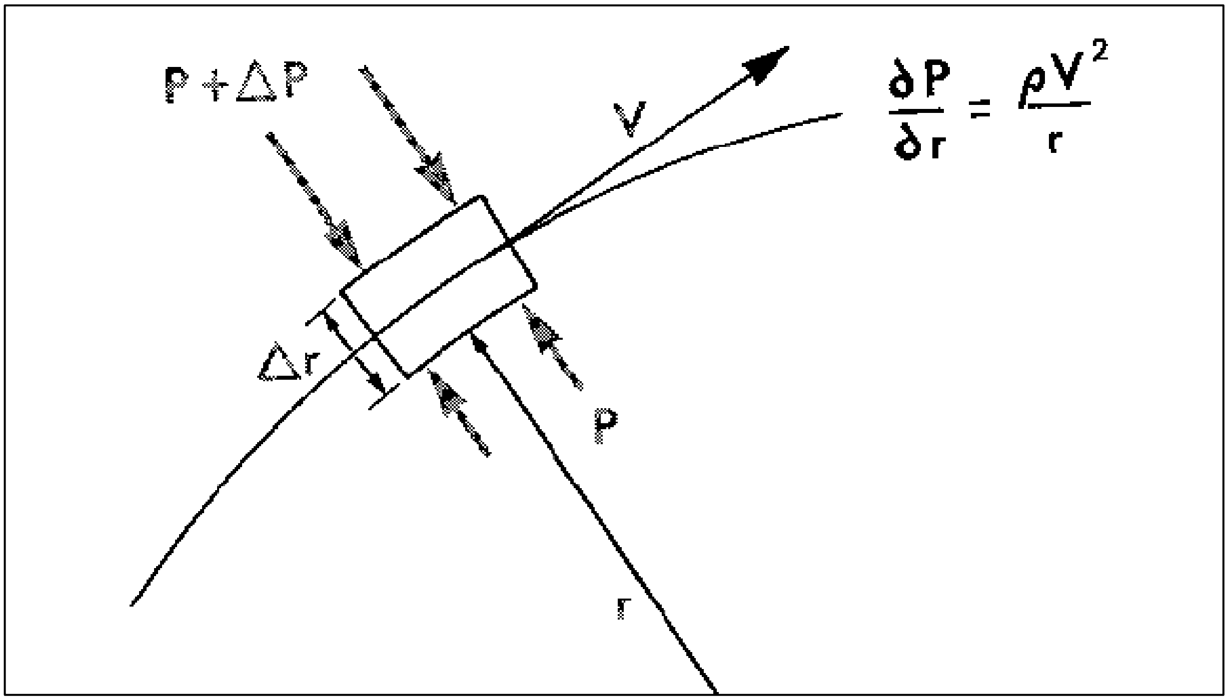

Figure 2.16: Control of pressure gradient and turbulence by (a) trailing-edge flaps and (b) multiple slots that minimize separation levels [29].

2.4 COMPUTATIONAL FLUID DYNAMICS ANALYSIS OF JET ENGINES

In [31] carried out research predicting the critical role of the CFD approach in analyzing the wind turbine inspired by the jet engine. The researchers relied on CFD numerical modeling and analysis to study the performance and speed profile of the wind turbine. Also, they analyzed induced flow’s curly shroud.

Their analysis and simulation results revealed that the shrouded wind turbine contributed to power coefficient improvements of 8.6%. The enhanced power coefficient ranged between

0.35 and 0.38. Further, it was found that the curly shroud caused an increase in the inlet speed and a pressure drop due to swirl formation in the wind turbine.

In [32] carried out research analyzing the beneficial impacts and advantageous role of CFD adoption in several turbomachinery applications, including jet engines' gas turbines. They used large eddy simulations based on CFD principles to analyze the performance and characteristics of their investigated gas turbine. Also, they applied Reynolds averaged Navier-Stoked approach, which is a critical CFD tool, to model and analyze the performance of the gas turbine.

Their research analysis revealed that using large eddy simulations and Reynolds averaged Navier-Stoked approach contributed to numerous benefits and strengths, mirrored by higher accuracy, significant robustness, and large efficiency. Furthermore, it was found that these two CFD approaches resulted in higher effectiveness and reliability compared with the experimental work.

In [33] conducted a study examining the critical contributions to modeling a microturbine numerically depending on the CFD approach. The researcher relied on collecting data from a flight test. They reported that analyzing microturbines is greatly vital as their employment in light personal aircraft and unmanned aerial vehicles has significantly grown in the last decades.

Nonetheless, they witness limited adoption due to their lower durability and less efficiency. For this reason, further simulation work and modeling are required to improve their reliability and performance, thus, increasing their engagement in aviation. In this context, The researcher used modeling and simulations of the microturbine using CFD principles.

Their modeling and simulation results indicated that microturbines modeling and simulation played a critical role in studying the performance and characteristics of the microturbine. Also, modeling and simulation of microturbines via CFD principles provides the potential to enhance their lifetime, design engines' control system, and improve their performance.

In [34] researched examining the significant role of CFD principles in modeling, simulating, and analyzing a fully coupled turbojet engine with the equilibrium running lines. The researcher implemented a thermodynamic cycle analysis of a small-scale turbojet engine under various operating conditions, considering the equilibrium running line. They applied single meshing from the intake area to the exhaust region of the whole engine.

They used the iterative Secant approach for the CFD to determine the fuel flow rate desired to achieve better matching of the turbine power and the compressor. Their simulation and modeling analysis revealed that using thermodynamic cycle analysis and iterative Secant approach juxtaposed with CFD principles provided higher reliability, accuracy, and performance than traditional analysis approaches, as the numerical results agreed with the experimental work associated with the assessment of the thrust, equivalence ratio, fuel, and air mass flow rate, and diffuser-combustor interface, making CFD approach highly helpful and useful for monitoring the development and design of small-scale gas turbines of jet engines.

In [35] conducted a study exploring the practical relevance and major significance of CFD principles in designing and modeling the jet engine. They reported that CFD has been widely employed and has become an attractive approach to analyzing aviation parameters of the jet engine. The researchers depended on a comparative analysis of the results of three CFD software tools, which are SolidWorks, OpenFOAM, and Fluent 6.3.

They analyzed the longitudinal coordinate and height bouncy effect in the jet engine. Their numerical modeling and simulations revealed that using CFD in aviation provided higher accuracy, reliability, and performance in terms of fluid flow analysis and the prediction of several aviation parameters.

For [36] published a paper investigating the critical contributions and major role of CFD principles in analyzing and modeling the performance of the gas microturbine of the KJ66 engine. The researchers relied on three-dimensional modeling and simulations of the gas microturbine using Autogrid/OMNIS™ software package.

Based on the researchers’ numerical modeling and simulations, it was found that using CFD provided higher accuracy and successful results associated with the analysis and performance of the gas microturbine of the KJ66 engine.

In addition, the results indicated that employing CFD principles allowed researchers to find a solution for the entire engine depending on a single simulation problem. [37] implemented a study devoted to analyzing the performance of OSA aircraft's engine depending on the CFD approach. The researchers applied three-dimensional simulations and modeling of the OSA aircraft's engine, focusing on analyzing the performance of a simplified design of the engine's nacelle.

Depending on the CFD simulations and modeling, the findings indicated that employing CFD had successfully helped predict several variables of the OSA aircraft's engine, which helped improve its performance.

In [38] carried out research identifying the role of the CFD approach in analyzing the performance of the jet engine. In addition, the researchers employed CFD to analyze the amount of NOx flue gases. They reported that the difficulties in designing higher-performance combustion systems did not greatly change in the last decades. However, the approach used in the analysis has been changed into a more complicated analysis procedure. The researchers studied the original design and applied some boundary conditions. They applied CFD using SolidWorks and ANSYS software tools.

Their modeling and simulation results revealed that using CFD principles to model and analyze the jet engine, and its corresponding flue gases contributed to higher performance and accuracy compared with conventional analysis methods. [39]–[43] studied the critical role of coating in reducing turbulence and found that using coating for different mechanical components could minimize the turbulence properties. Moreover, they reported that to improve the performance of the compressor, it is vital to control and monitor the turbulence effects in this mechanical device, as shown in Figure 2.17.

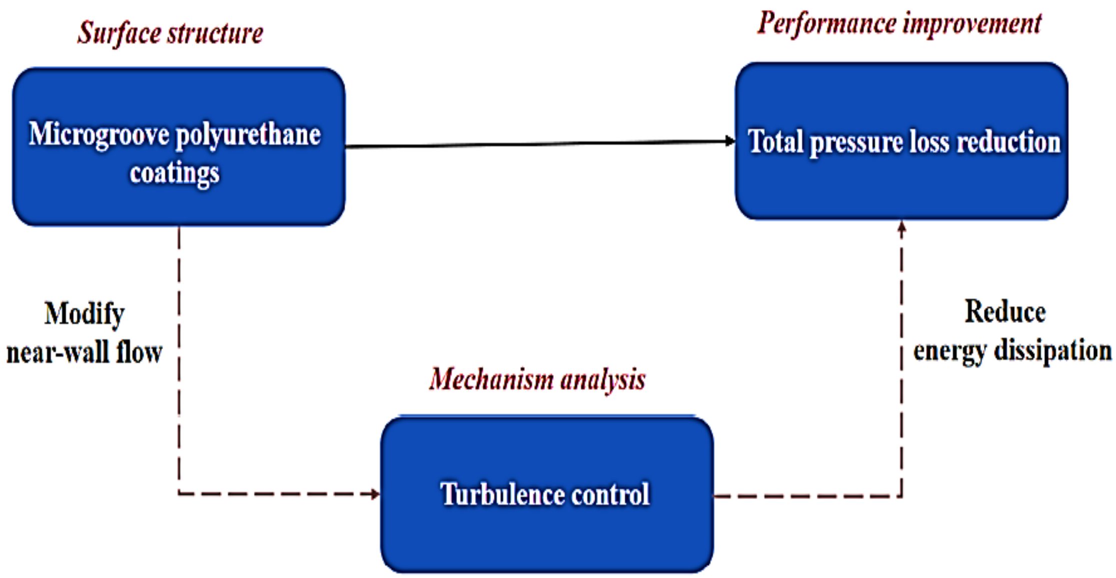

Figure 2.17: The performance improvements and turbulence control of the compressor using a micro-groove polyurethane coating layer [41].

In addition, [41] used a test section related to the compressor cascade to investigate the turbulence in the compressor. Furthermore, the researcher explored the mechanical and dynamic behavior pertaining to turbulence intensity and overall pressure using a flow channel that assesses the surface of the compressor cascade. The results of these examinations are shown in Figure 2.18.

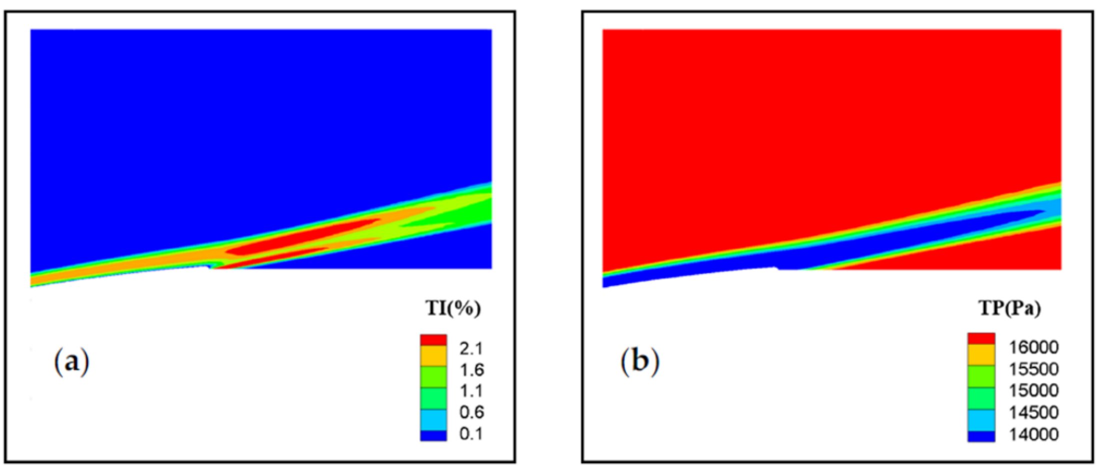

Figure 2.18: The testing results linked to turbulence intensity and overall pressure profiles closer to the section surface, including (a) values of turbulence intensity and (b) contours of overall pressure [41].

It can be inferred from Figure 2.18 that the energy conversion assessed using the flow channel for the compressor cascade is remarkably associated with the overall pressure loss, taking into account that the overall pressure value comprises static and dynamic pressure components. Thus, the energy conversion between static and dynamic pressures may not result in overall pressure loss. However, the viscous decadence of the flow field would cause the overall pressure loss. This overall pressure loss is primarily created by virtue of the flow field. In addition, it can be noted from Figure 2.5 that the centric area related to the turbulence intensity that has higher overall pressure loss is located closer to the near-wall zone. At the same time, the overall pressure loss would decline in those zones. Hence, it can be observed that the turbulence intensity value contributed to a robust advantageous relationship with the overall pressure loss across the flow field. Also, [41] depended on some critical formulas and relationships to validate their results. The results associated with the coating layer surface shape of micro-groove polyurethane material are described in Figure 2.19.

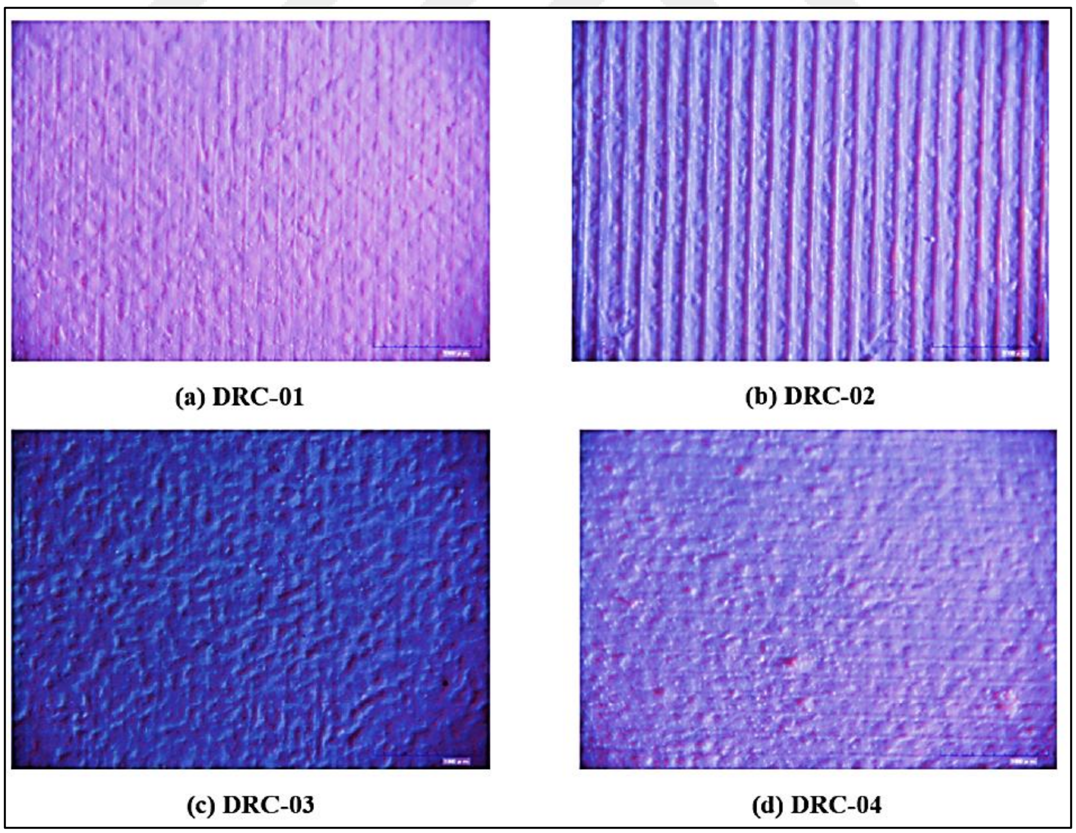

Figure 2.19: The research results related to the micro-groove polyurethane coating layer on the compressor [41].

It can be inferred from Figure 2.19 that DRC-2 and DRC-1 had singular directions related to the groove structure. The groove dimensions related to DRC-2 and DRC-1 equal 80 μm and 50 μm, respectively. On the other hand, DRC-4 and DRC-3 have multiple directions of grooves. The scale related to the groove structure of DRC-4 and DRC-3 reaches approximately 80 μm and 50 μm, respectively. Furthermore, [41] investigated the 3D configurations pertaining to the micro-groove polyurethane coating layer structure, which is expressed in Figure 2.20.

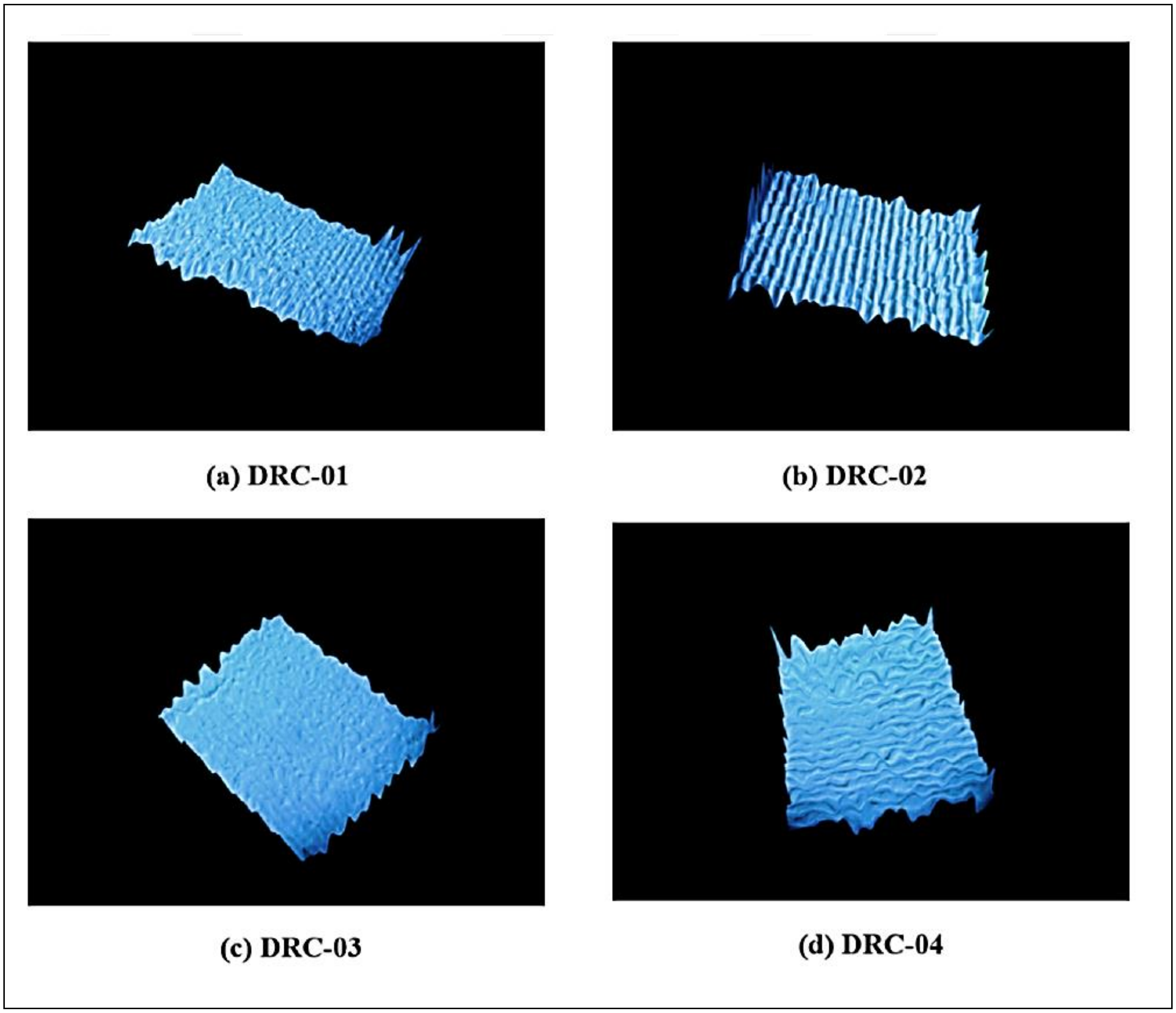

Figure 2.20: 3D configurations related to the micro-groove polyurethane coating layer structure [41].

These 3D layers of the micro-groove polyurethane coating structure, presented in Figure (2.7), are obtained by selecting fluorinated acrylate polymer molecules as polyacrylate nanospheres.

Then they are manufactured via a template-free and inexpensive emulsion polymerization approach in which the surface morphology of the coating is controlled. The shells related to the fluorinated acrylate polymer molecules are synthesized according to the PS-AA core that is provided via polymerization process. The testing apparatus used to predict the turbulence parameters of the micro-groove polyurethane coating is shown in Figure 2.21.

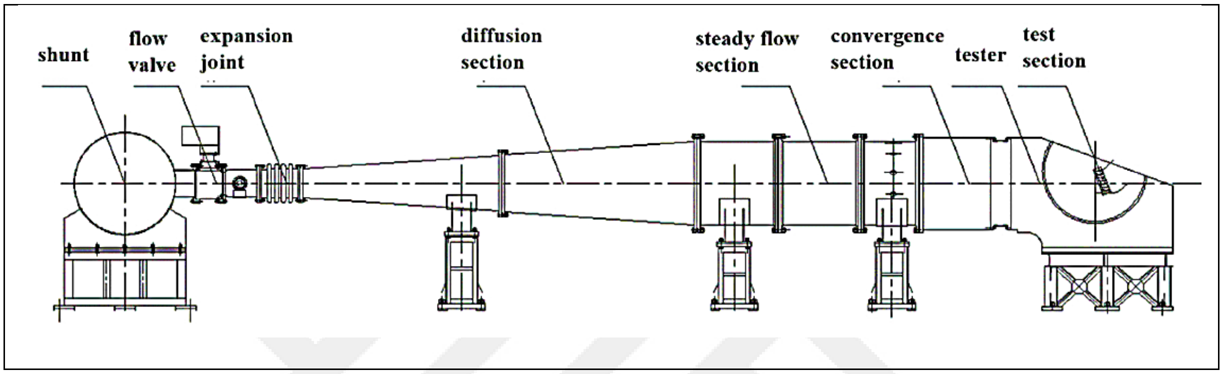

Figure 2.21: The turbulence testing apparatus of the coating [41].

A physical configuration of the testing apparatus, expressed in Figure (2.8), is shown in Figure 2.22.

Figure 2.22: A physical architecture of the testing apparatus [41].

Besides, [41] employed some formulas to assess some parameters linked to the turbulence characteristics of the compressor when the micro-groove polyurethane coating layer is applied. One example of the critical equations utilized in their work include the Mach number of the inlet flow, denoted by M_1, which is expressed by:

$$M_{1,in} = \sqrt{\frac{2}{k-1}\left(\left(\frac{P_1^*}{P_{1,i}}\right)^{\frac{k-1}{k}} - 1\right)} \tag{2.2}$$

And:

$$M_1 = \frac{1}{n}\sum_{i=-1}^{n} M_{1,i} \tag{2.3}$$

Where k presents an isentropic indicator, i is the assessment point, n is the overall number of assessment points, P_1^* is the overall inlet pressure, and P_1 presents the value of the static inlet pressure.

Mach number is a remarkably critical index employed in various applications of fluid dynamics. This number can offer an indication and a comparison between the magnitude of sound velocity and the fluid flow amount. It is developed by Ernst Mach (1838 to 1916). This parameter is also vital in aerodynamic applications, like aircraft and automotive investigations [44]. Particular dynamic forces could rise in case the plane or sport car speed gets closer to the critical values of the Mach number. A lower Mach number (less than 1) would indicate subsonic flow properties. On the other hand, a Mach number that is larger than one can indicate supersonic flow [45]. Also, a lower Mach number means a higher velocity corresponding with higher turbulence rates and turbulent properties (inversely proportional). While large Mach numbers indicate steady and calm (laminar) flow characteristics [46]. However, these indications are not always appropriate to describe the laminar and turbulent characteristics of fluid flow. Reynolds number is more appropriate to examine those two features in fluid dynamics and fluid mechanics [47].

They also defined the local overall pressure loss coefficient, denoted by γ_i, which can be expressed using the formula:

$$\gamma_i = \frac{P^*_{1,i} - P^*_{2,i}}{P^*_{1,i}} \tag{2.4}$$

Where $P^*_{2,i}$ presents the overall outer pressure.

When the overall local pressure loss coefficient, γ_i, is selected in the curve of pressure loss, its maximum amount can be denoted by γ_{max}. Also, the mean area of the overall pressure loss coefficient, γ, can be expressed in the formula:

$$\gamma = \frac{1}{n}\sum_{i=-1}^{n} \gamma_i \tag{2.5}$$

Moreover, the loss reduction percent, ξ, can be expressed by:

$$\xi = \frac{\gamma_b - \gamma_s}{\gamma_b} \times 100\% \tag{2.6}$$

Where γ_b is the area-mean overall pressure loss coefficient according to the Blank condition. At the same time, γ_s presents the area-mean overall pressure loss coefficient related to other conditions.

The turning angle of the flow, which expresses the potential of compressor blades to guide the flow using a pre-defined flow path, can be expressed in the following formula:

$$\varphi = \alpha_{in} - \alpha_{out} \tag{2.7}$$

Where α_{in} is the angle of the flow at the inlet of the compressor, while α_{out} presents the flow angle at the outlet region.

Figure 2.23 illustrates the total pressure loss coefficient distribution using the coating configurations DRC-1, DRC-2, DRC-3, and DRC-4.

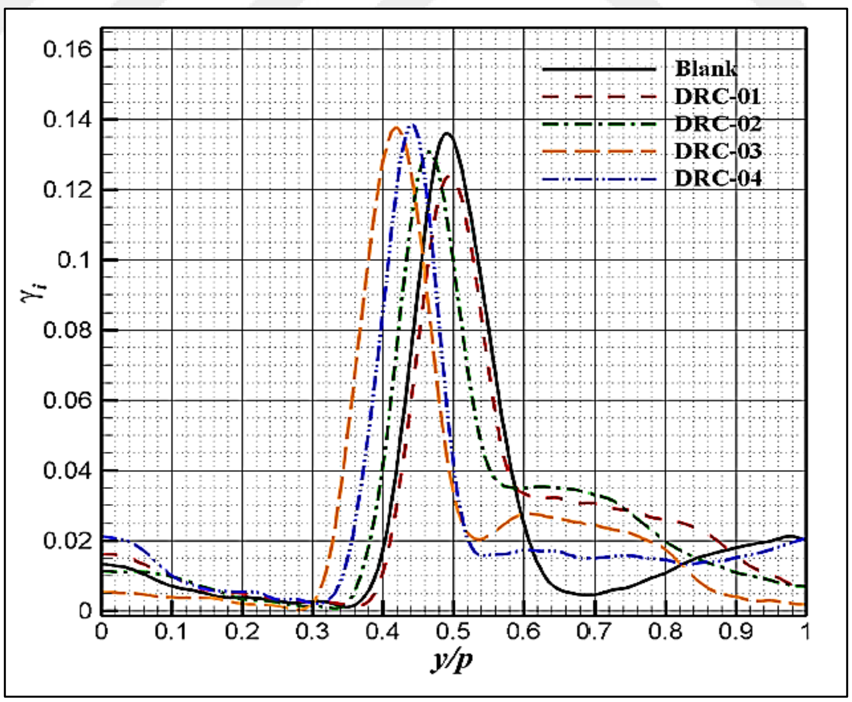

Figure 2.23: The total pressure loss coefficient distribution using the coating configurations DRC-1, DRC-2, DRC-3, and DRC-4 [41].

Also, the results indicated the area-mean overall pressure loss coefficient and loss reduction percent based on the four coating configurations DRC-1, DRC-2, DRC-3, and DRC-4.

$$\acute{u}_k = \sum_{a=-W}^{W} b_a r_{k+a} \tag{2.8}$$

Table 2.1: The area-mean overall pressure loss coefficient and loss reduction percent based on the four coating configurations DRC-1, DRC-2, DRC-3, and DRC-4.

Number	Sample	Area-Mean Overall Pressure Loss Coefficient, γ	The loss Reduction, ξ
1	Blank Case	0.0307273	---
2	DRC-1	0.0289236	5.87%
3	DRC-2	0.0304099	1.03%
4	DRC-3	0.0308256	−0.32%
5	DRC-4	0.0290237	5.54%

Further, the results of [41] indicated the maximum overall pressure loss coefficient and the wake area's width.

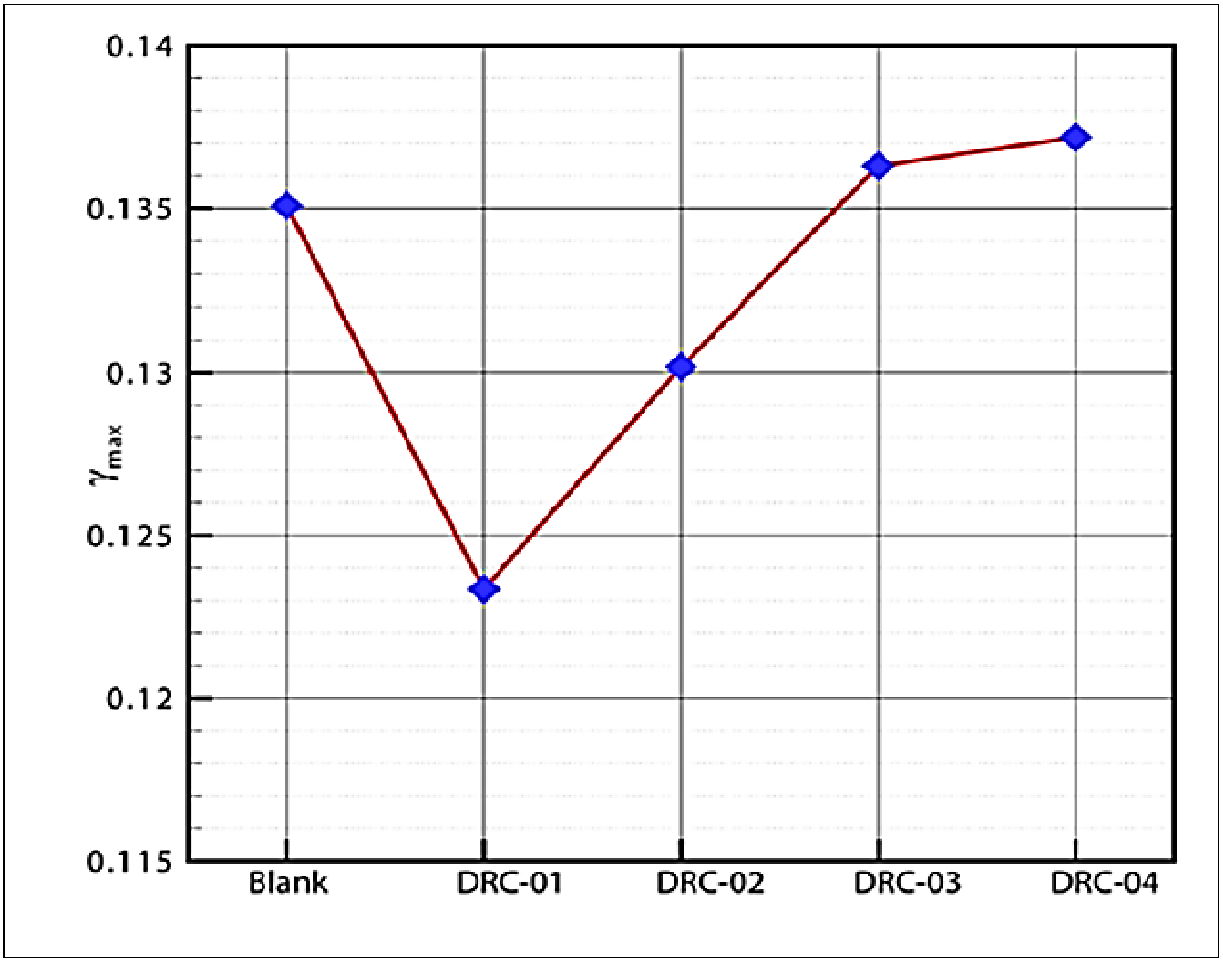

Figure 2.24: Maximum overall pressure loss coefficient [41].

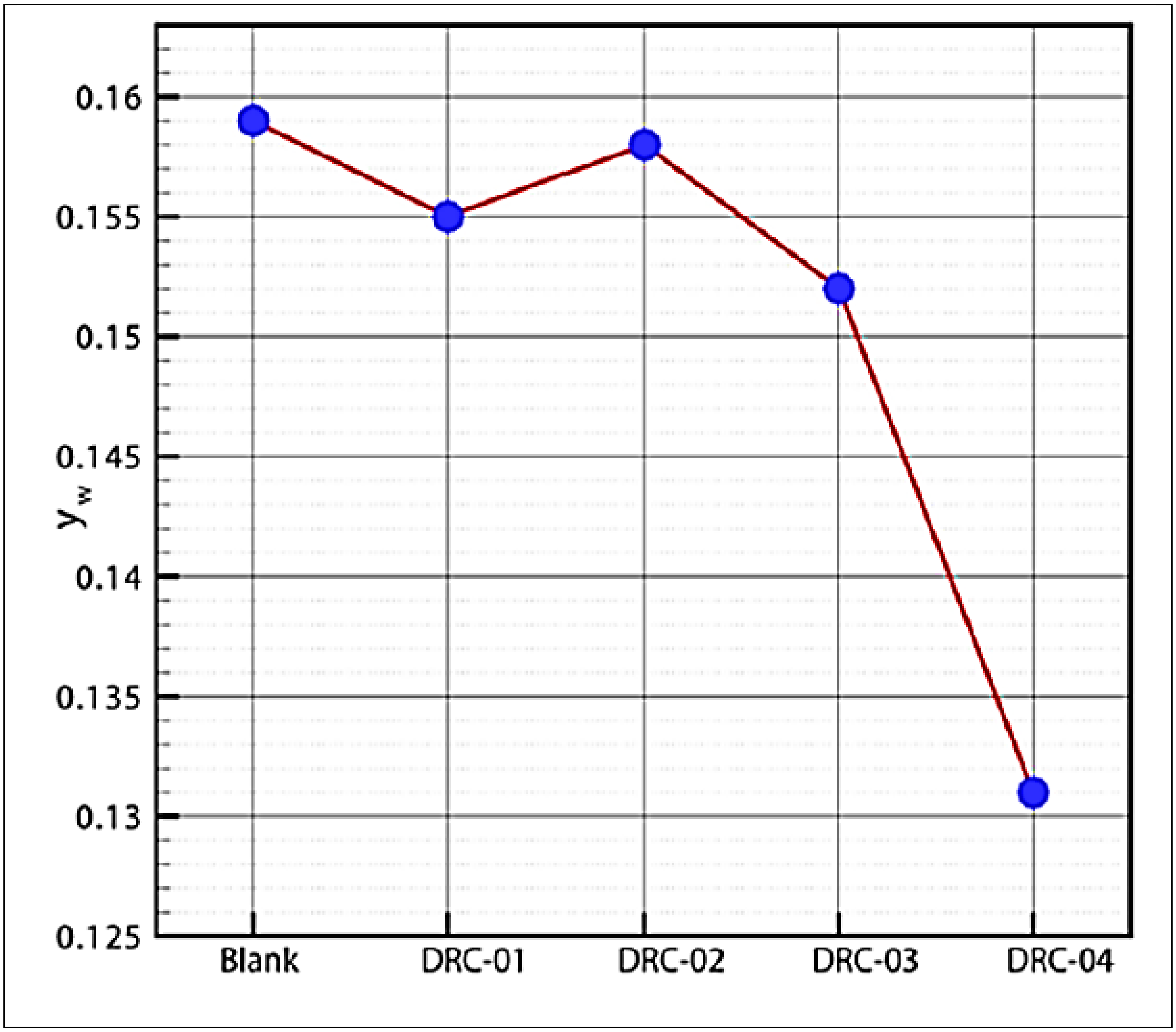

Figure 2.25: The wake area width [41].

2.5 VITAL EXAMPLES OF TURBULENCE GENERATION MODELS AND TRIP WIRE PRINCIPLES EMPLOYMENT

[48] guided an analysis exploring critical contributions and vital aspects of turbulence generation approaches employed to assess and evaluate the aerodynamic properties and turbulence characteristics of high-speed trains, focusing on the train's inter-car space area. The scholars investigated the aerodynamic features of braking plates located in this area and predicted some vital properties. They employed an experimental analysis through which a practical turbulence generation technique was adopted with the help of a wind tunnel. In

addition, to research the aerodynamic properties of this high-speed train, they used a shear–stress transport – turbulence model and an improved delayed detached eddy simulation. Both of these models are based on a shear–stress transport. They evaluated and analyzed the flow field and the aerodynamic performance of high-speed trains with varied aerodynamic braking plate layouts. In their study, a numerical method was utilized, and it was validated by means of an experimental wind tunnel test. According to the findings of the numerical and experimental research, it was determined that opening the plates that were installed in the inter-car space would significantly increase the aerodynamic drag of the train. This result was especially true for large downstream plates, which experienced relatively small fluctuations in the aerodynamic forces in comparison to large upstream plates. In addition, the research outputs revealed that the braking plates had a considerable impact on the downstream degrees of the inter-space area's turbulence. This significant effect might, in turn, cause an interaction with the external flow to bring about a reduction in the wake profile. [49], [50] conducted an analysis exploring and assessing some turbulence generation methods to investigate and identify some aerodynamic characteristics and properties to enhance the design and mechanical performance of aircraft. The scholars analyzed a case study representing a glider working on solar power. In addition, the focus of their research was on the development of a glider that has a significant potential of solar endurance, which would allow for an increased amount of time spent in the air. When compared to a standard glider, the glider's weight needed to be reduced, and its aerodynamic performance needed to be improved by applying vortex generators to the wingspan. These were the limits placed on the design. The design related to every individual component was developed by working through a number of stages with similar situations. In addition, a decision matrix design approach was utilized in order to make the component selections, which included some aspects, including vortex turbulence generators and solar panels. Their investigation made use of the ANSYS 18.1 software package, considering K-Omega SST turbulence generation and simulations process to successfully simulate the glider operating at a variety of speeds and angles of attack for the purpose of aerodynamics optimization. The installation of the vortex generators resulted in an increase in lift force between 160 N and 192 N, as demonstrated by their findings. The glider's wings are covered in 16 solar cells, each of which is capable of producing a power value of 57.6 W. Their research was constrained by the fact that the validation procedures involved physical testing in a wind tunnel. Because of this, the researchers depended on CFD simulations that were verified using data that

was public. Their study provides specific information regarding the idea of a boundary layer, the design process, the simulation of the glider, and the configuration of the glider, including the wingspan and total length. If the glider is equipped with vortex generators and solar panels, it should be able to maintain a flight time of six hours which is the least duration. [50] carried out a simulation work investigating the turbulence generation techniques' critical contributions and benefits on the performance and aerodynamic properties of sport cars. They investigated a case study of the NASCAR Gen 6 Cup car. In addition, the impacts of turbulence modeling on the RANS CFD simulations of a full-scale NASCAR Gen 6 Cup car were adopted using three different eddy viscosity turbulence models. These models were the realizable, the AKN (k-ε), and the SST (k-ω). A finite volume code with an unstructured, primarily hexahedral or trimmed mesh of 115 million cells was used to successfully finish the simulations. The delta drag and lift force plots along the vehicle model, as well as the generated delta scalar sceneries of pressure and velocity fields, demonstrated the prediction differences that exist amongst the various turbulence models. The discrepancies that were observed in the flow fields that were predicted were explained in terms of the differences that were observed in the vortical flow fields that were derived using the Q-criterion. According to the findings of the simulation, the effects of the turbulence modeling were likely to be most noticeable in sections that are both recirculated and separated. Due to under-predictions of the velocity gradients in the separated and wake regions, the realizable (k-ε) model demonstrated an inability to properly capture vortex-dominated flows, particularly towards the rear end of the vehicle. This result was especially noticeable in comparison to the AKN and SST models. The SST model projected vortex shedding that was comparable to the AKN in the majority of the vehicle body, with the exception of those on the decklid and off of the spoiler. Despite this, its poor performance in predicting total downforce calls for additional inquiry. When compared to the other two models, the AKN model appears to be superior since the predictions that it generates most closely align with the data from the wind tunnel in terms of drag, total downforce, and front-to-rear vehicle balance.
Regarding the trip wire principles employed in turbulence generation investigations, an experimental investigation is executed by [51] to assess and evaluate the aerodynamic impacts and properties related to polymer injection on the design development associated with a zero-pressure-variation bypass transitioning boundary layer linked to a flat plate. This investigation takes into consideration the two-dimensional trip wire principles. The development of the bypass transition process that is induced by a two-dimensional trip wire in Newtonian and polymer-injected flow can be characterized by using planar particle photo velocimetry. Furthermore, this study employed planar laser-induced fluorescence assessments that were carried out at multiple streamwise stations. In order to investigate the influence

of polymer injection both within the wake of the trip wire and within the laminar boundary layer upstream of the trip, two distinct trip positions in relation to the injection slot are taken into consideration. The transition process begins in a separated shear layer downstream of the trip wire. Here, a rapid amplification of the velocity perturbations brought about by an inflectional Kelvin-Helmholtz instability leads to the shedding of vortices, which is then followed by a breakdown into turbulence. When the polymer is injected, a transition process very similar to the one described above is observed. However, a more rapid initial increase of perturbations is seen, which results in an earlier transition. In spite of this, the beginning of the polymer effect may be observed at the final transition stages. This leads to a large reduction in the amount of drag experienced in the growing turbulent boundary layer.

A manuscript that was published by [52] investigating the mechanical and aerodynamic properties of aircraft from the perspective of the critical benefits and significance of turbulence generation techniques and trip-wire principles. An airfoil from a NACA 0012 wind turbine was the subject of a case study that the writers considered. According to what they found, the effectiveness related to wind turbines is severely impacted by the dynamic stall. As a result, the investigation looked into the consequences of applying state-of-the-art trip wire passive flow-control equipment to a NACA 0012 airfoil that was going through a dynamic stall at high angles of attack. 20,000 was thought to be the correct value for the Reynolds number. For the purpose of determining unstable lift, surface pressure assessments were carried out. When higher rotation-amount airfoil motion is stopped, an increase in flow occurs at the leading edge. This is because the airfoil imparts momentum onto the fluid during rotation, which causes the fluid to move faster. The effect of the increased flow at the leading edge is a rapid leading-edge air-flow separation because of the significant unfavorable pressure gradient caused by the increased flow. For settings with a high rotation rate, the leading-edge trip wire showed limited capacities in managing the boundary layer separation. This was evidenced by reductions in the ultimate post-stall lift and lift fluctuation. The production related to vortex shedding associated with the leading edge, which is analogous to bluff body separation, greatly dwarfed the vortex structures that were formed by the trip wire, which meant that the benefits of the trip wire were restricted. Under flow circumstances that have passed the stall point, the trip wire has very little of an effect on the significant-scale von-Karman vortex growth that happened as a result of load fluctuations. The use of a trip wire caused a reduction in the maximum lift, but changes in its diameter did not affect the stall angle of attack in any significant way.

A study executed by [53] aimed to identify the critical role of aeroplane model tests using air tunnels and turbulence generators in assessing and investigating the aerodynamic properties and mechanical performance of aircraft. The scholars depended on vortex-turbulence generation equipment and a wind tunnel through which experimental evaluations and tests were conducted to examine the performance and aerodynamic characteristics related to the aeroplane. Specifically, an approach of ice form modification was presented for use by Unmanned Aerial Vehicles (UAVs) considering constrained amounts of electrical power in order to accomplish effective anti-/de-icing at the leading edge of the wing. The lift and drag coefficients, as well as the suction-side velocity fields, of a NACA0012 finite wing model with 3D-printed bits of simulated ice mounted on it are measured using a six-component force balance and a Particle Imaging Velocimetry (PIV). They employed some calculation methods to assess turbulence characteristics, including the dimensionless ice shape length (w/c), which indicates the portion related to the spanwise length linked to a single ice shape part to the length of the chord. In addition, they depended on dimensionless modulation ratio (w/ λ), which explains the spanwise length of the non-icing area between two adjacent single ice shape pieces. Based on the findings, the coefficient related to the wing lift for a constant w/λ initially rises and then falls with increasing w/c, with a maximum value between 0.1 and 0.2. Wing lift coefficient increases as w/ decreases. The acceleration effect of the flow field in the non-icing area, which reduces the separation area, and the cross-flow resulting from the streamwise vortices and turbulence characteristics associated with the non-icing area to the icing area, which promotes the mixing of the flow field, are both responsible for the periodic variation of the flow separation area along the spanwise direction (similar to vortex generators). The derived modulation rule is validated by flight testing, and it provides direction for the ice shape modulation strategy employment for UAVs that are not entirely anti-/de-icing under extreme weather circumstances. Furthermore, it was found that utilizing turbulence vortex generators and wind tunnel tests helped classify and determine critical aerodynamic properties and mechanical performance related to the NACA0012 airfoil model with the help of particle imaging velocimetry principles. Figure 2.26 represents the ice-shape model of the aircraft explored under vortex-turbulence generation and wind tunnel test.

Figure 2.26: The ice-shape aeroplane model investigated under vortex-turbulence generation conditions [53].

[54] guided a study investigating the substantial contributions of turbulence generation techniques (including vortex generators) and ship model testing methods (which comprised a towing tank) in identifying significant aerodynamic properties and performance of a four-screw ship. Besides, the scholars carried out an experimental investigation in a towing tank using a particle image velocimetry (PIV) measurement device to determine the typical wake left by a ship equipped with four propellers. Further, they employed some critical turbulence formulas to investigate the aerodynamic properties of the ship. These equations and calculation methods to assess turbulence included the Reynolds-averaged Navier–Stokes (RANS) method to carry out computational research on the ship's viscous flow fields at various scales. An in-depth analysis was performed on the scale effect on the axial nominal wake field inside and outside propeller discs. The results demonstrated that the CFD results and the PIV data satisfactorily agreed with one another. Additionally, it was discovered that the inner and outside propeller discs had distinct circumferential distribution patterns of the axial nominal wake field, particularly in the zone behind the brackets. This was one of the findings that emerged from the research. When various radii were taken into consideration, it was found that the inside propeller produced a mean wake fraction that was generally greater than that of the outside propeller. The mean axial wake fraction is relatively large in the inner radius area (0.3 r/R 0.6) for both the inside and the outside propellers, whereas it is relatively small and almost coincident in the outer radius area (0.7 r/R) at different scales. This result is because the inner and outer propellers are closer together. Furthermore, turbulence and aerodynamic features associated with the four-screw ship model under

turbulence generation considerations were obtained, as shown in the vortex (vorticity) profile in Figure 2.27.

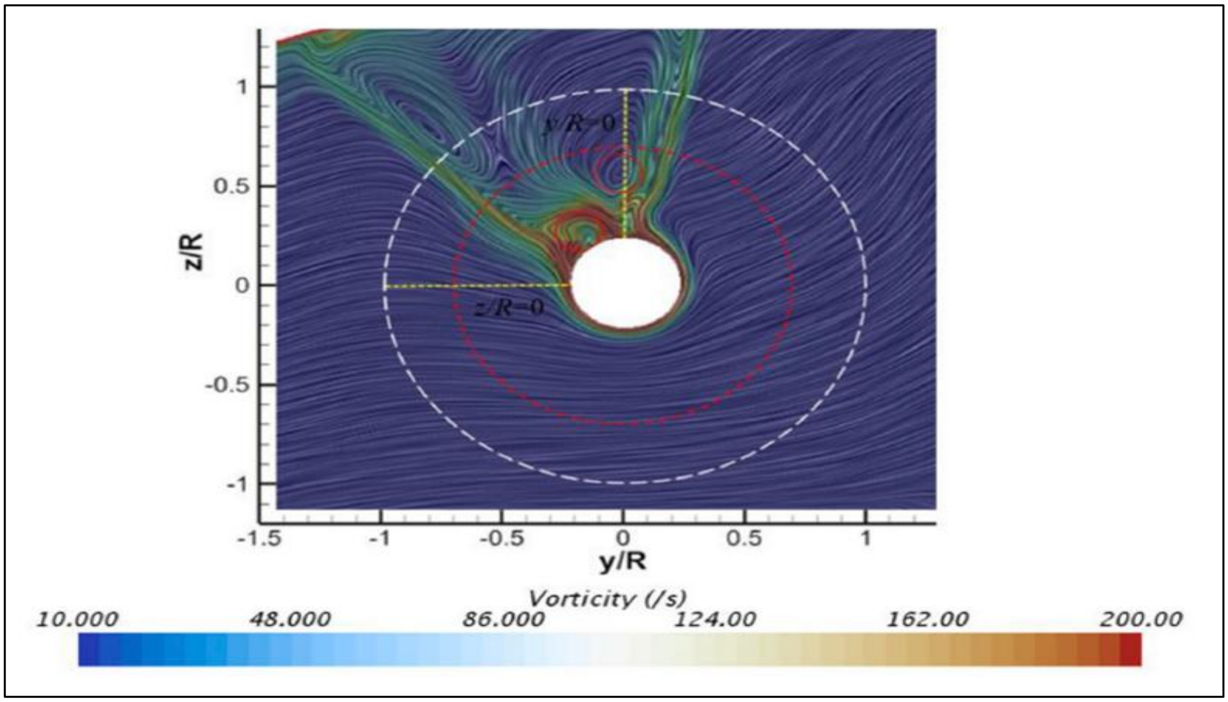

Figure 2.27: The turbulence vorticity investigations and generation related to the four-screw ship [54].

In addition, Figure 2.28 illustrates the employment of the towing test applied for ships.

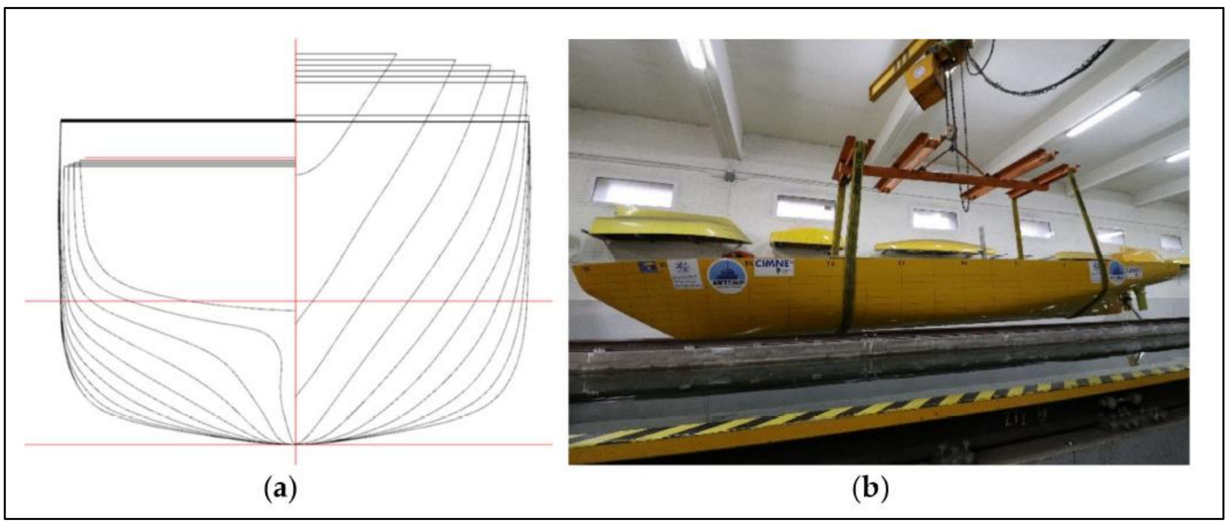

Figure 2.28: A towing test conducted for ships, including (a) a general configuration of the ship's body and (b) modeling of the ship developed for turbulence experimental analysis [55].

Also, other towing tests conducted for ships can be represented in Figure 2.29.

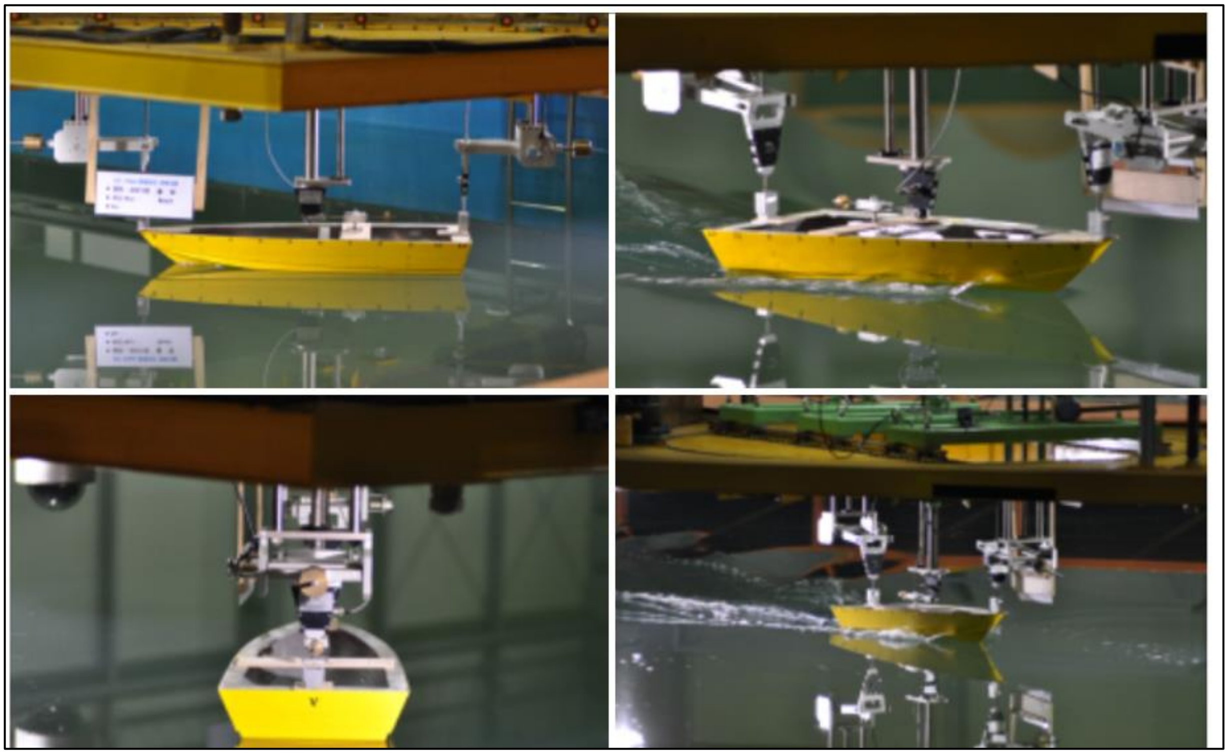

Figure 2.29: Different configurations and layouts of towing tests carried out to assess turbulence for typical ship models [56].

[57] conducted an analysis investigating the aerodynamic properties of a vehicle in a pilot wind tunnel developed in Canada. The scholars underlined the fact that turbulence is known to have an effect on both the aerodynamic and aeroacoustics performance of ground vehicles. What is not completely understood are the aspects of turbulence that have an effect on the performance, as well as the ways in which those aspects can be utilized in a consistent manner for the goals of aerodynamic design and evaluation. Road Turbulence System is the name given to the project that was developed as a result of collaboration between Transport Canada and the National Research Council of Canada (NRC) with the purpose of developing a system for creating road-representative turbulence in the NRC 9 m Wind Tunnel (RTS). This endeavor was carried out in support of a wider effort that aimed to examine new and developing technologies for reducing the amount of drag that heavy-duty vehicles experience. In order to build the RTS for use in the NRC 9 m Wind Tunnel with a 30% scale model of a heavy-duty truck, a procedure that included multiple stages of the design was utilized. This paper provided documentation of this process, which included 1) an on-road measurement campaign to identify those

target wind characteristics, 2) small-scale concept-development efforts to identify a passive approach to the problem, and 3) commissioning the full-sized RTS in the NRC 9 m Wind Tunnel. The wind spectrum that was produced by the RTS was an excellent match to the measurements that were taken on the target road. In order to compare the results of measurements (depending on turbulence generation calculation methods) taken in smooth and road-representative turbulent wind conditions, a model of a heavy-duty vehicle scaled down to thirty percent was utilized. Besides, to assess the turbulence similarity of their model with the effective Reynolds number, they used the following formula:

$$Re_{Model} \equiv Re_{Triple\ Point} \tag{2.8}$$

It has also been indicated that turbulent flow lowers the Reynolds number sensitivity of bluff bodies and raises the effective Reynolds number associated with the flow circumstances via a forced transition process. This can result in an improvement in the simulation of scaled-model experiments. Figure 2.30 indicates the variation of the drag coefficient of the heavy-duty vehicle with the Reynolds number. Furthermore, the measurements showed differences in the characteristics of the vehicle's drag, as well as differences in the drag-reductions associated with add-on devices such as side-skirts and boat-tails. These differences highlight the significance of representative turbulence for ground-vehicle aerodynamic evaluations.

Regarding the turbulence similarities based on their laboratory tests of the heavy-duty vehicle, it was found that yaw-sweeps assessments revealed some differences and divergence between the turbulence constraints and Reynolds n umber values. They discovered that in the low-wind-angle, the smooth flow condition provided significant turbulence rates and Reynolds number similarities to some turbulence cases investigated in their work, including VB, C6Q, and C7F circumstances. The C3S8 condition has a drag coefficient that is 10% higher at zero wind angle than the smooth-flow condition.

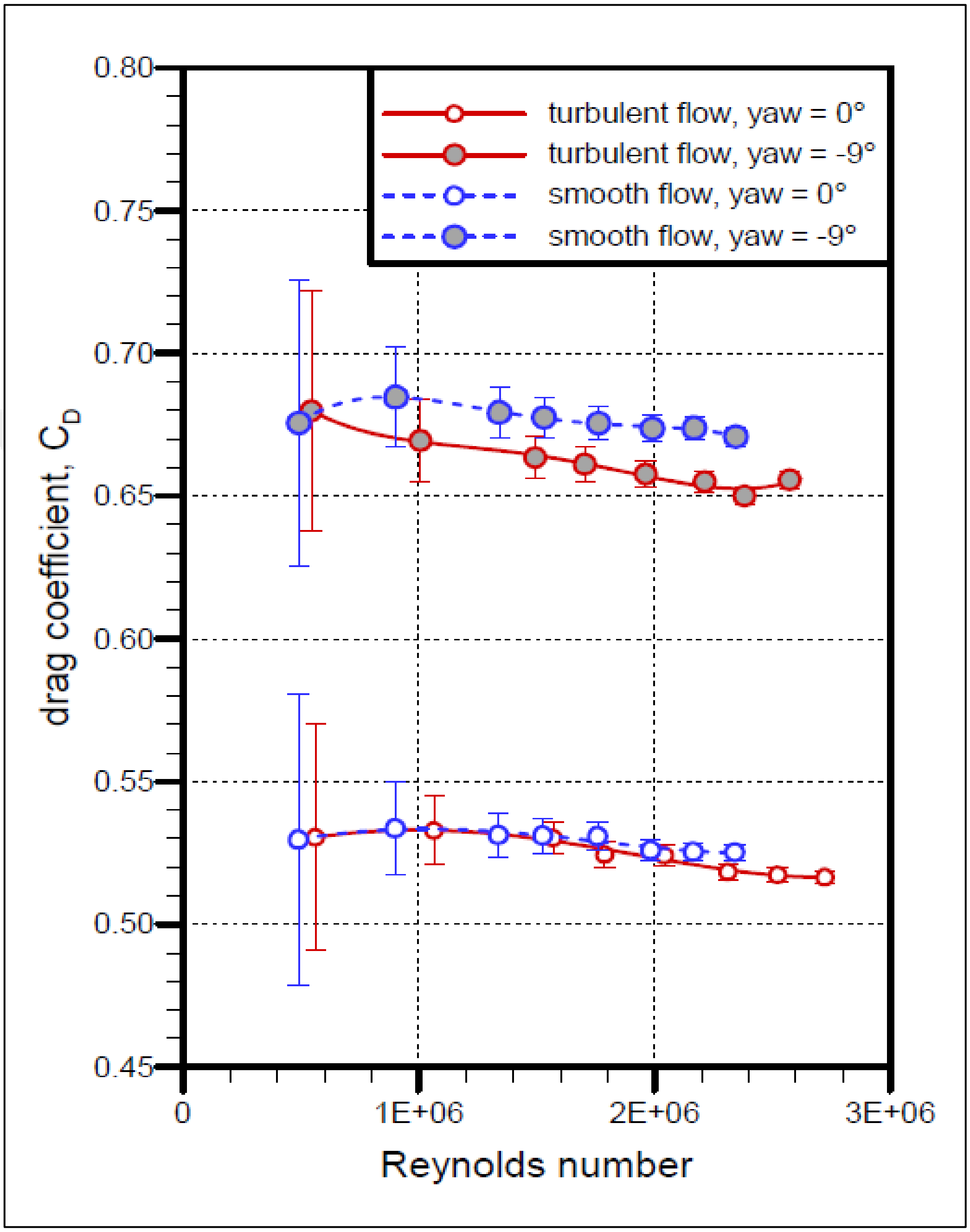

Figure 2.30: The variation of the drag coefficient of the heavy-duty vehicle with the Reynolds number [57].

Also, Figure 2.31 illustrates the tractor-trailer model investigated in the Canadian Wind Tunnel with a total length of 9 m.

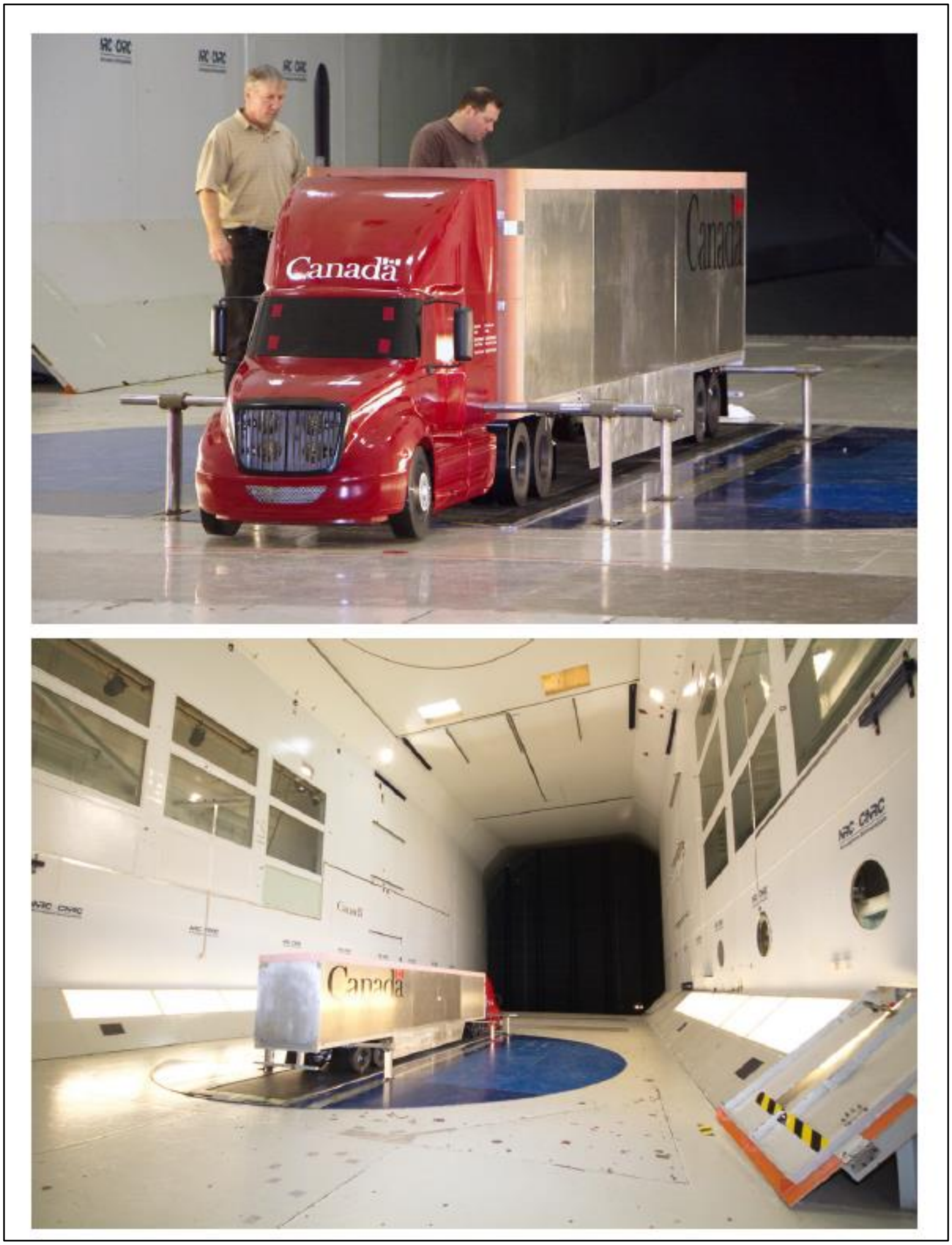

Figure 2.31: The tractor-trailer model investigated in the Canadian Wind Tunnel with a total length of 9 m [57].

Also, Figure 2.32 describes the turbulence generation techniques adopted to test the aerodynamic properties of the vehicle in a 9 m pilot Canadian wind tunnel.

Figure 2.32: The turbulence generation techniques adopted to test the aerodynamic properties of the vehicle in a 9 m pilot Canadian wind tunnel [57].

2.6 LITERATURE REVIEW CONTRIBUTIONS SUMMARY

The major results and relevances of each paper investigated in this work can be summarized in Table 2.2.

Table 2.2: Literature review publications reviewed in this work.

#	Author(s)	Year	Paper Title	Major Contributions
1	Dhalwala, M., Bayram, A., Oshkai, P., & Korobenko, A.	2022	Performance and near-wake analysis of a vertical-axis hydrokinetic turbine under a turbulent inflow	Their analysis results revealed that the performance of the turbine slightly declined when the turbulent flow existed. Moreover, the findings confirmed that the turbulent inflow contributed to significant fluctuations in the instantaneous power coefficient, affecting the fatigue life of some parts in the hydrokinetic vertical-axis turbine.
2	Yamamoto, K., Watanabe, T., & Nagata, K.	2022	Turbulence generated by an array of opposed piston-driven synthetic jet actuators	The research analysis revealed that the highly intermittence nature related to supersonic synthetic jets caused large-scale turbulence intermittency. In addition, the research results indicated that the turbulent flow's Mach and Reynold numbers at the chamber center region reached 0.01 and 1,000, respectively. Furthermore, it was observed that despite that the turbulent Mach number was not high at the center of the chamber, the turbulence generation process was significantly affected by compressibility because of supersonic jet flow. For this reason, the density variation is present in turbulence conditions.

Table 2.2: Literature review publications reviewed in this work. "tables Continued"

#	Author(s)	Year	Paper Title	Major Contributions
3	Dhamankar, N. S., Blaisdell, G. A., & Lyrintzis, A. S.	2018	Overview of turbulent inflow boundary conditions for large-eddy simulations	Their literature analysis revealed that STG is better than other methods to analyze the turbulent inflow characteristics due to its effectiveness and remarkable practicality in various industrial applications associated with turbulence. Furthermore, they found that the STG approach plays a critical role in predicting the inflow turbulence features of several engineering problems. Nonetheless, the lack of knowledge and experience regarding the turbulence and its quantitative aspects formulate a limiting factor facing practical and effective implementation of the STG approach. Moreover, Dhamankar et al. reported that engineers face several difficulties in generating realistic turbulent inflow fluctuations for problems that analyze inflow turbulence aspects. Additionally, they reported that using the STG approach and producing realistic turbulence circumstances is considerably significant and practical to comprehensively analyze and investigate inflow turbulence behavior using the large-eddy simulations and further large-scale turbulence analysis methods.

Table 2.2: Literature review publications reviewed in this work. "tables Continued"

#	Author(s)	Year	Paper Title	Major Contributions
4	Xiong, D., Yang, Y., & Wang, Y.	2022	An Improved Synthetic Eddy Method for Generating Inlet Turbulent Boundary Layers	Based on their numerical analysis, the results revealed that their enhanced synthetic eddy approach generated turbulent fluctuations with higher accuracy and the findings were greatly closer to the direct numerical simulation outputs in their experiment. Moreover, they found that the skin friction coefficient of their enhanced synthetic eddy approach for turbulence generation recovered faster and had low dimensionless speed at the outer region of the boundary layer compared with the conventional synthetic eddy approach employed for turbulence generation.
5	Gand, F., & Huet, M.	2021	On the generation of turbulent inflow for hybrid RANS/LES jet flow simulations	Their numerical simulation results revealed that the Mach and Reynolds numbers reached 0.9 and 1,000,000, respectively. In addition, the findings confirmed that there was a small area at the jet nozzle that had robust shear layer fluctuations and uncertainties, which led to the rapid development of three-dimensional turbulent flow at the mixing boundary layer. Gand and Huet reported that their results are vital for scholars and engineers to fully understand the turbulent modeling of the nozzle boundary layer relying on jet flow modeling and simulation.

Table 2.2: Literature review publications reviewed in this work. "tables Continued"

#	Author(s)	Year	Paper Title	Major Contributions
6	Shur, M., Strelets, M., Travin, A., Spalart, P., & Suzuki, T.	2018	Unsteady simulations of a fan/outlet-guide-vane system: Aerodynamics and turbulence	Their comparative analysis revealed that using the STG method provided a low-cost analytical technique to understand and investigate these three aspects. Moreover, the findings confirmed that using the STG method, zonal technique, and Reynolds-averaged Navier–Stokes formulas provided higher reliability, cost-effectiveness, and performance to investigate and understand the turbulence behavior, noise, and performance of the engine's fan. Additionally, the researchers depended on the STG approach besides zonal technique and Reynolds-averaged Navier–Stokes formulas to analyze the engine's fan in terms of noise, performance, and turbulence features.

Table 2.2: Literature review publications reviewed in this work. "tables Continued"

#	Author(s)	Year	Paper Title	Major Contributions
7	Blake, J. D.	2020	A Coupled Large Eddy Simulation-Synthetic Turbulence Method for Predicting Jet Noise	They found that using the STG technique provides higher accuracy and significant effectiveness in controlling and reducing the noise and turbulence aspects in the jet engine. Furthermore, their simulation and modeling affirmed that using Fourier mode-based stochastic turbulence approach offered higher cost-effectiveness in analyzing the jet engine noise and turbulence compared with other synthetic eddy techniques for small-scale analysis. Nevertheless, the synthetic eddy turbulent approach provided higher effectiveness in analyzing and understanding turbulence for high-scale turbulence applications. In addition, the critical benefits and substantial role of the STG approach were identified and classified in predicting the noise, performance, and turbulence properties of a jet engine.

Table 2.2: Literature review publications reviewed in this work. "tables Continued"

#	Author(s)	Year	Paper Title	Major Contributions
8	Morsbach, C., & Franke, M.	2019	Analysis of a synthetic turbulence generation method for periodic configurations	Their numerical simulation and research analysis indicated that using the STG process contributed to significant effectiveness and performance compared with other conventional turbulence analysis approaches. Furthermore, their research findings confirmed that employing the STG process is greatly practical for several industrial turbomachinery and aerogenic applications. In addition, the researchers employed a large-eddy simulation process to study the Reynolds stresses, energy spectra, and two-point correlations.
9	Martinez-Sanchis, D., Sternin, A., Sternin, D., Haidn, O., & Tajmar, M.	2021	Analysis of periodic synthetic turbulence generation and development for direct numerical simulations applications	Their analysis revealed that using the STG approach and Fourier synthetic turbulence technique helped provide effective neutralizing at the injection area of the engine. Moreover, they found that these two methods offered higher cost-effective techniques for analyzing the turbulence and noise of the engine compared with traditional turbulence analysis methods. The type of turbulence generation methods used in their study includes the STG and Fourier synthetic turbulence analysis, considering Navier–Stokes formulas.

Table 2.2: Literature review publications reviewed in this work. "tables Continued"

#	Author(s)	Year	Paper Title	Major Contributions
10	Shobayo, O. O., & Walters, D. K.	2020	Evaluation of a Statistically Targeted Forcing Method for Synthetic Turbulence Generation in Large-Eddy Simulations and Hybrid RANS-LES Simulations	Their simulations and research analysis confirmed that the STG method, targeted forcing technique, and hybrid large-eddy Reynolds-averaged Navier-Stokes CFD modeling and simulation offered higher flexibility in analyzing the velocity and turbulence profiles. Also, using these turbulence generations approaches contributed to the successful reproduction of the required statistical distributions for homogenous turbulent flow. The methods of turbulence analysis they used in their research are the STG approach, targeted forcing technique, and large eddy turbulence mechanism. Furthermore, they used hybrid large-eddy Reynolds-averaged Navier-Stokes CFD modeling and simulation to analyze the velocity and turbulence profile.

Table 2.2: Literature review publications reviewed in this work. "tables Continued"

#	Author(s)	Year	Paper Title	Major Contributions
11	Patruno, L., & Ricci, M.	2018	A systematic approach to the generation of synthetic turbulence using spectral methods	Their research analysis revealed that their proposed method provided several critical strengths in studying and analyzing the turbulence characteristics, mirrored by its simplicity and generality. Furthermore, their proposed method offered effective and direct control over several turbulence scales. Also, the new approach was capable of targeting anisotropic fields with higher robustness. They used the STG approach and proposed a new turbulence analysis approach with spectral approaches, considering Taylor's assumption and divergence-free conditions.
12	Nandi, T. N., Kröger, H., Yeo, D., & Kornev, N.	2018	Assessment of a synthetic inflow turbulence generator for prediction of neutrally stratified atmospheric flows	Their research analysis confirmed that the STG technique had higher potential in providing perfect continuity conditions and generating turbulence with the desired statistics. In addition, their findings indicated that using the STG approach allows researchers to obtain valuable results related to Computational Wind Engineering (CWE) applications. The researchers depended on the STG method through which spatially distributed turbulent zones (spots) were employed to produce the flow profile related to the boundary layer conditions of the neutrally stratified atmospheric flow.

Table 2.2: Literature review publications reviewed in this work. "tables Continued"

#	Author(s)	Year	Paper Title	Major Contributions
13	Sunhazim, N. S. A. M., Zawawi, F. M., Abidin, U., Samion, S., Ismail, K., & Ismail, A. M. M.	2022	CFD Investigation on The Jet-Engine Inspired Wind Turbine	Their analysis and simulation results revealed that the shrouded wind turbine contributed to power coefficient improvements of 8.6%. The enhanced power coefficient ranged between 0.35 and 0.38. Further, it was found that the curly shroud caused an increase in the inlet speed and a pressure drop due to swirl formation in the wind turbine. The researchers relied on CFD numerical modeling and analysis to study the performance and speed profile of the wind turbine. Also, they analyzed induced flow's curly shroud.
14	Chen, Z. X., Langella, I., & Swaminathan, N.	2019	The role of CFD in modern jet engine combustor design	Their research analysis revealed that using large eddy simulations and Reynolds averaged Navier-Stoked approach contributed to numerous benefits and strengths, mirrored by higher accuracy, significant robustness, and large efficiency. Furthermore, it was found that these two CFD approaches resulted in higher effectiveness and reliability compared with the experimental work. They used large eddy simulations based on CFD principles to analyze the performance and characteristics of their investigated gas turbine. Also, they applied Reynolds averaged Navier-Stoked approach for CFD analysis.

Table 2.2: Literature review publications reviewed in this work. "tables Continued"

#	Author(s)	Year	Paper Title	Major Contributions
15	Erario, M. L., Giorgi, M. G. D., & Przysowa, R.	2022	Model-based dynamic performance simulation of a microturbine using flight test data	Their modeling and simulation results indicated that microturbines modeling and simulation played a critical role in studying the performance and characteristics of the microturbine. Also, modeling and simulation of microturbines via CFD principles provides the potential to enhance their lifetime, design engines' control system, and improve their performance. They reported that analyzing microturbines is greatly vital as their employment in light personal aircraft and unmanned aerial vehicles has significantly grown in the last decades. Nonetheless, they witness limited adoption due to their lower durability and less efficiency. For this reason, further simulation work and modeling are required to improve their reliability and performance, thus, increasing their engagement in aviation. In this context, Erario et al. used modeling and simulations of the microturbine using CFD principles.

Table 2.2: Literature review publications reviewed in this work. "tables Continued"

#	Author(s)	Year	Paper Title	Major Contributions
16	Briones, A. M., Caswell, A. W., & Rankin, B. A.	2021	Fully Coupled Turbojet Engine Computational Fluid Dynamics Simulations and Cycle Analyses Along the Equilibrium Running Line	Their simulation and modeling analysis revealed that using thermodynamic cycle analysis and iterative Secant approach juxtaposed with CFD principles provided higher reliability, accuracy, and performance than traditional analysis approaches, as the numerical results agreed with the experimental work associated with the assessment of the thrust, equivalence ratio, fuel, and air mass flow rate, and diffuser-combustor interface, making CFD approach highly helpful and useful for monitoring the development and design of small-scale gas turbines of jet engines. They used the iterative Secant approach for the CFD to determine the fuel flow rate desired to achieve better matching of the turbine power and the compressor.

Table 2.2: Literature review publications reviewed in this work. "tables Continued"

#	Author(s)	Year	Paper Title	Major Contributions
17	Synylo, K., Krupko, A., Zaporozhets, O., & Makarenko, R.	2020	CFD simulation of exhaust gases jet from aircraft engine	Their numerical modeling and simulations revealed that using CFD in aviation provided higher accuracy, reliability, and performance in terms of fluid flow analysis and the prediction of several aviation parameters. They reported that CFD has been widely employed and has become an attractive approach to analyzing aviation parameters of the jet engine. The researchers depended on a comparative analysis of the results of three CFD software tools, which are SolidWorks, OpenFOAM, and Fluent 6.3. They analyzed the longitudinal coordinate and height bouncy effect in the jet engine.
18	Teixeira, M., Romagnosi, L., Mezine, M., Baux, Y., Anker, J., Claramunt, K., & Hirsch, C. ().	2018	A methodology for fully coupled CFD engine simulations, applied to a micro gas turbine engine	Based on the researchers' numerical modeling and simulations, it was found that using CFD provided higher accuracy and successful results associated with the analysis and performance of the gas microturbine of the KJ66 engine. The researchers relied on three-dimensional modeling and simulations of the gas microturbine using Autogrid/ OMNIS™ software package. In addition, the results indicated that employing CFD principles allowed researchers to find a solution for the entire engine depending on a single simulation problem.

Table 2.2: Literature review publications reviewed in this work. "tables Continued"

#	Author(s)	Year	Paper Title	Major Contributions
19	Olejnik, A., Dziubiński, A., & Kiszkowiak, Ł.	2022	CFD simulation of engine nacelle cooling on pusher configuration aircraft	Depending on the CFD simulations and modeling, the findings indicated that employing CFD had successfully helped predict several variables of the OSA aircraft's engine, which helped improve its performance. The researchers applied three-dimensional simulations and modeling of the OSA aircraft's engine, focusing on analyzing the performance of a simplified design of the engine's nacelle.
20	Pasalkar, S. M., Shaikh M. S., Pipulyawala M. M.	2020	Design and CFD Analysis of Combustion Chamber of Jet Engine to Reduce Formation of NOx	Their modeling and simulation results revealed that using CFD principles to model and analyze the jet engine, and its corresponding flue gases contributed to higher performance and accuracy compared with conventional analysis methods. In addition, the researchers employed CFD to analyze the amount of NOx flue gases. They reported that the difficulties in designing higher-performance combustion systems did not greatly change in the last decades. However, the approach used in the analysis has been changed into a more complicated analysis procedure. The researchers studied the original design and applied some boundary conditions. They applied CFD using SolidWorks and ANSYS software tools.

Table 2.2: Literature review publications reviewed in this work. "tables Continued"

#	Author(s)	Year	Paper Title	Major Contributions
21	Sarvari, A. A., Heris, S. Z., Mohammadpourfard, M., Mousavi, S. B., & Estellé, P.	2022	Numerical investigation of TiO2 and MWCNTs turbine meter oil nanofluids: Flow and hydrodynamic properties	The research results indicated that using nano coating layer of TiO2 would significantly reduce the turbulence impact and turbulent characteristics in the turbine.
22	Wang, L., Wang, C., Qin, S., Lan, X., Sun, G., You, B., ... & Lu, H.	2022	Experimental Study on Performance of Transonic Compressor Cascade with Microgroove Polyurethane Coatings	The research findings revealed that employing micro-groove polyurethane coating layers compressor would remarkably minimize the turbulence effects in the compressor.
23	Liyue, W. A. N. G., Cong, W. A. N. G., Shuyue, W. A. N. G., Sheng, Q. I. N., Gang, S. U. N., Bo, Y. O. U., & Zhong, Y.	2022	A boundary surrogate model for micro/nano grooved surface structure applied in turbulence flow control over airfoil	The study outputs confirmed that utilizing micro-nano coating layer on the surface of the airfoil would improve its performance due to the reduction of turbulent flow effects and turbulence characteristics.

Table 2.2: Literature review publications reviewed in this work. "tables Continued"

#	Author(s)	Year	Paper Title	Major Contributions
24	Jun, T. A. O., Gang, S. U. N., Gang, W. U., Liqiang, G. U. O., Zhong, Y., Meng, W. A. N. G., & Bo, Y. O. U.	2019	An innovative study on low surface energy micro-nano coatings with multilevel structures for laminar flow design	The study outputs indicated that using micro-nano coating layer could achieve better laminar flow effects and reduce turbulence impact.
25	Guinness, I., & Persoons, T.	2021	Passive Flow Control for Drag Reduction on a Cylinder in Cross-Flow Using Leeward Partial Porous Coatings	The work findings affirmed that using partial porous coating would minimize the effects of turbulence and drag force values.

2.6 CHAPTER SUMMARY

Based on reviewing several peer-reviewed articles and research publications in the literature review, it can be inferred that the CFD approach and STG process play a critical role in enabling effective modeling, simulation, and analysis of jet engines, providing a higher level of accuracy, reliability, and performance in predicting the turbulence characteristics.

These aspects can help engineers and scholars conduct further improvements and modifications on the jet engines and investigate their key strengths and weaknesses to enhance their efficiency and performance.

Moreover, it can be inferred from the literature that there are variant CFD methods and STG techniques employed by scientists that helped analyze turbulence characteristics and jet engine features successfully, offering a higher level of flexibility and precision.

In this work, a jet engine is modeled and analyzed using CFD principles via the STAR-CCM+ 2022.1 software package to understand its turbulence characteristics and analyze its performance.

3. RESEARCH METHODOLOGY

3.1 INTRODUCTION

This chapter describes the research methodology followed in conducting this study. In addition, this chapter illustrates the theory and mathematical model associated with the synthetic turbulence generation approach for jet engines and turbines used in several engineering applications.

Furthermore, chapter three shows some details related to the software package used in this study to analyze, model, and simulate a 3D modeling of the jet engine investigated in this thesis.

3.2 RESEARCH METHODOLOGY

This work is carried out depending on a research approach that followed a group of phases to investigate the critical contribution and role of the synthetic turbulence generation approach in studying and analyzing the turbulence behavior in jet engines.

Firstly, the study depends on a comprehensive literature review through which several research peer-reviewed articles and academic publications were addressed to discuss and analyze the turbulence behavior in the jet engine and turbines in different mechanical engineering applications, including automobiles and ships.

In the second phase of this research, a case study of a jet engine is selected depending on some specifications and characteristics related to its operation and use, which include the following aspects:

i. The jet engine is Rolls-Royce RB211 jet engine (Figure 3.1 a).
ii. It is implemented and employed to power the Boeing 757 (Figure 3.1 b).
iii. This engine is three stage jet engine.
iv. It has four stages, which are:
    a. Intake stage,
    b. Compression stage,
    c. Combustion stage,

d. Exhaust stage.

v. It is a three-spool jet engine, which comprise:

a. Propeller spool,

b. Booster spool,

c. Compressor spool.

vi. The fuel used to operate this engine is kerosene.

Figure 3.1: Configuration of (a) Rolls-Royce RB211 jet engine, and (b) Boeing 757.

In addition, Appendix A shows more details on the components of the Rolls-Royce RB211 jet engine. In the third phase of this research, the boundary conditions and major assumptions were taken into account to carry out the numerical modeling and simulation analysis of the Rolls-Royce RB211 jet engine. These boundary conditions assumptions include: (According to [58])

a. The inlet pressure is 14.69 psi (1.01 bar).

b. The outlet pressure is 70.0 psi (4.83 bar).

c. The temperature at the inlet of the turbo engine is the ambient temperature (25 C),

d. The temperature in the combustion chamber at full power is 2,000 °C. (Cooling is used as metal parts melt at 1,300 ºC) [59].

e. The temperature at the outlet of the turbojet engine is roughly 540 ºC.

In the fourth stage, a comparative analysis is implemented to determine the contribution of the nano-ceramic layer employment to coat the jet engine and reduce the impact of high turbulence pressure and temperature during the combustion process and at the outlet of the jet engine.

An assumption was considered in using the nano ceramic layer associated with its thickness. The thickness of the nano ceramic SiO_2 coating layer used for the jet engine equals 1,000 nm [19]. The mechanical and thermophysical properties of the nanomaterial ceramic coating - SiO_2 are illustrated in Table 3.1.

Table 3.1: Some mechanical and thermophysical properties of the nanomaterial ceramic coating - SiO_2 [60], [61].

Property	Value *
Structure	Amorphous
Melting Temperature	Approximately 1,600 ºC
Density	2,200 kg/m^3
Dielectric Strength	10,000,000 V/m
Thermal Conductivity (@ 27 ºC)	1.4 W/mK
Dielectric Constant	3.9
Refractive Index	1.46
Specific Heat Capacity	745 J/kg.K

It can be indicated from Table (3.1) that this nano-ceramic layer can effectively protect the inner body and internal metal components and mechanical parts of the jet engine due to the larger melting point of the SiO2 (1,600 ºC) compared with jet engine metals melting point (1,300 ºC).

In this fourth stage of this research, a comparative analysis is carried out, considering the use and no use of SiO2 nanomaterial ceramic coating.

The Simcenter starccm+ 2022.1.1 software package is used to make simulations and 2D and 3D modeling of the jet engine.

Firstly, no coating is used. Secondly, 1,000 nm of SiO_2 nanomaterial ceramic coating layer is applied to the internal body of the jet engine to protect its mechanical components from turbulence, high pressure, and temperature impacts.

In the fifth stage of this work, modifications and adjustments are implemented to correct, validate, and verify the analysis findings obtained from the software program.

Finally, conclusions and recommendations are proposed to help CFD experts and turbulence professionals carry out further improvements and critical enhancements to the research outputs of this study.

Figure 3.2 presents a summary of the research methodology flowchart.

3.3 CASE STUDY DESCRIPTION

The Rolls-Royce RB211 jet engine relies on four stages to generate the necessary kinetic power to help the aircraft take off. Through the first stage (intake phase), air enters the jet engine using a propeller.

In the second stage, the air is compressed using an air compressor to reach a high-pressure value.

In the combustion stage, the highly compressed air is mixed with fuel and ignited. The chemical energy stored in the high-pressure air ignited with fuel would produce a considerable value of kinetic energy that can help the airplane fly. At the final stage of combustion, the exhaust gases go out from the combustion chamber and out of the jet engine into the atmosphere.

It is worth mentioning that the jet engine compressor consists of several compression stages to make the compression ratio high as possible and maximize the kinetic power essential for the aircraft [62].

[63] reported that the Rolls-Royce RB211 jet engine has the potential to produce a significant thrust power, which ranges between 182.5 kN and 264.4 kN (or between roughly 41,030 Ibf and 59,450 Ibf).

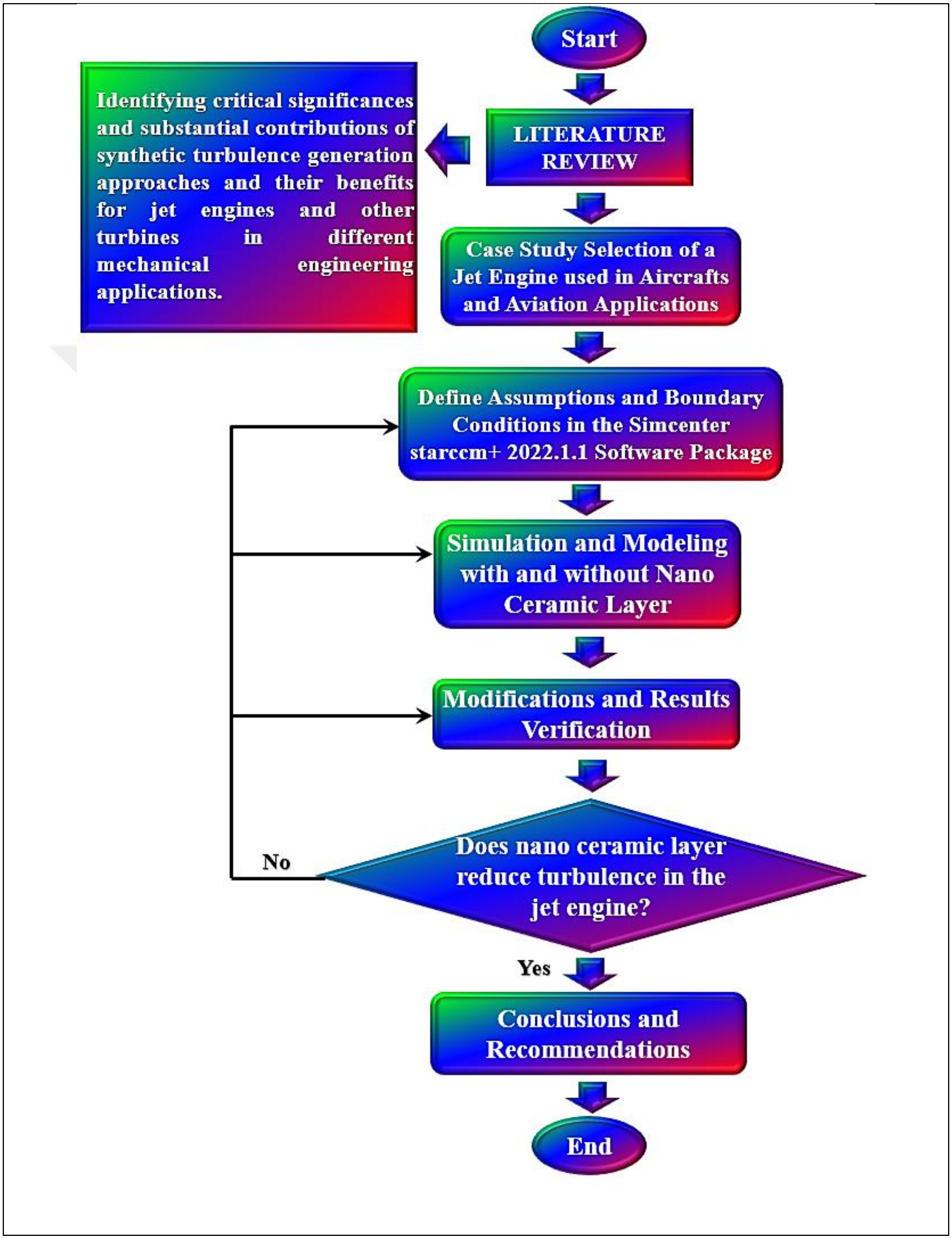

Figure 3.2: The research methodology flowchart.

Figure (3.3) presents a schematic diagram and energy profile (in horsepower) of the jet engine investigated in this work. The jet engine comprises two major sections.

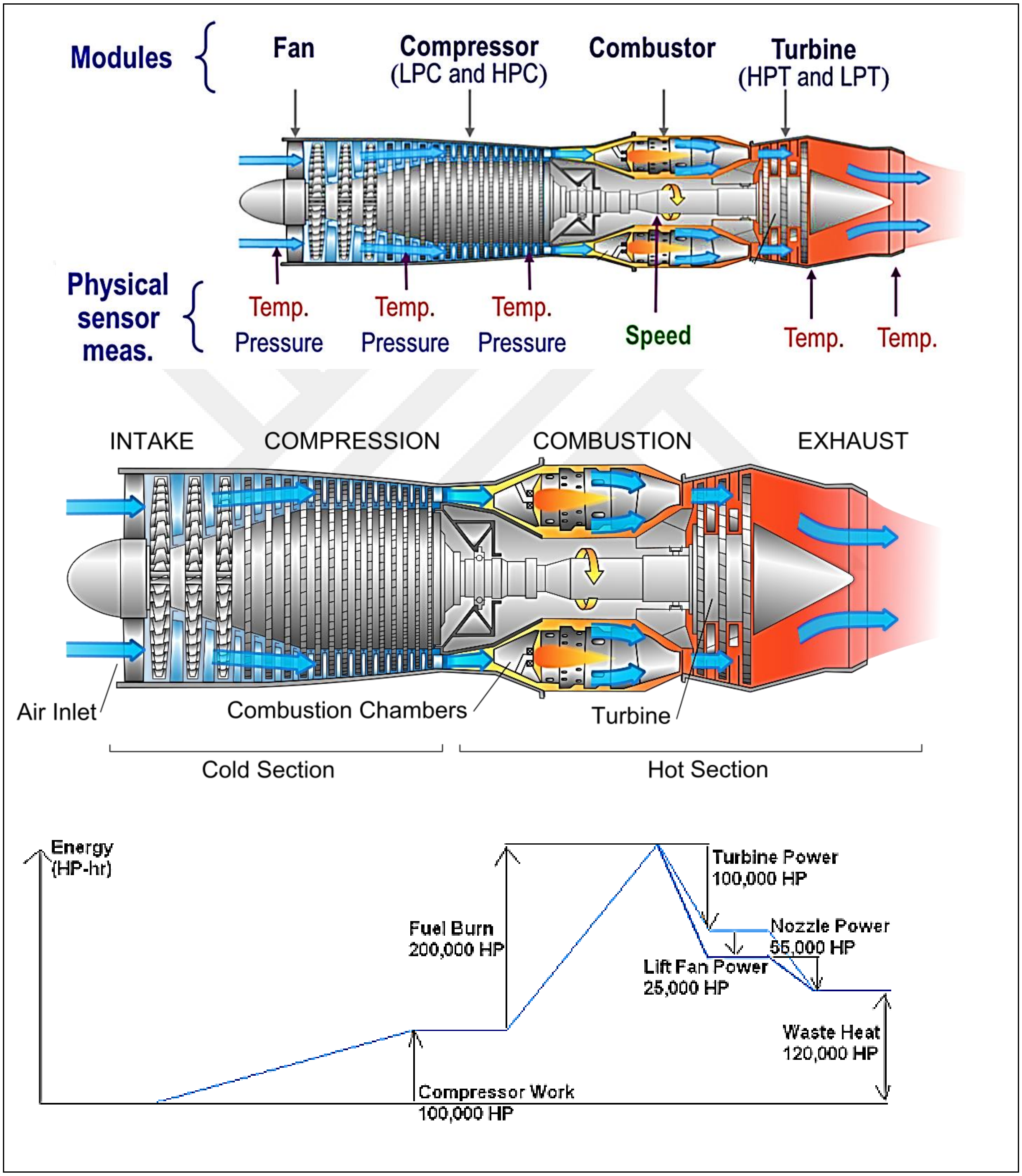

Figure 3.3: The major components of the aircraft jet engine and the horsepower profile [64], [65].

From Figure 3.3, the first section is the cold section in which cold air from the ambient is dragged and enters the jet engine using a fan driven by the jet engine.

Also, during the compression process, the air pressure can amount to 70 psi (4.83 bar) [66]. The air velocity can rise as well, juxtaposed with the pressure increase. The inlet speed of air at the inlet stage of the jet engine reaches 55.56 m/s.

When the air exits the compressor, its velocity reaches 194.44 m/s [67]. Furthermore, the jet engine contains a hot section in which flue gases resulting from the combustion process flow at a high temperature (ranging from 600 ºC to 700 ºC) [68].

Also, it can be inferred from Figure 3.3 that higher values of horsepower can be obtained in the hot section where the combustion of highly pressurized air takes place. Also, the kinetic power reaches its maximum value at the combustion stage. Then, it declines when reaching the exhaust phase, where hot flue gases flow with higher thrust and energy to drive the aircraft.

3.3 THEORY AND MATHEMATICAL MODEL

This section comprises the theoretical equations and formulas developed by several scholars to investigate the parameters of jet engines. The following paragraphs illustrate these theoretical expressions and mathematical relationships.

3.3.1 Turbulent Kinetic Energy

Turbulent kinetic energy (TKE) can be described as the kinetic energy associated with turbulence flow. The general formula of TKE can be expressed in the following relationship [69]:

$$TKE = \frac{1}{2}\left(\overline{(u')^2} + \overline{(u')^2} + \overline{(w')^2}\right) \tag{3.1}$$

Where u, v, and w are the velocity components in the x-, y-, and z-directions. They are given by [69]:

$$\overline{u'} = \frac{1}{T}\int_0^T (u(t) - \bar{u})dt = 0 \quad (3.2)$$

$$\overline{v'} = \frac{1}{T}\int_0^T (v(t) - \bar{v})dt = 0 \quad (3.3)$$

$$\overline{w'} = \frac{1}{T}\int_0^T (w(t) - \bar{w})dt = 0 \quad (3.4)$$

And [69]:

$$\overline{(u')^2} = \frac{1}{T}\int_0^T (u(t) - \bar{u})^2 dt \geq 0 \quad (3.5)$$

$$\overline{(v')^2} = \frac{1}{T}\int_0^T (v(t) - \bar{v})^2 dt \geq 0 \quad (3.6)$$

$$\overline{(w')^2} = \frac{1}{T}\int_0^T (w(t) - \bar{w})^2 dt \geq 0 \quad (3.7)$$

$$u' = u - \bar{u} \quad (3.8)$$

$$v' = v - \bar{v} \quad (3.9)$$

$$w' = w - \bar{w} \quad (3.10)$$

3.3.2 Turbulent Velocity

The turbulent velocity of the jet engine is investigated and described by [70], who employed the Navier-Stokes formula to express the turbulence velocity, which is given by [70]:

$$\frac{\partial u_j}{\partial x_j} = 0 \quad (3.11)$$

$$\frac{\partial u_i}{\partial t}+\frac{\partial}{\partial x_j}\left(u_j u_i\right)=-\frac{\partial}{\partial x_i}\left(\frac{P}{\rho_o}\right)+\frac{\partial}{\partial x_j}\left[v_m\left(\frac{\partial u_i}{\partial x_j}+\frac{\partial u_j}{\partial x_i}\right)-\frac{2}{3}v_m\frac{\partial u_k}{\partial x_k}\delta_{ij}\right] \quad (3.12)$$

Where:

u	The air velocity
P	The air pressure
ρ_o	The air density
v_m	The air viscosity
x	The space dimension (jet turbine) across which the air flows
δ_{ij}	The deflection angle of the air

The deflection angle, δ_{ij}, can be expressed using the relationship [71]:

$$\delta_{ij}=\tan^{-1}\left(\frac{V_{A,x}}{V_{A,y}}\right) \quad (3.13)$$

Where $V_{A,x}$ presents the air velocity (at point A) in the x-direciton, while $V_{A,y}$ is the air velocity at the same point in the y-direction. Taking into account that the pressure and velocity are expressed in terms of the fluctuation and mean components, which are $P = P' + \bar{P}$ and $u = u' + \bar{u}$, and making some reductions in the length of the Navier-Stokes formula, the Reynolds averaged method (RANS) equation becomes [70]:

$$\frac{\partial \bar{u}_i}{\partial t}+\frac{\partial}{\partial x_j}\left(\bar{u}_j\bar{u}_i\right)=-\frac{\partial}{\partial x_i}\left(\frac{\bar{P}}{\rho_o}\right)+\frac{\partial}{\partial x_j}\left[v_m\left(\frac{\partial \bar{u}_i}{\partial x_j}+\frac{\partial \bar{u}_j}{\partial x_i}-\frac{2}{3}v_m\frac{\partial \bar{u}_k}{\partial x_k}\delta_{ij}\right)-\overline{u_i'u_j'}\right] \quad (3.14)$$

Where $\overline{u_i'u_j'}$ presents the term of RANS Reynold stress, which can be expressed via the formula [70]:

$$\overline{u_i'u_j'}=-v_t\left(\frac{\partial u_i}{\partial x_j}+\frac{\partial u_j}{\partial x_i}-\frac{2}{3}\frac{\partial u_k}{\partial x_k}\delta_{ij}\right)+\frac{2}{3}(SKE)\delta_{ij} \quad (3.15)$$

Where SKE is the specific kinetic energy. The first term after the equal sign presents the isotropic component of Reynolds stress, while the second term expresses the deviatoric part. Substituting equation (3.15) into equation (3.14) leads to [70]:

$$\frac{\partial u_i}{\partial t} + \frac{\partial}{\partial x_j}\left(u_j u_i\right) = -\frac{\partial}{\partial x_i}\left(\frac{\bar{P}}{\rho_o}\right) + \frac{\partial}{\partial x_j}\left[(v_m + v_t)\left(\frac{\partial u_i}{\partial x_j} + \frac{\partial u_j}{\partial x_i} - \frac{2}{3} v_m \frac{\partial u_k}{\partial x_k}\delta_{ij}\right)\right] \tag{3.16}$$

$$\tilde{P} = \bar{P} + \frac{2}{3}\rho_o (SKE)\delta_{ij} \tag{3.17}$$

Where $\tilde{P}$ is the modified average air pressure, which absorbed the isotropic components in the Reynold stress equation, while v_t is the turbulent viscosity.

3.3.3 Reynold and Mach Number

Reynolds number is essential to describe the turbulence characteristics of the air flowing across the jet engine. It can be expressed by [72]:

$$Re = \frac{\rho V d}{\mu} \tag{3.18}$$

Where:

ρ	The air density
V	The dynamic air velocity
d	The internal jet engine diameter
μ	The air dynamic viscosity

[73] mentioned that Re can laminar when:

$$10{,}000 <\approx Re <\approx 1{,}000{,}000;$$

At the same time, the airflow can be turbulent when the Re:

$$1{,}000{,}000 <\approx Re <\approx 10{,}000{,}000{,}000;$$

These facts are illustrated in Figure (3.4), in which C_f is the skin friction drag coefficient.

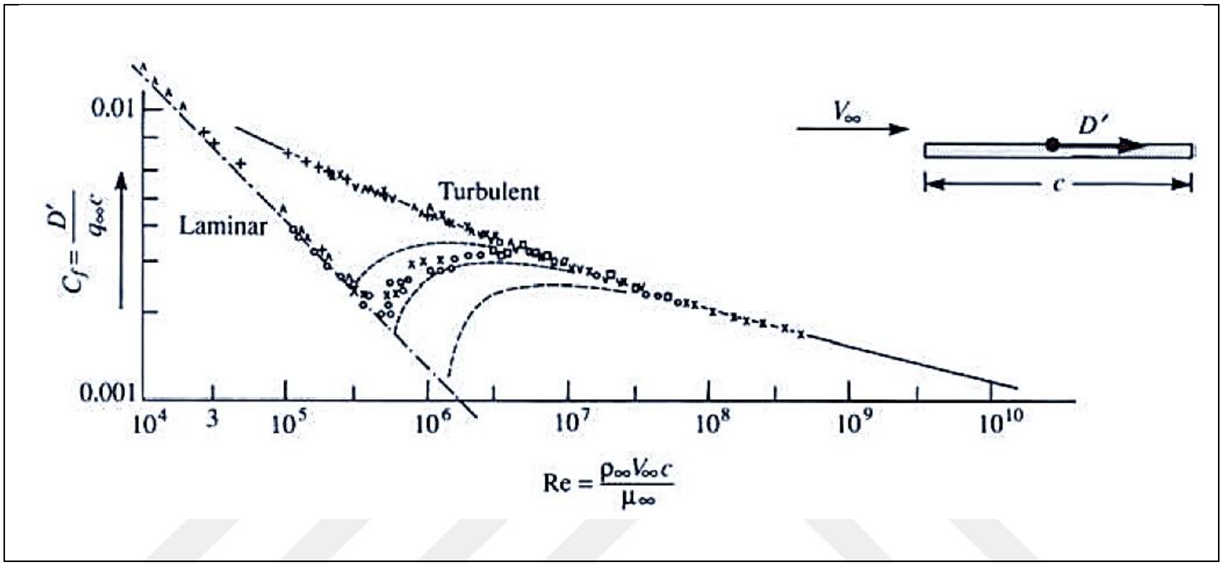

Figure 3.4: Variation of turbulent and laminar flow presenting the Reynolds number [73].

Furthermore, the Mach number can be described depending on the formula:

$$M = \frac{V}{a} \tag{3.19}$$

Where a presents the sound speed. The values of the Mach number of a jet engine can be expressed in Figure (3.5).

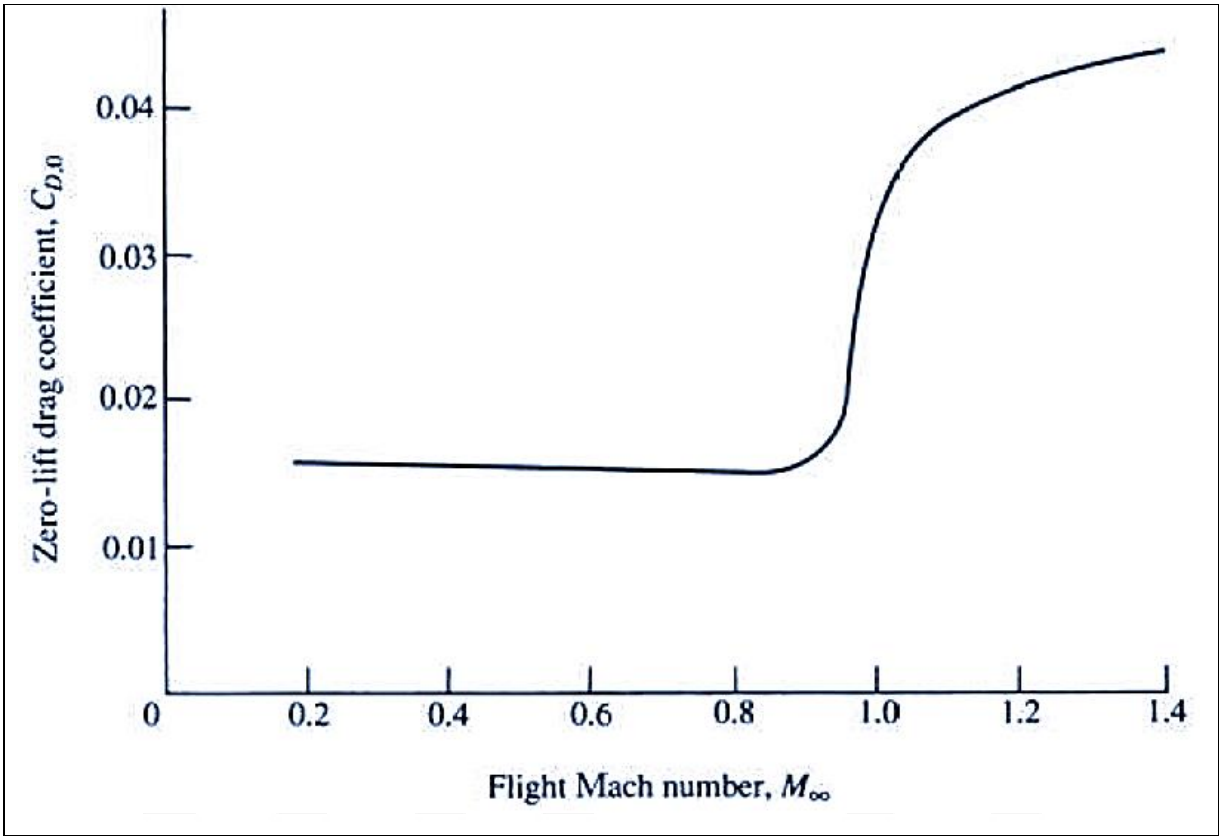

Figure 3.5: Mach number of a jet engine in aircraft [73].

In addition, a reflection of other effects or parameters related to different turbulence applications is possible through the latent space, as reported by [74], who stated that generative adversarial networks could learn the universal nature of the Reynolds number effect by capturing the similarity aspects hidden in the chaotic turbulence generation data.

Furthermore, [75] analyzed the use of Reynolds number correlations based on the Kármán-Howarth formula, which can describe different turbulence characteristics and turbulence models in which double- and triple-points of velocity are taken into account. They mentioned that Reynolds number similarity related to double-/ triple-point velocity values could be addressed using the expression:

$$Re = Const \quad (3.20)$$

They continued:

$$\sigma = 1\ , \qquad \overline{u'^2} \sim t^{-1}\ , \qquad l \sim l^{\frac{1}{2}} \quad (3.21)$$

Where:

σ	The finite Reynolds number
$\overline{u'^2}$	The velocity fluctuations
l	The integral length scale
t	The time

However, these formulas related to the Kármán-Howarth relationship are used when the Reynolds number is constant, considering double-/triple-point velocity rates. Hence, [75] investigated another Kármán-Howarth expression to assess the Reynolds number for different turbulence cases when double, and triple-point velocity models are employed. They stated that isotropic turbulence is an idealized turbulent state in which the turbulent fluctuations are statistically uniform in all directions, corresponding to isotropic turbulence generation (in which an idealized state of turbulence model has statistically uniform fluctuations of the turbulent flow in all directions). This formula is also applied to the double/ triple-velocity scheme. The following correlation expresses it:

$$\frac{\partial \overline{u'^2(t)}\, f(r,t)}{\partial t} = \frac{1}{r^4}\frac{\partial}{\partial r}\left[r^4\left(\left(\overline{u'^2}(t)\right)^{\frac{3}{2}} h(r,t) + 2v\frac{\partial \overline{u'^2(t)}\, f(r,t)}{\partial r}\right)\right] \tag{3.22}$$

Besides, this formula can be expressed depending on the Fourier space as shown in the relationship:

$$\frac{\partial E(k,t)}{\partial t} = -T(k,t) - 2vk^2 E(k,t) \tag{3.23}$$

Where k, f, t, h, r, and v represent some coefficients associated with the normalized two- and triple-point velocity relationship in which $Re \rightarrow \infty$.

3.3.4 Engine Pressure Ratio

Engine Pressure Ratio (EPR) is a critical parameter that can express the amount of air pressure amount related to the turbulent air flowing through the jet engine. It can be described using the formula, depending on the information in Figure 3.6:

$$EPR = \frac{P_{Tot,8}}{P_{Tot,2}} = \frac{P_{Tot,3}}{P_{Tot,2}} = \frac{P_{Tot,4}}{P_{Tot,3}} = \frac{P_{Tot,5}}{P_{Tot,4}} = \frac{P_{Tot,8}}{P_{Tot,5}} \quad (3.24)$$

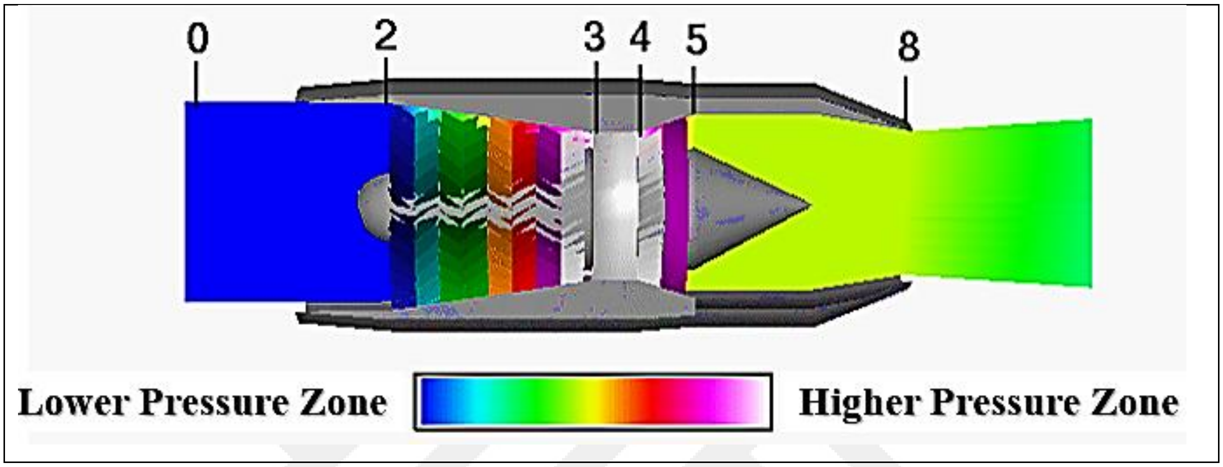

Figure 3.1: Jet engine major zones [76].

3.3.5 Turbulent Viscosity

The turbulent viscosity (or eddy viscosity), μ_{Turb}, can be described as a measure of the turbulent flow momentum of air due to eddies helping activate the internal air friction which is larger than the friction in laminar flow.

Turbulent viscosity plays a critical role in fluid dynamics and it can be more complicated when the air is mixed with other fluids such as liquid fuel in the combustion chamber of the jet engine [77]. The turbulent viscosity can be expressed by [77]:

$$\mu_{Turb} = \frac{C_{TED}\rho k_{Turb}^2}{\varepsilon} \quad (3.25)$$

Where:

C_μ	The turbulent model constant value (which equals 0.09)
k_{Turb}	The internal turbulence kinetic energy
TED	The rate of turbulent energy dissipation

3.4 NUMERICAL MODELING AND SIMULATION

In this section, more details are illustrated and addressed regarding the computational fluid dynamics' critical principles, modeling and simulation approach, and software package used in this work. The following paragraphs describe these details.

3.4.1 Computational Fluid Dynamics

CFD has witnessed great attention and interest from several scholars and engineers worldwide. CFD plays a critical role in helping scientists carry out numerical analysis and evaluation of various fluid mechanics problems to help determine the behavior of fluid and its turbulence and laminar characteristics [78], [79]. CFD approach is considered as a branch of fluid dynamics that is concerned with analyzing and resolving mechanical engineering problems associated with fluid motion (mainly water and air).

The solution to the CFD problem depends on defining some boundary conditions that help identify the structure and properties of the fluid investigated in fluid mechanics. Currently, CFD analysis has become greatly practical and beneficial due to the development of high-speed processors and better computer programs that can predict different turbulence characteristics of the fluid with higher levels of speed and accuracy [80], [81].

Therefore, new CFD programs can analyze highly complicated mechanical engineering problems which are involved in extreme working conditions, such as very high pressure and temperature values, including supersonic aircraft and jet engines.

Further, significant applications of CFD comprise the aerospace industry, flight testing, weather and climate parameters simulation, wind turbine investigations, combustion engines, and biological engineering [82]–[84]. CFD enables a comprehensive understanding of different fluid phenomena, such as combustion [85], [86].

One example of critical CFD approaches implemented for analyzing the turbulence of fluids is the Reynolds-averaged Navier–Stokes (RANS) technique. Through this approach, turbulence modeling can be executed to estimate the Reynolds stresses via solving a group of governing formulas. The RANS method can also handle unsteady and highly turbulent fluid flows flexibly [87].

3.4.2 Modeling and Simulation

One of the practical and critical applications associated with CFD is its potential to make numerical modeling and simulations. Two-dimensional (2D) and three-dimensional (3D) modeling and numerical simulations of variant mechanical components related to fluid mechanics enable mechanical engineers and designers to visualize the fluid's moments, pressure, temperature, velocity, forces, and turbulence behavior. 2D and 3D modeling and numerical simulations can forecast the turbulent kinetic energy and some vital fluid elements, which contain Reynolds and Mach numbers, turbulent viscosity, density, internal energy, specific kinetic energy, specific enthalpy, and specific entropy.

It also helps determine vital variables and significant parameters that play an important role in controlling and monitoring the turbulence in several small- and large-scale mechanical devices, like aircraft, jet engines, automobiles, and ships [88]–[90]. In this context, CFD software tools require some boundary conditions and research approaches to carry out the numerical modeling and simulations. One of these approaches is meshing.

Through the meshing process, the mechanical device is divided into a large number of small elements that have different shapes and dimensions, as making the modeling and simulation of the whole mechanical device (like a jet engine or wind turbine) would cause a high number of errors [91]. The reason for these errors is due to the large complexity of the mechanical device in which not all components of this device are similar in shape and size.

To solve this problem, the entire system can be divided into very small elements, and modeling and simulation processes can be applied to each element to come up with a significant rate of accuracy and quality. Nevertheless, the more complex the shape is, the more elements are used, and thus, the more time and effort are required from the software tool to calculate the needed parameters and make numerical simulations [92].

3.4.3 Software Package

The software package used in this work is the STAR-CCM+ 2022.1 software package. Commonly, ANSYS and OpenFOAM software tools are broadly employed by designers and mechanical engineers to execute CFD analysis through numerical modeling and simulations.

Notwithstanding, Siemens has been working to develop novel software that can handle complex geometries and run simulations and modeling with considerable accuracy and speed compared with other software programs. Consequently, Simcenter STAR-CCM+ 2022.1 was developed, enabling accelerated graphic processing of different mechanical geometries related to fluids which are handled using the CFD analysis.

Additionally, Simcenter STAR-CCM+ 2022.1 program can help scholars minimize higher costs and budgets linked to the hardware requirements to run the simulations effectively with lower power consumption. Major advantages and key strengths of the Simcenter STAR-CCM+ 2022.1 program include its high potential to handle the CFD analysis of nonstationary fluids, besides treating constant and steady density flows.

Some fluid formulas and CFD principles are defined in this software to support scientists in investigating the turbulence behavior of fluids, such as the RANS approach, Reynolds stresses modeling, and Delayed Detached eddy simulation (DDES). Also, this software supports different field functions and fluid benchmarks. Using Simcenter STAR-CCM+ 2022.1 program allows the reduction of CPU costs calculations and power consumption by roughly seventy percent [93].

3.5 RESULTS VALIDATION

The research findings that will be obtained from the numerical simulations and 2D and 3D modeling of the jet engine using the Simcenter STAR-CCM+ 2022.1 software package will be verified, modified, and validated to make sure that the outcomes are connected and consistent with the results of other scholars. The results will be validated depending on CFD experts' and fluid mechanics professionals' points of view.

Their consultation and opinion would be beneficial and helpful in determining the effectiveness, reliability, and practicality of the Simcenter STAR-CCM+ 2022.1 software's numerical modeling and simulation analysis. Those CFD professionals and fluid mechanics experts will locate significant strengths and critical weaknesses associated with the outputs attained with the program.

Furthermore, results validation will be carried out by comparing the research outcomes with other scholars and researchers who have rich experience and knowledge in CFD and fluid mechanics and have research publications similar to this work. Therefore, closer results and higher consistency of these research outcomes to other scholars will prove higher reliability and validity of this research.

4. RESULTS AND DISCUSSIONS

4.1 GENERAL

This chapter presents major thesis findings associated with the numerical analysis and simulation work conducted via the STAR-CCM+ 2022.1 software package to validate the contribution of the STG approach. It also presents the CFD analysis before and after a thin layer of a nano-ceramic layer is implemented. Moreover, chapter four shows the research discussions that relate the research outputs to other scientists' results.

4.2 CAD DESIGN OF THE JET ENGINE

Before the jet engine was simulated and numerically modeled in the STAR-CCM+ 2022.1 software package, it was built and designed in the AutoCAD software. Figure 4.1 illustrates the design of the jet engine based on a 3D environment. It can be shown from Figure 4.1 that the jet engine contains two major compressors near the air inlet.

Then, a protective cast iron shield (colored grey) covers the region in which the combustion of air mixed with fuel occurs. Then, the flue gases resulting from the combustion process flow through four turbines which can generate the kinetic power required for the aircraft to fly.

The four turbines and the exhaust gases belong to the hot section, while inlet air and the two compressors belong to the cold section.

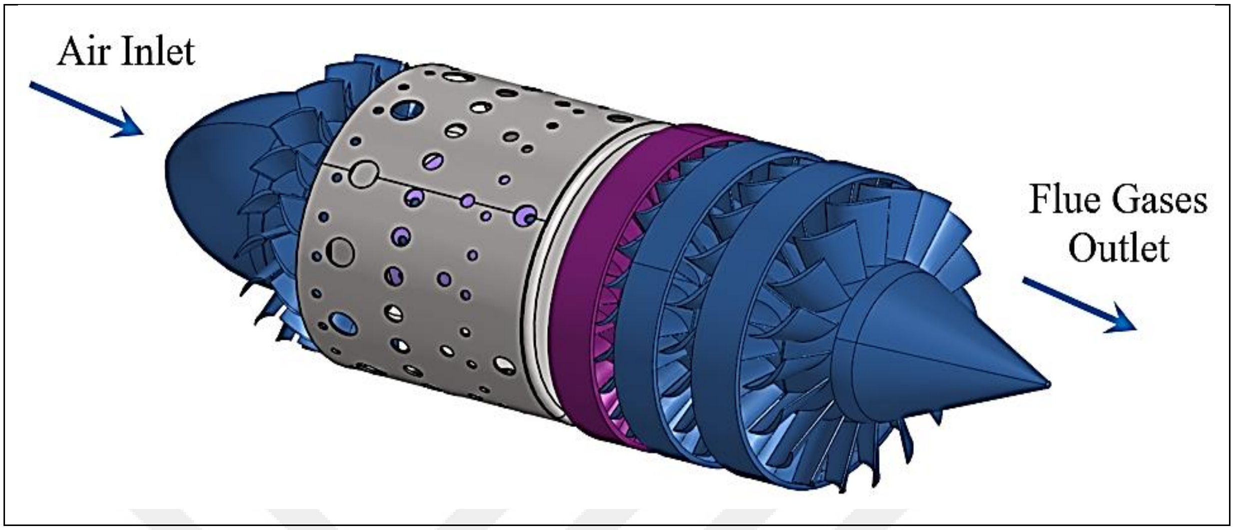

Figure 4.1: A 3D design of the jet engine investigated in this research.

When the cast iron protective shield is removed from the combustion chamber, the 3D design of the jet engine becomes as illustrated in Figure (4.2).

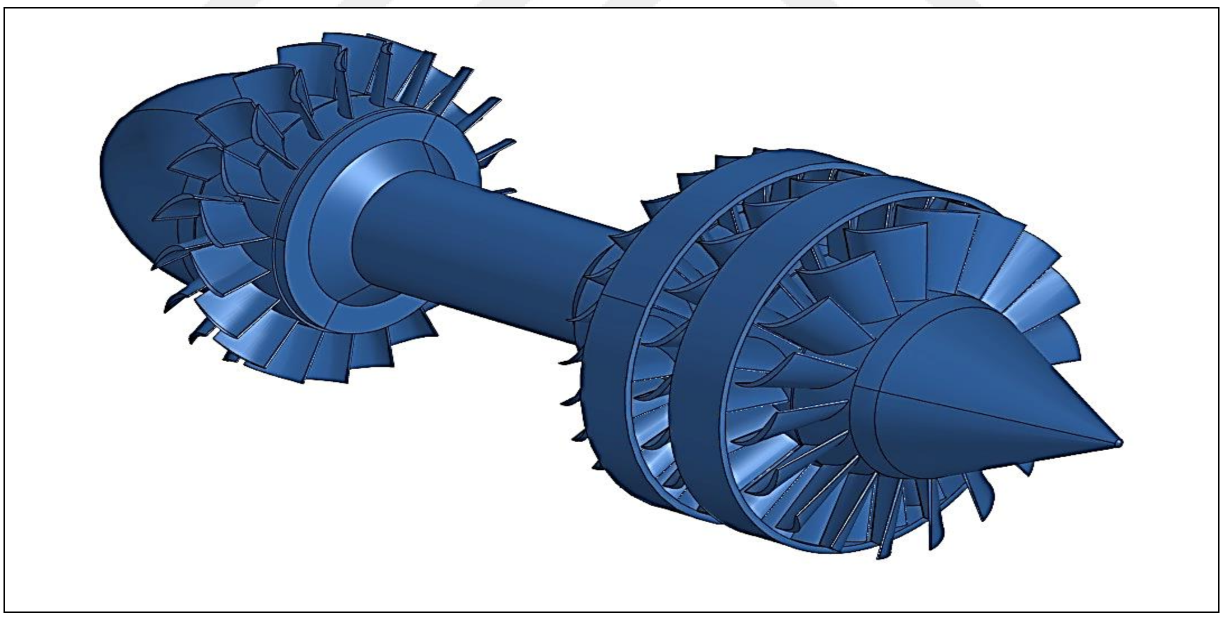
Figure 4.2: The 3D design of the jet engine without the protective shields.

Cast iron protective shield in the combustion chamber is not the only part that covers and protects the internal body of the jet engine. There are also outer casting components that cover the whole jet engine and separate its entire elements from the exterior environment. Figure (4.3) presents the whole components of the jet engine considering the outer casting.

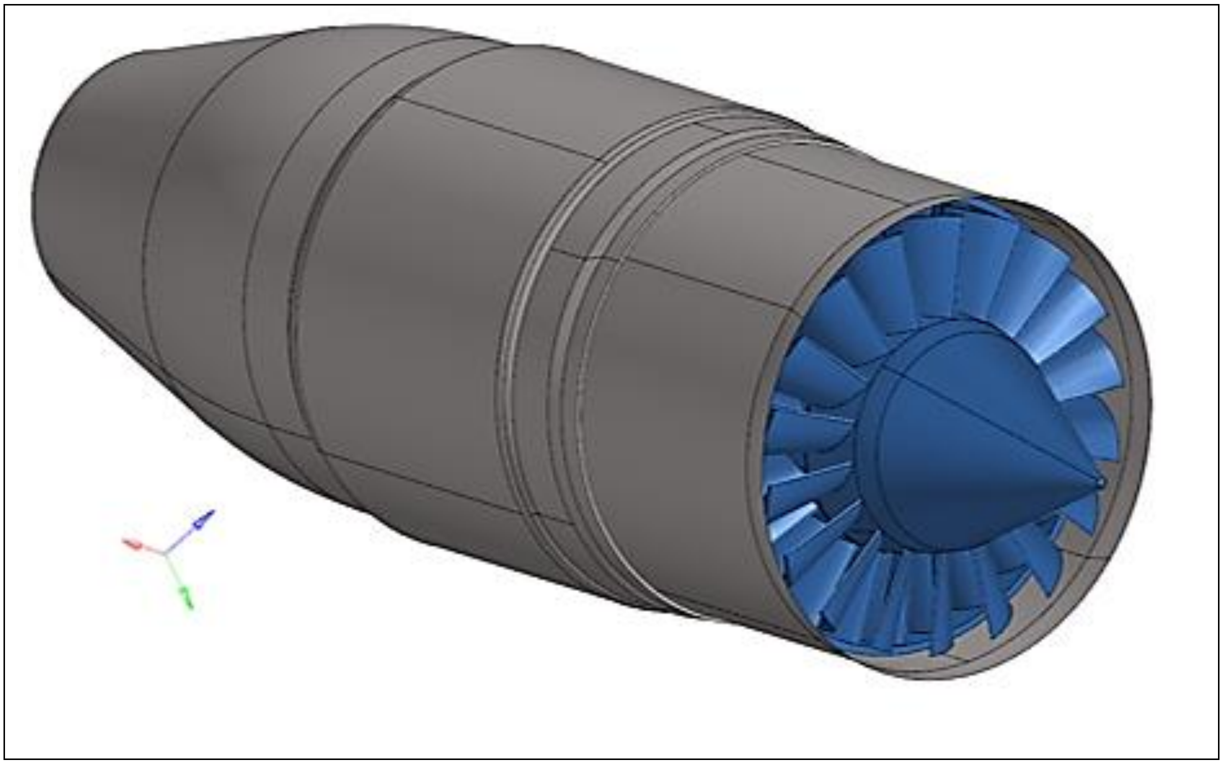

Figure 4.3: The jet engine shielding the whole components.

The actual dimensions of the jet engine are expressed in Figure (4.4).

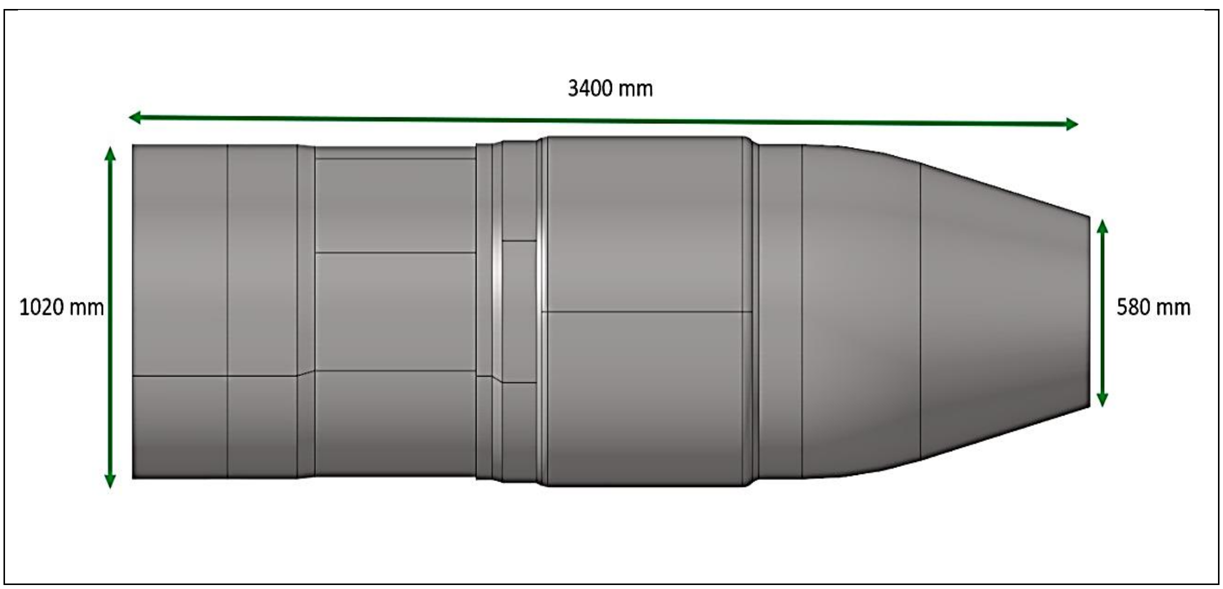

Figure 4.4: The actual dimensions of the jet engine.

4.3 MESHING ANALYSIS OF THE JET ENGINE

The meshing process is employed in this work to divide the whole jet engine into very small elements that can have simple shapes and sizes to enable effective modeling and numerical simulation analysis with higher accuracy. The meshing specifications related to this research are described in Table (4.1).

Table 4.1: The meshing process specifications and boundary conditions.

Parameter	Value
Number of elements	20,867,700
Shape of Mesh	Tetrahedral Elements
Base Size	20 mm
Minimum Surface Size	2.0 mm
Minimum surface size for the Compressor and Turbines	0.3 mm
Surface Curvature	35 Pts/Circle
Number of Prism Layers	8
Prism Layer Total Thickness	10 mm
Prism Layer Stretching	1.5
Volume Growth Rate	1.2

The meshing process of the whole engine is applied, as indicated in Figure (4.5).

Figure 4.5: The meshing procedure implemented to the whole jet engine.

Also, the meshing process is applied to the inner parts of the jet engine, as shown in Figure (4.6).

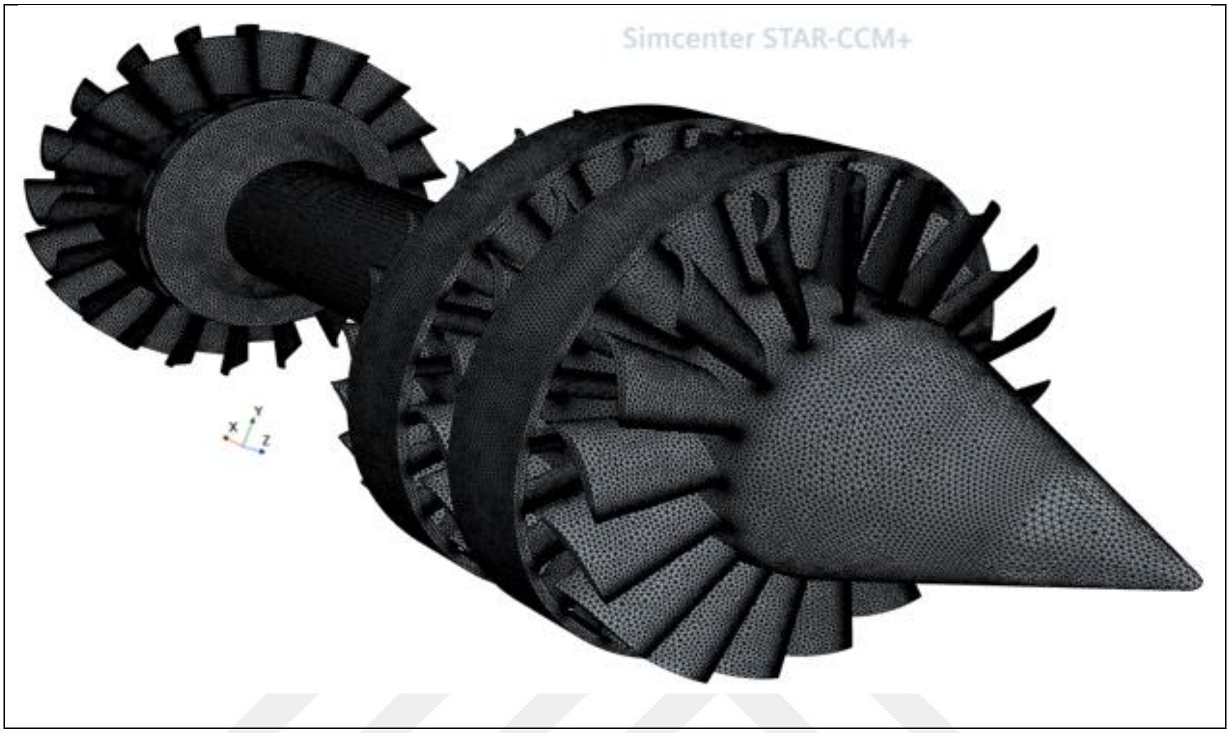

Figure 4.6: Meshing process applied to the inner parts of the jet engine.

From the meshing process implemented, it was found that the meshing elements were more regular at the surface area of the inlet and outlet of the jet engine. Nonetheless, meshing elements at impellers of turbines and compressors have some constraints, as impellers have more shape complexity compared with the surface area of the inlet and outlet regions of the jet engine, which are both described in Figure (4.7).

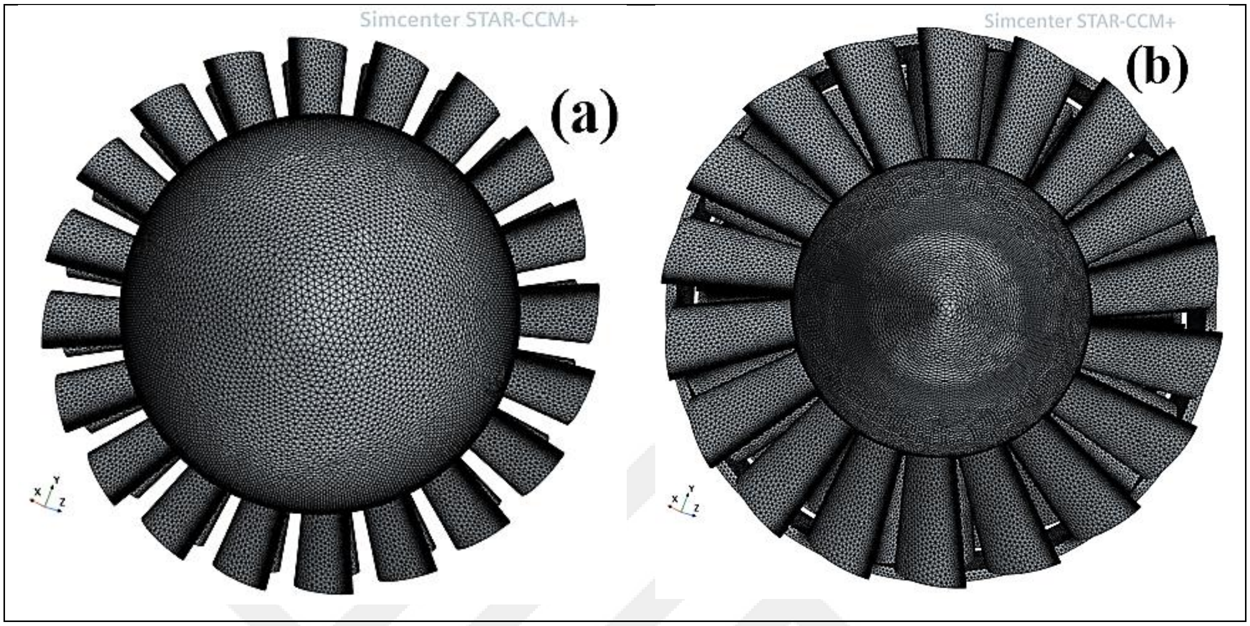

Figure 4.7: Meshing of the jet engine: (a) inlet compressors, (b) outlet turbines.

Following the successful meshing process of all jet engine components, CFD analysis is applied, and numerical simulations are executed to find some critical parameters related to the turbulence behavior of the jet engine before and after applying a thin layer of nano-ceramic coating.

4.4 CFD ANALYSIS OF TURBULENT VISCOSITY

After conducting the numerical simulation and modeling analysis, the STAR-CCM+ 2022.1 software package revealed the profile of turbulent viscosity before and after using a thin layer of nano-ceramic coating. Figure (4.8) presents the simulation results of the jet engine related to turbulent viscosity before and after using a thin layer of nano-ceramic coating.

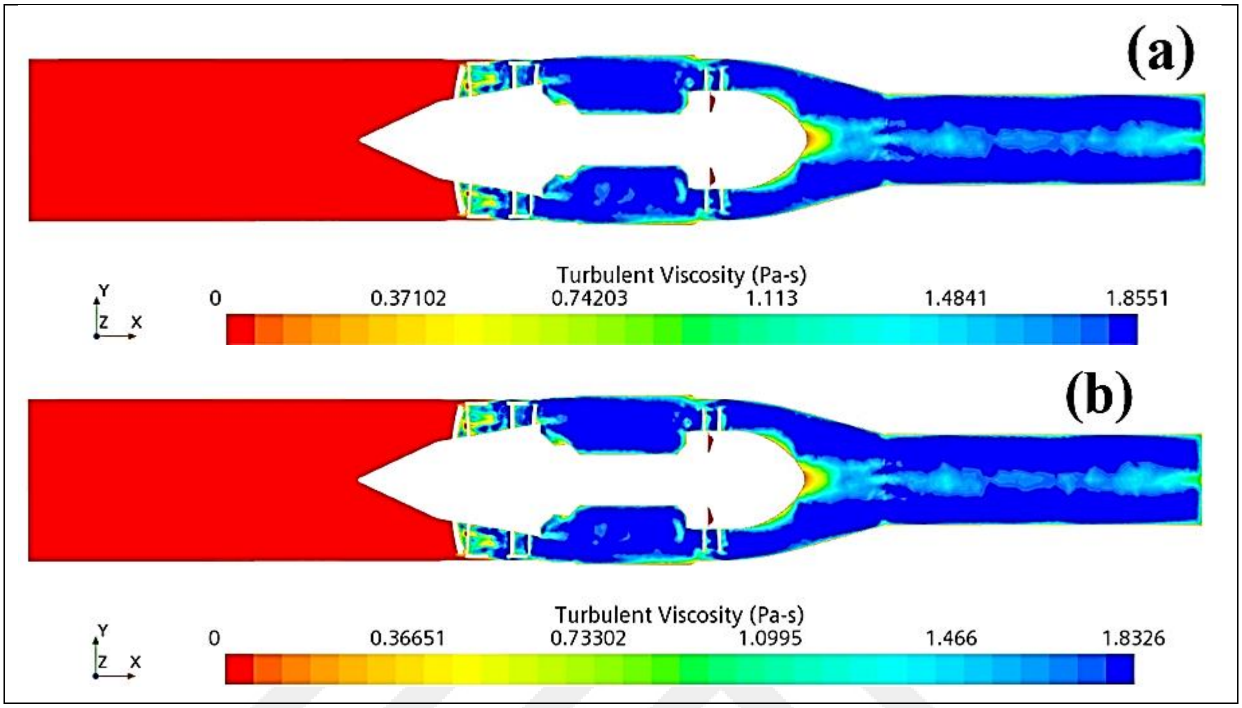

Figure 4.8: The jet engine's turbulent viscosity, (a) before and (b) after using a thin layer of nano-ceramic coating.

It can be inferred from Figure (4.8) that the turbulent viscosity ranges between roughly 0.37102 Pa.s and 1.8551 Pa.s. When the thin layer of nano ceramic coating is employed, the range of turbulent viscosity becomes between 0.33178 Pa.s and 1.6589 Pa.s, which indicates that using a thin layer of nano ceramic coating can reduce the turbulence behavior in the jet engine, leading to a decline in the turbulent viscosity. Also, it is indicated that the turbulent viscosity is high in the exhaust region of the jet engine and low at the inlet of the engine.

4.5 CFD ANALYSIS OF TURBULENT KINETIC ENERGY

The numerical simulation and modeling analysis conducted via the STAR-CCM+ 2022.1 software package provided the profile of the turbulent kinetic energy before and after using a thin layer of nano-ceramic coating. Figure (4.9) presents the simulation results of the jet engine related to the turbulent kinetic energy before and after using a thin layer of nano-ceramic coating.

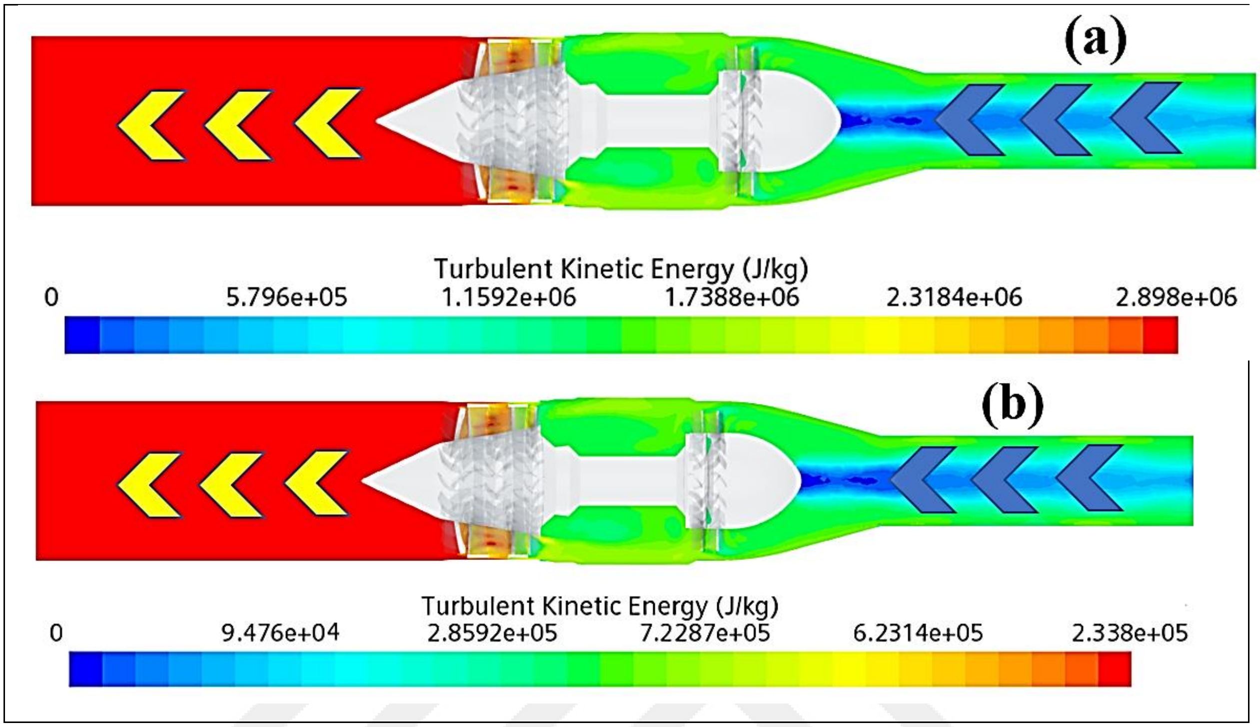

Figure 4.9: The jet engine's turbulent kinetic energy, (a) before and (b) after using a thin layer of nano-ceramic coating.

It is concluded from Figure (4.9) that the turbulent kinetic energy ranges between approximately 5.796×10^5 J/kg and 2.898×10^6 J/kg. After applying the thin layer of nano-ceramic coating, it was found that the range of turbulent kinetic energy becomes between 9.476×10^4 J/kg and 2.338×10^5 J/kg, explaining that using a thin layer of nano ceramic coating can reduce the turbulence behavior in the jet engine, leading to a decline in the turbulent kinetic energy.

4.6 CFD ANALYSIS OF THE STATIC PRESSURE

The numerical simulation and modeling analysis carried out by the STAR-CCM+ 2022.1 software package offered the profile of the static pressure before and after using a thin layer of nano-ceramic coating. Figures (4.10), (4.11), and (4.12) present the simulation results of the jet engine related to the static pressure before and after using a thin layer of nano-ceramic coating.

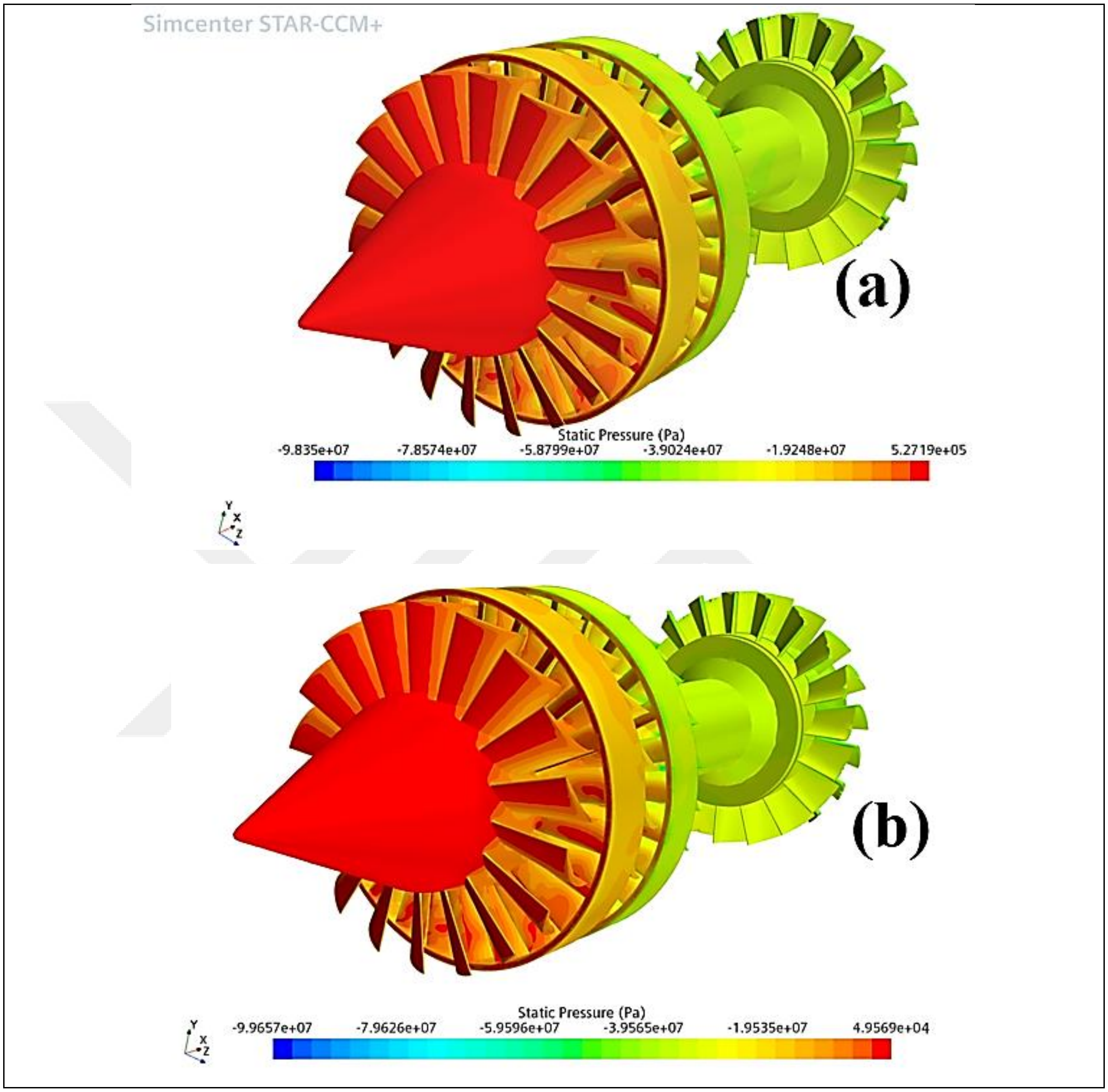

Figure 4.10: The jet engine's static pressure, (a) before and (b) after using a thin layer of nano-ceramic coating.

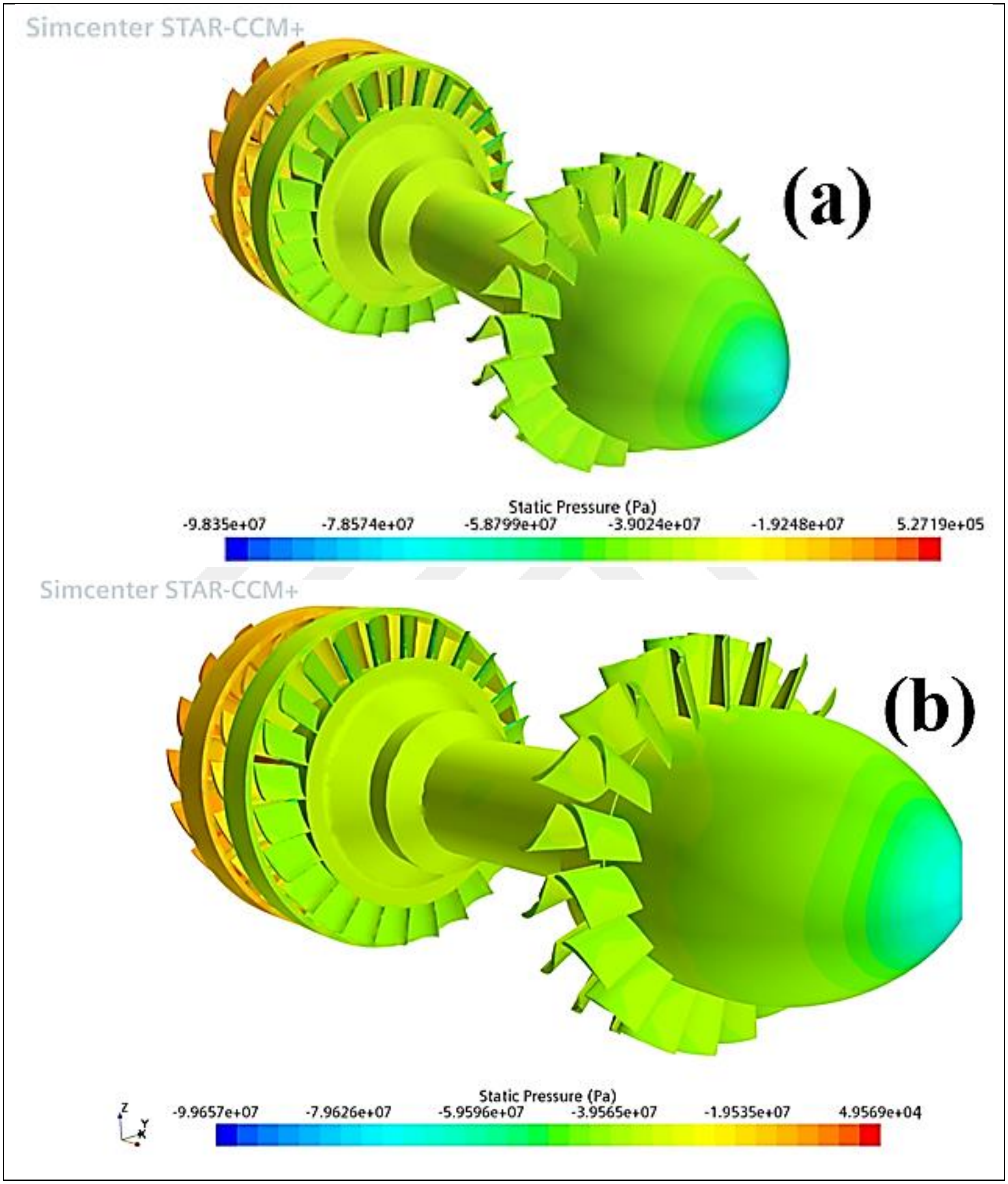

Figure 4.11: The jet engine's static pressure, (a) before and (b) after using a thin layer of nano-ceramic coating. (A second view).

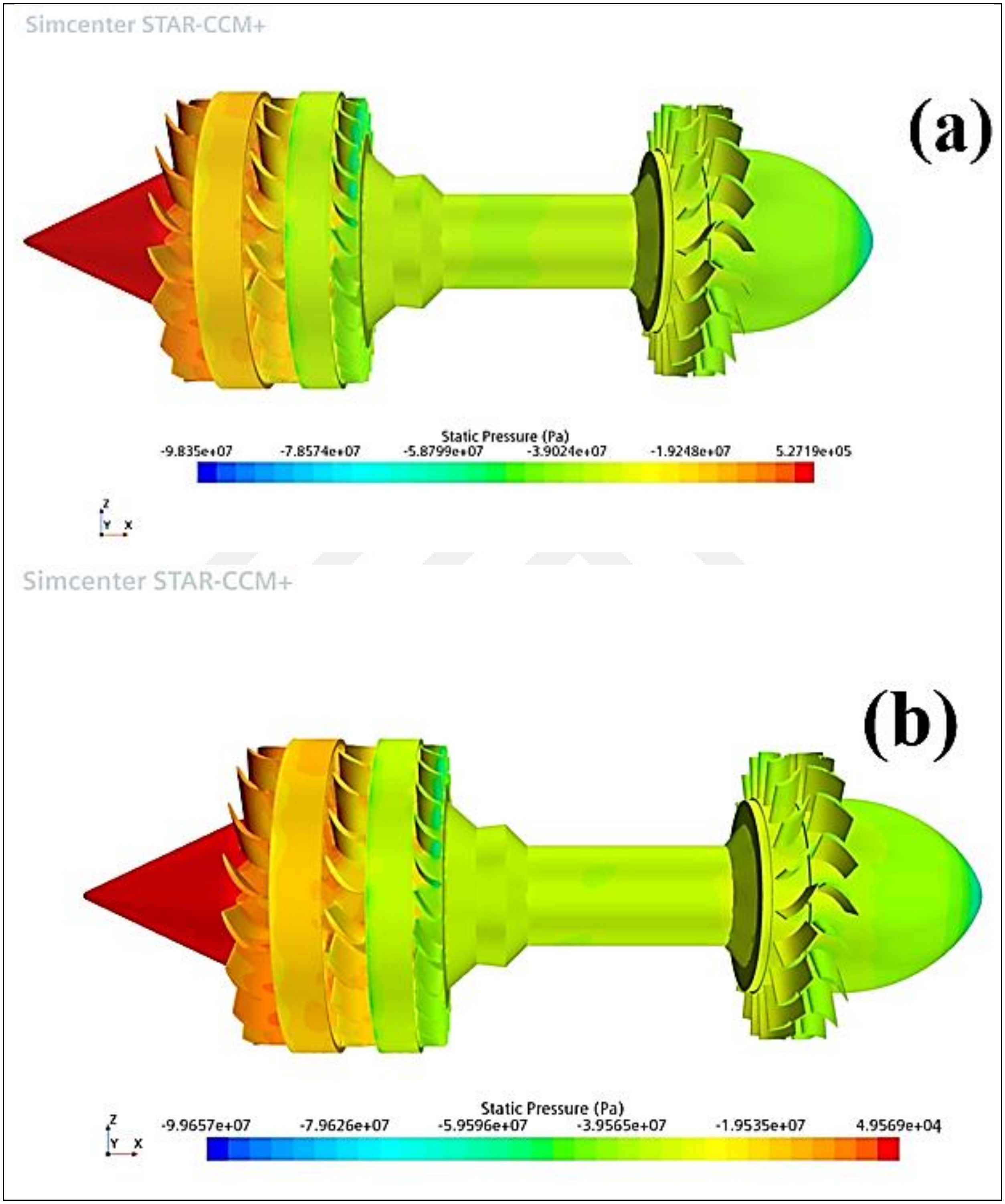

Figure 4.12: The jet engine's static pressure, (a) before and (b) after using a thin layer of nano-ceramic coating. (A third view).

It is concluded from Figures (4.10), (4.11), and (4.12) that the maximum jet engine's static pressure is 5.272×10^5 Pa before the thin layer of nano-ceramic coating is applied. After using the thin layer of nano-ceramic coating, it was found that the maximum jet engine's static pressure had slightly declined to 4.956×10^4 Pa. In addition, the minus sign of pressure (which exists at the jet engine's propeller) indicates that the pressure is very low compared with the adjacent region (which is the compressor). In the exhaust region, the pressure is very high, where flue gases have higher thrust to provide driving power for the aircraft.

4.7 CFD ANALYSIS OF THE TOTAL PRESSURE

The numerical simulation and modeling analysis executed by the STAR-CCM+ 2022.1 software package indicated the profile of the total pressure before and after using a thin layer of nano-ceramic coating. Figure (4.13) presents these simulation results.

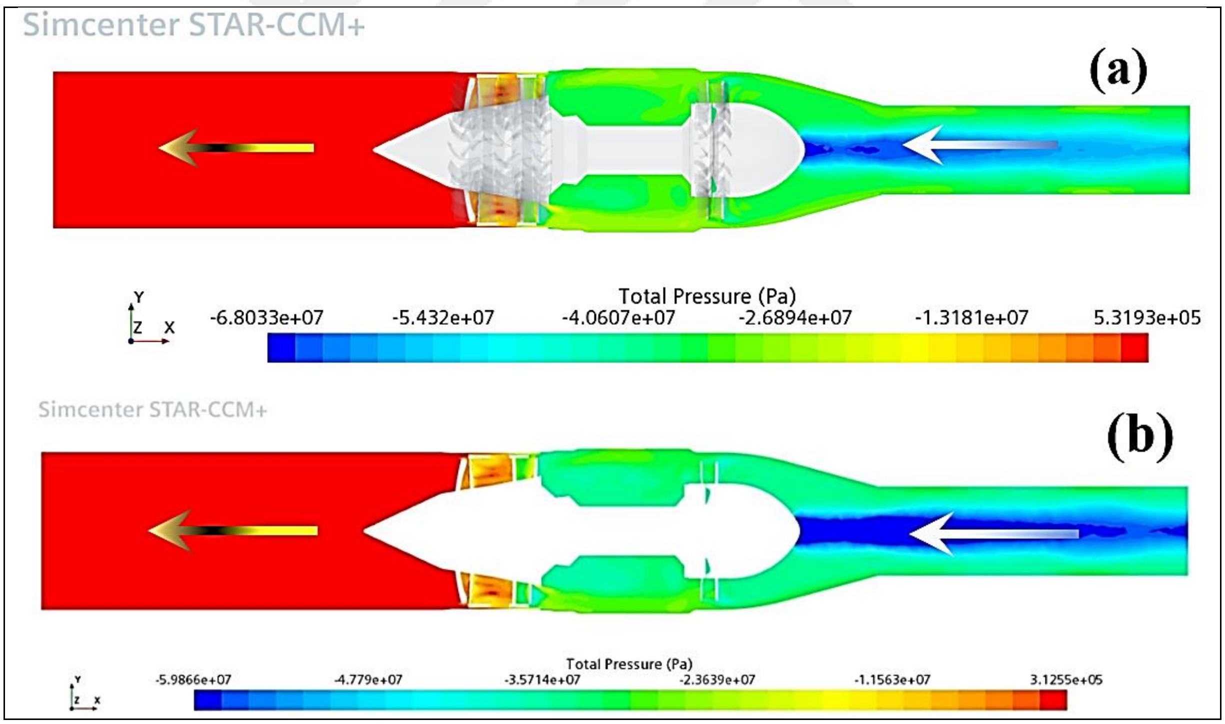

Figure 4.13: The jet engine's total pressure, (a) before and (b) after using a thin layer of nano-ceramic coating.

It can be concluded from Figure (4.13) that the total pressure of the jet engine ranges between roughly −4.0607 × 107 Pa and 5.3193 × 105 Pa before the thin layer of nano-ceramic coating is applied. After using the thin layer of nano-ceramic coating, it was found that the total pressure of the jet engine ranges between around −3.5714 × 107 Pa and 3.1255 × 105 Pa, explaining that the turbulent characteristics have declined after the coating is applied, which is mirrored by lower pressure. Also, maximum pressure of the jet engine (red color) occurs at its outlet. A negative sign of the pressure at the inlet expresses that the atmospheric pressure is very low compared with the inner region and exhaust zone of the jet engine.

4.8 CFD ANALYSIS OF THE TURBULENT VELOCITY

Besides the previous results, the numerical simulation and modeling analysis performed via the STAR-CCM+ 2022.1 software package indicated the profile of the turbulent velocity before and after using a thin layer of nano-ceramic coating.

Figure (4.14) presents the 2D velocity profile, while Figure (4.15) indicates a 3D modeling of turbulent velocity before and after the coasting process.

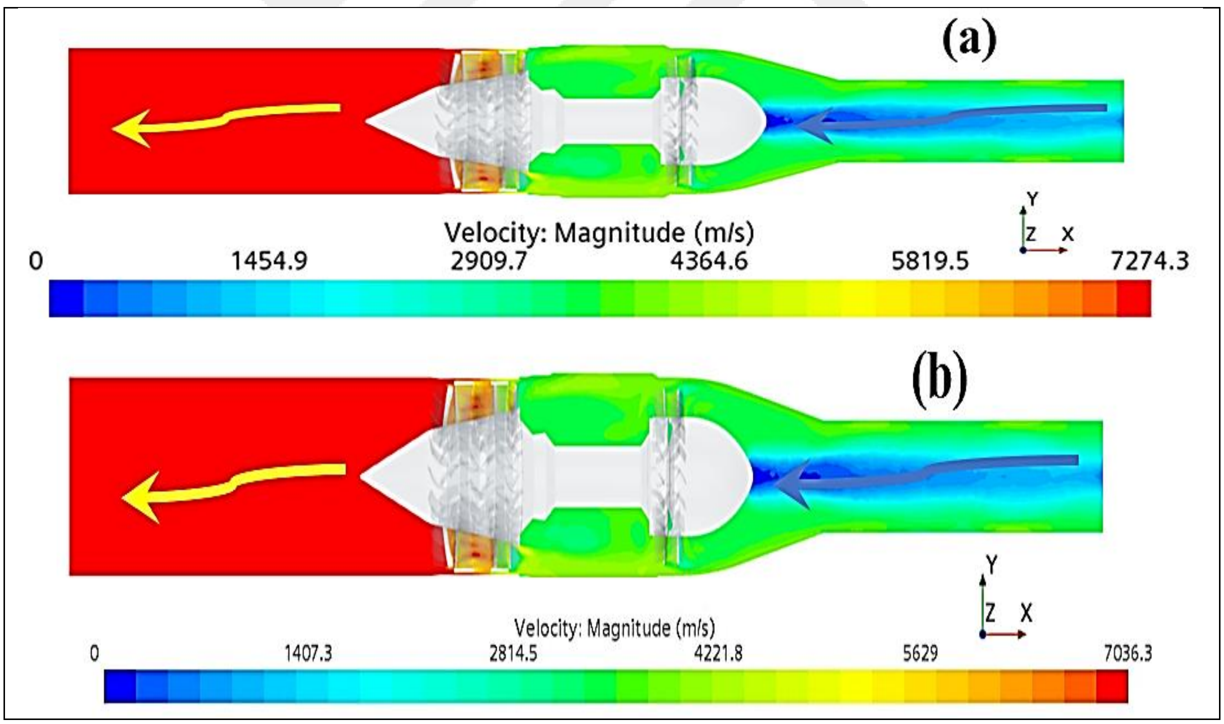

Figure 4.14: The jet engine's 2D turbulent velocity, (a) before and (b) after using a thin layer of nano-ceramic coating.

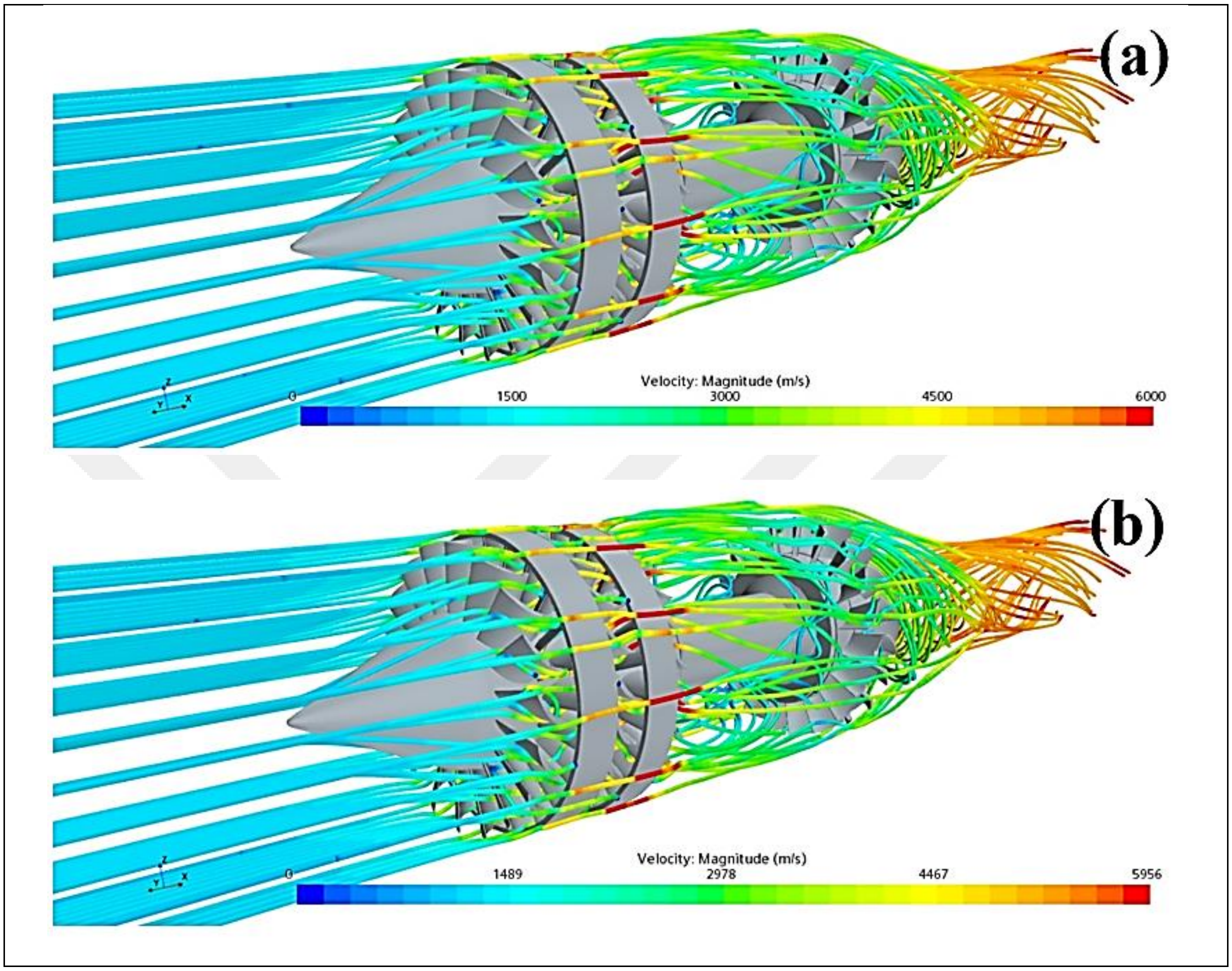

Figure 4.15: The jet engine's 3D turbulent velocity, (a) before and (b) after using a thin layer of nano-ceramic coating.

It can be inferred from Figures (4.14) and (4.15) that the turbulence velocity of the jet engine is higher when no coating is used than that when the coating is applied in both 2D and 3D models, which can indicate that using a nano-ceramic coating layer would reduce turbulence charactersitcis and turbulence velocity.

4.9 CFD ANALYSIS OF THE MACH NUMBER

Additional to these findings, the modeling analysis and numerical simulations, carried out using the STAR-CCM+ 2022.1 software package, indicated the profile of the Mach number before and after using a thin layer of nano-ceramic coating. Figure (4.16) presents the Mach number profile.

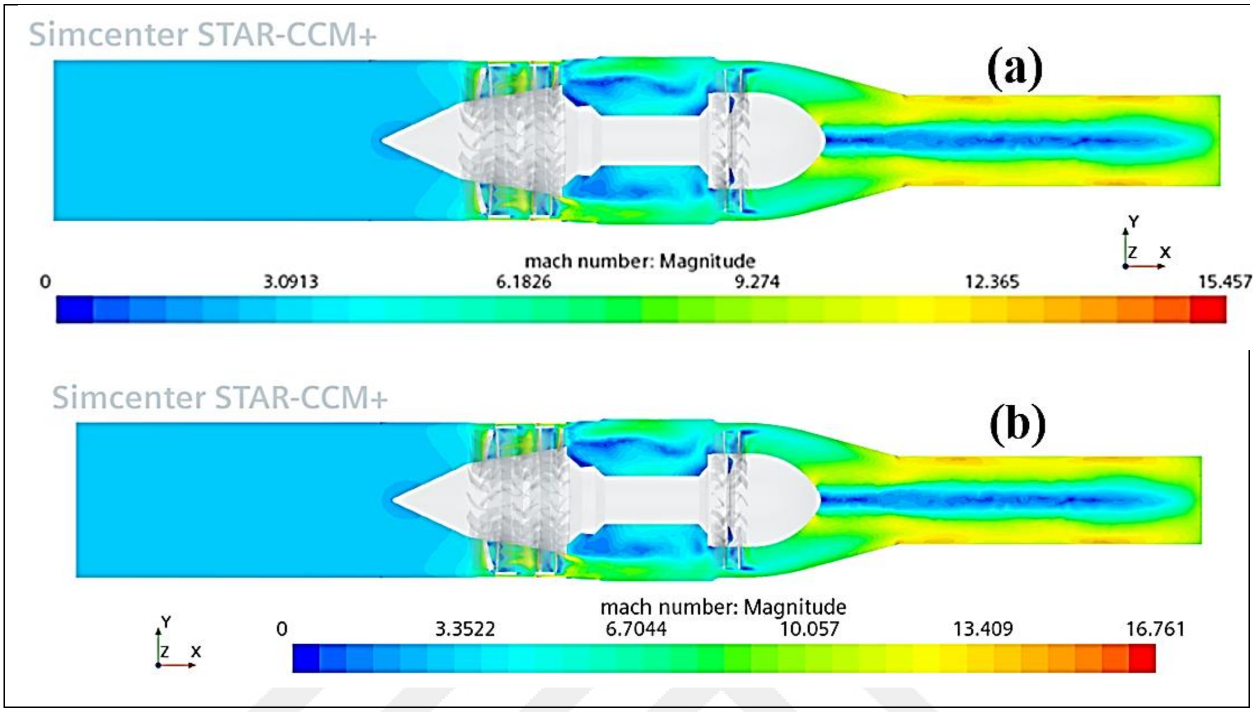

Figure 4.16: The jet engine's Mach number, (a) before and (b) after using a thin layer of nano-ceramic coating.

It is indicated from Figure (4.16) that the Mach number before the coating process is applied is within a range from around 3.0913 to 15.45. At the same time, its value has increased, reaching a range between about 3.3522 and 16.761. These numbers can point out that using the coating layer would reduce the turbulence behavior, which gives a lower Mach number. Also, it can be inferred from Figure (4.16) that the Mach number is very low in the exhaust region of the jet engine, indicating higher turbulence characteristics. On the other hand, lower turbulence exists at the inlet of the jet engine, which is mirrored by a higher Mach number.

4.10 CFD ANALYSIS OF THE REYNOLDS NUMBER

The modeling analysis and numerical simulations, performed by the STAR-CCM+ 2022.1 software package, provided the values of the Reynolds number before and after using a thin layer of nano-ceramic coating. However, no figures are expressed in terms of Reynolds number. It was found that the Reynolds number when no nano ceramic coating is used was higher than the case of the coating process (a Reynold number value of 1.34275×10^8 was obtained when no coating is used, which indicates higher turbulence properties, more significant velocity, high pressure, and higher turbulent viscosity). On the other hand, the Reynolds number in the case of nano ceramic coating is 8.80182×10^7, which shows that coating reduces the turbulence characteristics. Thus, the speed of flow is minimized, which leads to a decline in the Reynolds number. Overall, it can be inferred that coating can reduce the turbulence aspects in the jet engine, building on all presented results.

4.11 PERCENTAGES OF IMPROVEMENTS DUE TO COATING

The percentage error formula, expressed in the following equation, is used to calculate the percentage of improvement after the nano-ceramic coating layer is employed:

$$Coating\ Contribution\ of\ Improvment\ (\%) = \frac{New\ Value\ (After\ Coating) - Orignial\ Value (Before\ Coating)}{Orignial\ Value\ (Before\ Coating)} \tag{4.1}$$

Table (4.2) describes the calculation results of the coating contribution to the seven parameters related to the turbulence behavior in the jet engine.

Table 4.2: The calculation results of the coating contribution in the jet engine.

No.	Variable	Value Before Coating	Value After Coating	Enhancement Percentage
1	Turbulent Viscosity	1.8551 Pa.s	1.6589 Pa.s	10.58%
2	Turbulent Kinetic Energy	2.898×10^6 J/kg	2.338×10^5 J/kg	91.93%
3	Static Pressure	5.272×10^5 Pa	4.956×10^4 Pa	90.60%
4	Total Pressure	5.3193×10^5 Pa	3.1255×10^5 Pa	41.24%
5	Turbulent Velocity	6,000 m/s	5,956 m/s	0.73%
6	Mach Number	15.46	16.76	8.4%
7	Reynolds Number	1.34275×10^8	8.80182×10^7	34.46%

4.12 DISCUSSIONS

The results of this study indicated that using a nano-ceramic coating layer would reduce turbulence characteristics in the jet engine, which is mirrored by higher turbulent kinetic energy before the nano-ceramic coating layer is applied and lower turbulent kinetic energy after this coating layer is implemented.

This result is consistent with the results of [42], who conducted a study investigating the critical role of turbulence and drag force reduction using micro- and nano-coating surfaces and found that using micro- and nano-coating surfaces on the airfoil would significantly minimize the turbulence energy and drag force.

This result is also consistent with the findings of [43], who conducted an analysis identifying the critical role of micro-nano coating layer in minimizing the turbulence kinetic energy and drag force on the surface of the aircraft and found that using micro-nano coating layer on the surface of the aircraft helps reduce the turbulence kinetic energy and drag force that causes significant friction and reduce the aircraft flying performance.

The results of this research also revealed that using a nano-ceramic coating layer could minimize the values related to the static and total pressure in the jet engine, which is mirrored by higher static and total pressure values before the nano-ceramic coating layer is applied and lower static and total pressure amounts after this coating layer is implemented.

This result is consistent with the results of [41], who conducted an analysis classifying the critical contribution of the microgroove polyurethane coating process to minimize the total pressure of transonic compressor and found that using microgroove polyurethane coating layer would reduce the total pressure of the transonic compressor.

This result is also consistent with the findings of [40], who conducted an analysis exploring the beneficial role of TiO_2 nano-coating in reducing the turbulence pressure of a turbine and found that using this nanomaterial in the coating can increase the pressure drop (reduce turbulence pressure) in the turbine.

Furthermore, the research findings indicated that using a nano-ceramic coating layer could minimize the values related to the turbulent velocity in the jet engine, which is mirrored by higher turbulent velocity values before the nano-ceramic coating layer is applied and lower turbulent velocity amounts after this coating layer is implemented. Also, the research findings of this work indicated that the Mach number would increase when a nano-ceramic coating layer is used to protect the jet engine. The Mach number is low when no coating is employed, indicating that coating could reduce turbulence.

This result is consistent with the findings of [94], who carried out a study investigating the critical role of coating in reducing turbulence and found that using Leeward partial porous coating on the cylinder would reduce the turbulence characteristics. Moreover, the research results indicated that using a nano-ceramic coating layer would reduce the Reynolds number value, indicating a reduction in the turbulence behavior of the jet engine.

These results are consistent with the results of [40], who found that using nano-coating of TiO_2 in the turbine could reduce the turbulence properties and reduce the Reynolds number.

5. CONCLUSIONS AND RECOMMENDATIONS

5.1 INTRODUCTION

This chapter summarizes major conclusions obtained from the numerical analysis and modeling using the STAR-CCM+ 2022.1 software package. In addition, it suggests critical aspects and essential recommendations for future work that help students and scholars conduct further analysis and work to improve the findings and numerical outputs of this research.

5.2 CONCLUSIONS

This work is carried out to investigate the turbulence characteristics of a jet engine and investigate the synthetic turbulence generation techniques. The research depends on a systematic literature review by which synthetic turbulence generation techniques are reviewed and addressed. In addition, primary data are collected from a case study, which investigates the impact of adding a nano-ceramic coating layer on the Rolls-Royce RB211 jet engine on some turbulence parameters, including (1) turbulent viscosity, (2) turbulence kinetic energy, (3) static pressure, (4) total pressure, (5) turbulent velocity, (6) Mach number, and (7) Reynolds number. To analyze these parameters, the STAR-CCM+ 2022.1 software package is employed, which made 2D and 3D modeling and numerical simulations of the jet engine. Depending on the research numerical solution and simulation analysis, the critical study results can be summarized through the following paragraphs:

i. Using a nano-ceramic coating layer would reduce turbulence characteristics in the jet engine, which is mirrored by higher turbulent viscosity before the nano-ceramic coating layer is applied and lower turbulent viscosity after this coating layer is implemented by (%).
ii. Utilizing a nano-ceramic coating layer would reduce turbulence characteristics in the jet engine, which is mirrored by higher turbulent kinetic energy before the nano-ceramic coating layer is applied and lower turbulent kinetic energy after this coating layer is implemented.
iii. Employing a nano-ceramic coating layer could minimize the values related to the static pressure in the jet engine, which is mirrored by higher static pressure values before the

nano-ceramic coating layer is applied and lower static pressure amounts after this coating layer is implemented.

iv. Employing a nano-ceramic coating layer could minimize the values related to the total pressure in the jet engine, which is mirrored by higher total pressure values before the nano-ceramic coating layer is applied and lower total pressure amounts after this coating layer is implemented.

v. Using a nano-ceramic coating layer could minimize the values related to the turbulence velocity in the jet engine, which is mirrored by higher turbulence velocity values before the nano-ceramic coating layer is applied and lower turbulence velocity amounts after this coating layer is implemented.

vi. Using a nano-ceramic coating layer could increase the values associated with the Mach number in the jet engine, which is mirrored by lower Mach number values before the nano-ceramic coating layer is applied and larger Mach number amounts after this coating layer is implemented.

vii. Utilizing a nano-ceramic coating layer could reduce the values associated with the Reynolds number in the jet engine, which is mirrored by larger Reynolds number values before the nano-ceramic coating layer is applied and lower Reynolds number amounts after this coating layer is implemented.

viii. Overall, using a nano-ceramic coating layer would reduce turbulence effects in the jet engine investigated in this work.

5.3 RECOMMENDATIONS

Based on the research's numerical findings obtained from the simulation analysis and 2D and 3D modeling of the Rolls-Royce RB211 jet engine using the STAR-CCM+ 2022.1 software package, this work proposes a group of vital suggestions and critical recommendations that could help students and scholars carry out further research and investigations to improve the outputs of this study. These recommendations include the following aspects:

a. To conduct thermal analysis of the Rolls-Royce RB211 jet engine, analyze the temperature inside and outside the jet engine, and predict the effect of the nano-ceramic coating layer on the inner and outer temperature of the jet engine.

b. To use another software package that can provide faster calculation time and less effort to simulate the turbulence parameters of the jet engines flexibly.
c. To analyze other variables that are not investigated and estimated in this study, such as dynamic pressure, Weber number, Nusselt number, and drag force.

5.4 RESEARCH LIMITATIONS

Despite the successful results obtained from the, this research faced some obstacles and critical difficulties that limit the broad implementation of the numerical modeling and simulation analysis of the jet engine. The research's major challenges include:

i. A very long time and great computer calculation effort are required to evaluate and simulate the inner and outer temperature of the jet engine. Thus, the temperature parameter in this study was neglected.
ii. A large number of meshing elements due to the high complexity of the jet engine geometry caused a significant duration required to make simulations and numerical analyses of the jet engine.
iii. The few CFD experts and jet engine professionals made some limitations on consultations, advice, and help to verify the research results.

REFERENCES

[1] A. C. Barkett Botan, R. G. Ramirez Gustavo, G. L. Tiago Filho, and E. R. da Silva, "Optimization of a Draft Tube using Statistical Techniques- DOE and 2D Computational Fluid Dynamic Analysis," *Journal of Applied Fluid Mechanics*, vol. 14, no. 6, Nov. 2021, doi: 10.47176/jafm.14.06.32314.

[2] M. H. Zawawi *et al.*, "A review: Fundamentals of computational fluid dynamics (CFD)," 2018, p. 020252. doi: 10.1063/1.5066893.

[3] R. K. Raman, Y. Dewang, and J. Raghuwanshi, "A review on applications of computational fluid dynamics," *International Journal of LNCT*, vol. 2, no. 6, pp. 137–143, 2018.

[4] G. Tiwari, J. Kumar, V. Prasad, and V. K. Patel, "Utility of CFD in the design and performance analysis of hydraulic turbines — A review," *Energy Reports*, vol. 6, pp. 2410–2429, Nov. 2020, doi: 10.1016/j.egyr.2020.09.004.

[5] J. Klinner, A. Hergt, S. Grund, and C. E. Willert, "High-Speed PIV of shock boundary layer interactions in the transonic buffet flow of a compressor cascade," *Exp Fluids*, vol. 62, no. 3, p. 58, Mar. 2021, doi: 10.1007/s00348-021-03145-3.

[6] L. Bahrainirad, S. Hosseinverdi, and H. F. Fasel, "Laminar-Turbulent Transition in a Swept Low-Speed Boundary Layer," in *AIAA AVIATION 2022 Forum*, Jun. 2022. doi: 10.2514/6.2022-3633.

[7] M. Kadivar, D. Tormey, and G. McGranaghan, "A review on turbulent flow over rough surfaces: Fundamentals and theories," *International Journal of Thermofluids*, vol. 10, p. 100077, May 2021, doi: 10.1016/j.ijft.2021.100077.

[8] S. Heinz, "A review of hybrid RANS-LES methods for turbulent flows: Concepts and applications," *Progress in Aerospace Sciences*, vol. 114, p. 100597, Apr. 2020, doi: 10.1016/j.paerosci.2019.100597.

[9] Z. Tong, Y. A. N. G. Qing-shan, Y. A. N. Bo-wen, P. van Phuc, and W. A. N. G. Jing-xue, "Review of inflow turbulence generation methods with large eddy simulation for atmospheric boundary layer," *J Eng Mech*, vol. 37, no. 5, pp. 15–25, 2020.

[10] F. C. C. Galeazzo *et al.*, "Implementation of an Efficient Synthetic Inflow Turbulence-Generator in the Open-Source Code OpenFOAM for 3D LES/DNS Applications," in

High Performance Computing in Science and Engineering '20, Cham: Springer International Publishing, 2021, pp. 207–221. doi: 10.1007/978-3-030-80602-6_14.

[11] N. Jain *et al.*, "A Critical Review of Physical Models in High Temperature Multiphase Fluid Dynamics: Turbulent Transport and Particle-Wall Interactions," *Appl Mech Rev*, vol. 73, no. 4, Jul. 2021, doi: 10.1115/1.4051503.

[12] M. Matha, C. Morsbach, and M. Bergmann, "A comparison of methods for introducing synthetic turbulence," in *In ECCOMAS--ECFD 2018-6th European Conference on Computational Mechanics (Solids, Structures and Coupled Problems)/7th European Conference on Computational Fluid Dynamics*, 2018.

[13] T. Li, J. Zhang, M. M. Rashidi, and M. Yu, "On the Reynolds-Averaged Navier-Stokes Modelling of the Flow around a Simplified Train in Crosswinds," *Journal of Applied Fluid Mechanics*, vol. 12, no. 2, pp. 551–563, Mar. 2019, doi: 10.29252/jafm.12.02.28958.

[14] T. Watanabe, X. Zhang, and K. Nagata, "Direct numerical simulation of incompressible turbulent boundary layers and planar jets at high Reynolds numbers initialized with implicit large eddy simulation," *Comput Fluids*, vol. 194, p. 104314, Nov. 2019, doi: 10.1016/j.compfluid.2019.104314.

[15] C. García-Sánchez, J. van Beeck, and C. Gorlé, "Predictive large eddy simulations for urban flows: Challenges and opportunities," *Build Environ*, vol. 139, pp. 146–156, Jul. 2018, doi: 10.1016/j.buildenv.2018.05.007.

[16] M. Dhalwala, A. Bayram, P. Oshkai, and A. Korobenko, "Performance and near-wake analysis of a vertical-axis hydrokinetic turbine under a turbulent inflow," *Ocean Engineering*, vol. 257, p. 111703, Aug. 2022, doi: 10.1016/j.oceaneng.2022.111703.

[17] K. Yamamoto, T. Watanabe, and K. Nagata, "Turbulence generated by an array of opposed piston-driven synthetic jet actuators," *Exp Fluids*, vol. 63, no. 1, p. 35, Jan. 2022, doi: 10.1007/s00348-021-03351-z.

[18] N. S. Dhamankar, G. A. Blaisdell, and A. S. Lyrintzis, "Overview of Turbulent Inflow Boundary Conditions for Large-Eddy Simulations," *AIAA Journal*, vol. 56, no. 4, pp. 1317–1334, Apr. 2018, doi: 10.2514/1.J055528.

[19] D. Xiong, Y. Yang, and Y. Wang, "An Improved Synthetic Eddy Method for Generating Inlet Turbulent Boundary Layers," *Aerospace*, vol. 9, no. 1, p. 37, Jan. 2022, doi: 10.3390/aerospace9010037.

[20] F. Gand and M. Huet, “On the generation of turbulent inflow for hybrid RANS/LES jet flow simulations,” *Comput Fluids*, vol. 216, p. 104816, Feb. 2021, doi: 10.1016/j.compfluid.2020.104816.

[21] M. Shur, M. Strelets, A. Travin, P. Spalart, and T. Suzuki, “Unsteady Simulations of a Fan/Outlet-Guide-Vane System: Aerodynamics and Turbulence,” *AIAA Journal*, vol. 56, no. 6, pp. 2283–2297, Jun. 2018, doi: 10.2514/1.J056645.

[22] J. D. Blake, *A Coupled Large Eddy Simulation-Synthetic Turbulence Method for Predicting Jet Noise*. Hood Rd, Mississippi State, USA: Mississippi State University, 2020.

[23] C. Morsbach and M. Franke, “Analysis of a Synthetic Turbulence Generation Method for Periodic Configurations,” 2019, pp. 169–174. doi: 10.1007/978-3-030-04915-7_23.

[24] D. Martinez-Sanchis, A. Sternin, D. Sternin, O. Haidn, and M. Tajmar, “Analysis of periodic synthetic turbulence generation and development for direct numerical simulations applications,” *Physics of Fluids*, vol. 33, no. 12, p. 125130, Dec. 2021, doi: 10.1063/5.0071002.

[25] O. O. Shobayo and D. K. Walters, “Evaluation of a Statistically Targeted Forcing Method for Synthetic Turbulence Generation in Large-Eddy Simulations and Hybrid RANS-LES Simulations,” in *Volume 3: Computational Fluid Dynamics; Micro and Nano Fluid Dynamics*, Jul. 2020. doi: 10.1115/FEDSM2020-20376.

[26] L. Patruno and M. Ricci, “A systematic approach to the generation of synthetic turbulence using spectral methods,” *Comput Methods Appl Mech Eng*, vol. 340, pp. 881–904, Oct. 2018, doi: 10.1016/j.cma.2018.06.028.

[27] T. N. Nandi, H. Kröger, D. Yeo, and N. Kornev, “Assessment of a synthetic inflow turbulence generator for prediction of neutrally stratified atmospheric flows,” in *The 7th International Symposium on Computational Wind Engineering 2018*, Jun. 2018.

[28] M. van Dyke and M. van Dyke, *An Album of Fluid Motion*, 4th ed., vol. 176. Stanford, California, USA: Stanford: Parabolic Press, 1982.

[29] National Committee, *Illustrated Experiments in Fluid Mechanics: The NCFMF Book of Film Notes*. USA: MIT Press, 1972.

[30] Hartnett K., “For Fluid Equations, a Steady Flow of Progress,” *Quantamagazine*, 2020. https://www.quantamagazine.org/for-fluid-equations-a-steady-flow-of-progress-20200113/ (accessed Jan. 17, 2023).

[31] Nur Shamimi Amirah Md Sunhazim, Fazila Mohd Zawawi, Ummikalsom Abidin, Syahrullail Samion, Kamarulafizam Ismail, and Ainaa Maya Munira Ismail, “CFD Investigation on The Jet-Engine Inspired Wind Turbine,” *CFD Letters*, vol. 14, no. 2, pp. 72–80, Mar. 2022, doi: 10.37934/cfdl.4.2.7280.

[32] Z. X. Chen, I. Langella, and N. Swaminathan, “The Role of CFD in Modern Jet Engine Combustor Design,” in *Environmental Impact of Aviation and Sustainable Solutions*, IntechOpen, 2020. doi: 10.5772/intechopen.88267.

[33] M. L. Erario, M. G. de Giorgi, and R. Przysowa, “Model-Based Dynamic Performance Simulation of a Microturbine Using Flight Test Data,” *Aerospace*, vol. 9, no. 2, p. 60, Jan. 2022, doi: 10.3390/aerospace9020060.

[34] A. M. Briones, A. W. Caswell, and B. A. Rankin, “Fully Coupled Turbojet Engine Computational Fluid Dynamics Simulations and Cycle Analyses Along the Equilibrium Running Line,” *J Eng Gas Turbine Power*, vol. 143, no. 6, Jun. 2021, doi: 10.1115/1.4049410.

[35] K. Synylo, A. Krupko, O. Zaporozhets, and R. Makarenko, “CFD simulation of exhaust gases jet from aircraft engine,” *Energy*, vol. 213, p. 118610, Dec. 2020, doi: 10.1016/j.energy.2020.118610.

[36] M. Teixeira *et al.*, “A Methodology for Fully-Coupled CFD Engine Simulations, Applied to a Micro Gas Turbine Engine,” in *Volume 2C: Turbomachinery*, Jun. 2018. doi: 10.1115/GT2018-76870.

[37] A. Olejnik, A. Dziubiński, and Ł. Kiszkowiak, “CFD simulation of engine nacelle cooling on pusher configuration aircraft,” *Aircraft Engineering and Aerospace Technology*, vol. 93, no. 9, pp. 1421–1429, Nov. 2021, doi: 10.1108/AEAT-12-2020-0290.

[38] S. M. Pasalkar, Shaikh M. S., and Pipulyawala M. M., “Design and CFD Analysis of Combustion Chamber of Jet Engine to Reduce Formation of NOx,” *International Research Journal of Engineering and Technology (IRJET)*, vol. 7, no. 6, pp. 5172–5180, 2020.

[39] I. Guinness and T. Persoons, “Passive Flow Control for Drag Reduction on a Cylinder in Cross-Flow Using Leeward Partial Porous Coatings,” *Fluids*, vol. 6, no. 8, p. 289, Aug. 2021, doi: 10.3390/fluids6080289.

[40] A. Aghaei Sarvari, S. Zeinali Heris, M. Mohammadpourfard, S. B. Mousavi, and P. Estellé, “Numerical investigation of TiO2 and MWCNTs turbine meter oil nanofluids: Flow and hydrodynamic properties,” *Fuel*, vol. 320, p. 123943, Jul. 2022, doi: 10.1016/j.fuel.2022.123943.

[41] L. Wang *et al.*, “Experimental Study on Performance of Transonic Compressor Cascade with Microgroove Polyurethane Coatings,” *Fluids*, vol. 7, no. 6, p. 190, Jun. 2022, doi: 10.3390/fluids7060190.

[42] L. WANG *et al.*, “A boundary surrogate model for micro/nano grooved surface structure applied in turbulence flow control over airfoil,” *Chinese Journal of Aeronautics*, vol. 35, no. 2, pp. 62–73, Feb. 2022, doi: 10.1016/j.cja.2021.04.026.

[43] J. TAO *et al.*, “An innovative study on low surface energy micro-nano coatings with multilevel structures for laminar flow design,” *Chinese Journal of Aeronautics*, vol. 32, no. 3, pp. 577–584, Mar. 2019, doi: 10.1016/j.cja.2018.12.010.

[44] P. Krehl and M. van der Geest, “The Discovery of the Mach Reflection Effect and Its Demonstration in an Auditorium,” 2019, pp. 443–469. doi: 10.1007/978-3-030-04378-0_33.

[45] P. Liu, “Introduction to Celebrities in Fluid Mechanics,” in *A General Theory of Fluid Mechanics*, Singapore: Springer Singapore, 2021, pp. 581–641. doi: 10.1007/978-981-33-6660-2_8.

[46] P. E. Lapenna, R. Lamioni, P. P. Ciottoli, and F. Creta, “Low-Mach number simulations of transcritical flows,” in *2018 AIAA Aerospace Sciences Meeting*, Jan. 2018. doi: 10.2514/6.2018-0346.

[47] D. S. Oliveira and E. C. Teixeira, “Hydrodynamic characterization and flocculation process in helically coiled tube flocculators: an evaluation through streamlines,” *International Journal of Environmental Science and Technology*, vol. 14, no. 12, pp. 2561–2574, Dec. 2017, doi: 10.1007/s13762-017-1341-z.

[48] J. Niu, Y. Wang, R. Li, and F. Liu, “Comparison of Aerodynamic Characteristics of High-Speed Train for Different Configurations of Aerodynamic Braking Plates

Installed in Inter-Car Gap Region," *Flow Turbul Combust*, vol. 106, no. 1, pp. 139–161, Jan. 2021, doi: 10.1007/s10494-020-00196-0.

[49] S. Dol, S. S. Pervaiz, M. , B. K. Uzair, and M. M. Elzughbi, "Design of Solar-powered Endurance Glider with Vortex Generators," *Renewable Energy Research and Applications*, vol. 2, no. 1, pp. 1–8, 2021.

[50] C. Fu, M. Uddin, and A. C. Robinson, "Turbulence modeling effects on the CFD predictions of flow over a NASCAR Gen 6 racecar," *Journal of Wind Engineering and Industrial Aerodynamics*, vol. 176, pp. 98–111, May 2018, doi: 10.1016/j.jweia.2018.03.016.

[51] Y. Shah and S. Yarusevych, "Effect of polymer injection on the development of a trip-wire-induced bypass transitioning boundary layer," *Phys Rev Fluids*, vol. 7, no. 9, p. 093901, Sep. 2022, doi: 10.1103/PhysRevFluids.7.093901.

[52] R. R. Leknys, M. Arjomandi, R. M. Kelso, and C. H. Birzer, "Thin airfoil load control during post-stall and large pitch angles using leading-edge trips," *Journal of Wind Engineering and Industrial Aerodynamics*, vol. 179, pp. 80–91, Aug. 2018, doi: 10.1016/j.jweia.2018.05.009.

[53] L. XIE *et al.*, "Improving aircraft aerodynamic performance with bionic wing obtained by ice shape modulation," *Chinese Journal of Aeronautics*, Sep. 2022, doi: 10.1016/j.cja.2022.09.011.

[54] S. Sun, X. Chang, C. Guo, H. Zhang, and C. Wang, "Numerical investigation of scale effect of nominal wake of four-screw ship," *Ocean Engineering*, vol. 183, pp. 208–223, Jul. 2019, doi: 10.1016/j.oceaneng.2019.04.032.

[55] J. E. Gutiérrez-Romero, S. Ruiz-Capel, J. Esteve-Pérez, B. Zamora-Parra, and J. P. Luna-Abad, "Methodology Based on Photogrammetry for Testing Ship-Block Resistance in Traditional Towing Tanks: Observations and Benchmark Data," *J Mar Sci Eng*, vol. 10, no. 2, p. 246, Feb. 2022, doi: 10.3390/jmse10020246.

[56] C. H. Park, N. H. An, H. Y. Jang, and Y. W. Kwon, "A Study on the Characteristic of Motion and Resistance Performance from the Body Plan of Planning Leisure boat at low speed," *Journal of the Korea Society For Power System Engineering*, vol. 16, no. 4, pp. 17–23, Aug. 2012, doi: 10.9726/kspse.2012.16.4.017.

[57] B. R. McAuliffe and A. D'Auteuil, "A System for Simulating Road-Representative Atmospheric Turbulence for Ground Vehicles in a Large Wind Tunnel," *SAE*

International Journal of Passenger Cars - Mechanical Systems, vol. 9, no. 2, pp. 2016-01–1624, Apr. 2016, doi: 10.4271/2016-01-1624.

[58] Feigenoff C., "Generating Current as Well as Thrust from Jet Engines," *University of Virginia. School of Engineering and Applied Sciences*, Thornton Hall, 351 McCormick Road, Charlottesville, USA, 2018.

[59] C. Giehl, R. A. Brooker, H. Marxer, and M. Nowak, "An experimental simulation of volcanic ash deposition in gas turbines and implications for jet engine safety," *Chem Geol*, vol. 461, pp. 160–170, Jun. 2017, doi: 10.1016/j.chemgeo.2016.11.024.

[60] S. Y. Sia, E. Z. Bassyony, and A. A. D. Sarhan, "Development of SiO2 nanolubrication system to be used in sliding bearings," *The International Journal of Advanced Manufacturing Technology*, vol. 71, no. 5–8, pp. 1277–1284, Mar. 2014, doi: 10.1007/s00170-013-5566-9.

[61] K. A. Mohammed, A. R. A. Talib, N. A. Aziz, and K. A. Ahmed, "Three dimensional numerical investigations on the heat transfer enhancement in a triangular facing step channels using nanofluid," *IOP Conf Ser Mater Sci Eng*, vol. 152, p. 012057, Oct. 2016, doi: 10.1088/1757-899X/152/1/012057.

[62] O. Balli and H. Caliskan, "Energy, exergy, environmental and sustainability assessments of jet and hydrogen fueled military turbojet engine," *Int J Hydrogen Energy*, vol. 47, no. 62, pp. 26728–26745, Jul. 2022, doi: 10.1016/j.ijhydene.2022.04.180.

[63] A. Borysova, "Preliminary design of a mid-range aircraft with 227 passenger capacity," Bachelor Thesis, National Aviation University, Kyiv, 2021.

[64] Stephan Savarese, "Turbine Stator Blade Cooling and Aircraft Engines," *COMSOL Blog*, Burlington, MA, USA, Aug. 07, 2013.

[65] J. Zhang, P. Wang, R. Yan, and R. X. Gao, "Long short-term memory for machine remaining life prediction," *J Manuf Syst*, vol. 48, pp. 78–86, Jul. 2018, doi: 10.1016/j.jmsy.2018.05.011.

[66] Y. Ayele, T. Stuecken, and H. Schock, "A study of the influence of orifice diameter on a Dual Mode, Turbulent Jet Ignition engine through variable engine speed," *International Journal of Engine Research*, p. 146808742210977, May 2022, doi: 10.1177/14680874221097745.

[67] Blazingtrials, “Anatomy of a Jet Engine: The Compressor Section,” *Blazing Trails*, Palm Bay Florida, United States, Oct. 28, 2020.

[68] K. M. Döleker *et al.*, “Enhancing the wear and oxidation behaviors of the Inconel 718 by low temperature aluminizing,” *Surf Coat Technol*, vol. 412, p. 127069, Apr. 2021, doi: 10.1016/j.surfcoat.2021.127069.

[69] D. Flórez-Orrego, W. Arias, H. Velásquez, and D. López, “Experimental and CFD study of a single phase cone-shaped helical coiled heat exchanger: an empirical correlation,” in *In Proceedings of the 25th international conference on efficiency, cost, optimization, simulation and environmental impact of energy systems*, 2012, pp. 375–394.

[70] D. S. Weaver and S. Mišković, “A Study of RANS Turbulence Models in Fully Turbulent Jets: A Perspective for CFD-DEM Simulations,” *Fluids*, vol. 6, no. 8, p. 271, Jul. 2021, doi: 10.3390/fluids6080271.

[71] J.-F. Liu *et al.*, “Dual Synthetic Jets Actuator and Its Applications—Part II: Novel Fluidic Thrust-Vectoring Method Based on Dual Synthetic Jets Actuator,” *Actuators*, vol. 11, no. 8, p. 209, Jul. 2022, doi: 10.3390/act11080209.

[72] NASA, “Reynolds Number,” *NASA*, 2023.

[73] J. Anderson, *Fundamentals of Aerodynamics*, 6th ed. New York City: McGraw Hill Education, 2017.

[74] J. Kim and C. Lee, “Deep unsupervised learning of turbulence for inflow generation at various Reynolds numbers,” *J Comput Phys*, vol. 406, p. 109216, Apr. 2020, doi: 10.1016/j.jcp.2019.109216.

[75] M. Oberlack, “On the decay exponent of isotropic turbulence,” *PAMM*, vol. 1, no. 1, p. 294, Mar. 2002, doi: 10.1002/1617-7061(200203)1:1<294::AID-PAMM294>3.0.CO;2-W.

[76] “Pressure Variation of Jet Engine,” *National Aeronautics and Space Administration*, 2021.

[77] S. Zhang, Z. Yao, H. Wu, Q. Zhong, R. Tao, and F. Wang, “A New Turbulent Viscosity Correction Model With URANS Solver for Unsteady Turbulent Cavitation Flow Computations,” *J Fluids Eng*, vol. 144, no. 9, Sep. 2022, doi: 10.1115/1.4053958.

[78] C. Poon, “Measuring the density and viscosity of culture media for optimized computational fluid dynamics analysis of in vitro devices,” *J Mech Behav Biomed Mater*, vol. 126, p. 105024, Feb. 2022, doi: 10.1016/j.jmbbm.2021.105024.

[79] P. Liu, *Computational fluid dynamics. In A General Theory of Fluid Mechanics* . Singapore: Springer, 2021.

[80] R. Vinuesa and S. L. Brunton, “Enhancing computational fluid dynamics with machine learning,” *Nat Comput Sci*, vol. 2, no. 6, pp. 358–366, Jun. 2022, doi: 10.1038/s43588-022-00264-7.

[81] G. K. W. Kenway, C. A. Mader, P. He, and J. R. R. A. Martins, “Effective adjoint approaches for computational fluid dynamics,” *Progress in Aerospace Sciences*, vol. 110, p. 100542, Oct. 2019, doi: 10.1016/j.paerosci.2019.05.002.

[82] D. Kochkov, J. A. Smith, A. Alieva, Q. Wang, M. P. Brenner, and S. Hoyer, “Machine learning–accelerated computational fluid dynamics,” *Proceedings of the National Academy of Sciences*, vol. 118, no. 21, May 2021, doi: 10.1073/pnas.2101784118.

[83] M. Sekar, “Guest editorial: Computational fluid dynamics in aerospace engineering: recent advances,” *Aircraft Engineering and Aerospace Technology*, vol. 94, no. 4, p. 481, Mar. 2022, doi: 10.1108/AEAT-04-2022-363.

[84] A. Gupta, J. Pierce, K. Bera, E. G. Kikano, N. Shah, and R. C. Gilkeson, “Computational Fluid Dynamics in Cardiovascular Imaging,” *Advances in Clinical Radiology*, vol. 3, pp. 153–168, Sep. 2021, doi: 10.1016/j.yacr.2021.04.013.

[85] M. Zandie, H. K. Ng, S. Gan, M. F. Muhamad Said, and X. Cheng, “Review of the advances in integrated chemical kinetics-computational fluid dynamics combustion modelling studies of gasoline-biodiesel mixtures,” *Transportation Engineering*, vol. 7, p. 100102, Mar. 2022, doi: 10.1016/j.treng.2021.100102.

[86] S. Wijeyakulasuriya *et al.*, “Enabling Powertrain Technologies for Euro 7/VII Vehicles with Computational Fluid Dynamics,” *Transportation Engineering*, vol. 9, p. 100127, Sep. 2022, doi: 10.1016/j.treng.2022.100127.

[87] L. Criscuolo *et al.*, “Aeroacoustic Instability Analysis of Helmholtz Resonators Through High-Order Unsteady Reynolds-Averaged Navier–Stokes Simulations,” *AIAA Journal*, vol. 60, no. 6, pp. 3593–3602, Jun. 2022, doi: 10.2514/1.J061181.

[88] S. Thabet and T. H. Thabit, "CFD Simulation of the Air Flow around a Car Model (Ahmed Body)," *International Journal of Scientific and Research Publications (IJSRP)*, vol. 8, no. 7, Jul. 2018, doi: 10.29322/IJSRP.8.7.2018.p7979.

[89] N. Subramani, S. M., V. Kengaiah, and S. Prakash, "Numerical modeling on dynamics of droplet in aircraft wing structure at different velocities," *Aircraft Engineering and Aerospace Technology*, vol. 94, no. 4, pp. 553–558, Mar. 2022, doi: 10.1108/AEAT-04-2021-0115.

[90] A.-M. Chiroșcă and L. Rusu, "Comparison between Model Test and Three CFD Studies for a Benchmark Container Ship," *J Mar Sci Eng*, vol. 9, no. 1, p. 62, Jan. 2021, doi: 10.3390/jmse9010062.

[91] G. Bangga, A. Dessoky, Z. Wu, K. Rogowski, and M. O. L. Hansen, "Accuracy and consistency of CFD and engineering models for simulating vertical axis wind turbine loads," *Energy*, vol. 206, p. 118087, Sep. 2020, doi: 10.1016/j.energy.2020.118087.

[92] R. Borrell *et al.*, "Heterogeneous CPU/GPU co-execution of CFD simulations on the POWER9 architecture: Application to airplane aerodynamics," *Future Generation Computer Systems*, vol. 107, pp. 31–48, Jun. 2020, doi: 10.1016/j.future.2020.01.045.

[93] Frojd K., "Simcenter STAR-CCM+ 2022.1 Released! What's new? ," *Siemens*, Munich, Germany, 2022.

[94] I. Guinness and T. Persoons, "Passive Flow Control for Drag Reduction on a Cylinder in Cross-Flow Using Leeward Partial Porous Coatings," *Fluids*, vol. 6, no. 8, p. 289, Aug. 2021, doi: 10.3390/fluids6080289.

APPENDIX A

Details of the Rolls-Royce RB211 Jet Engine

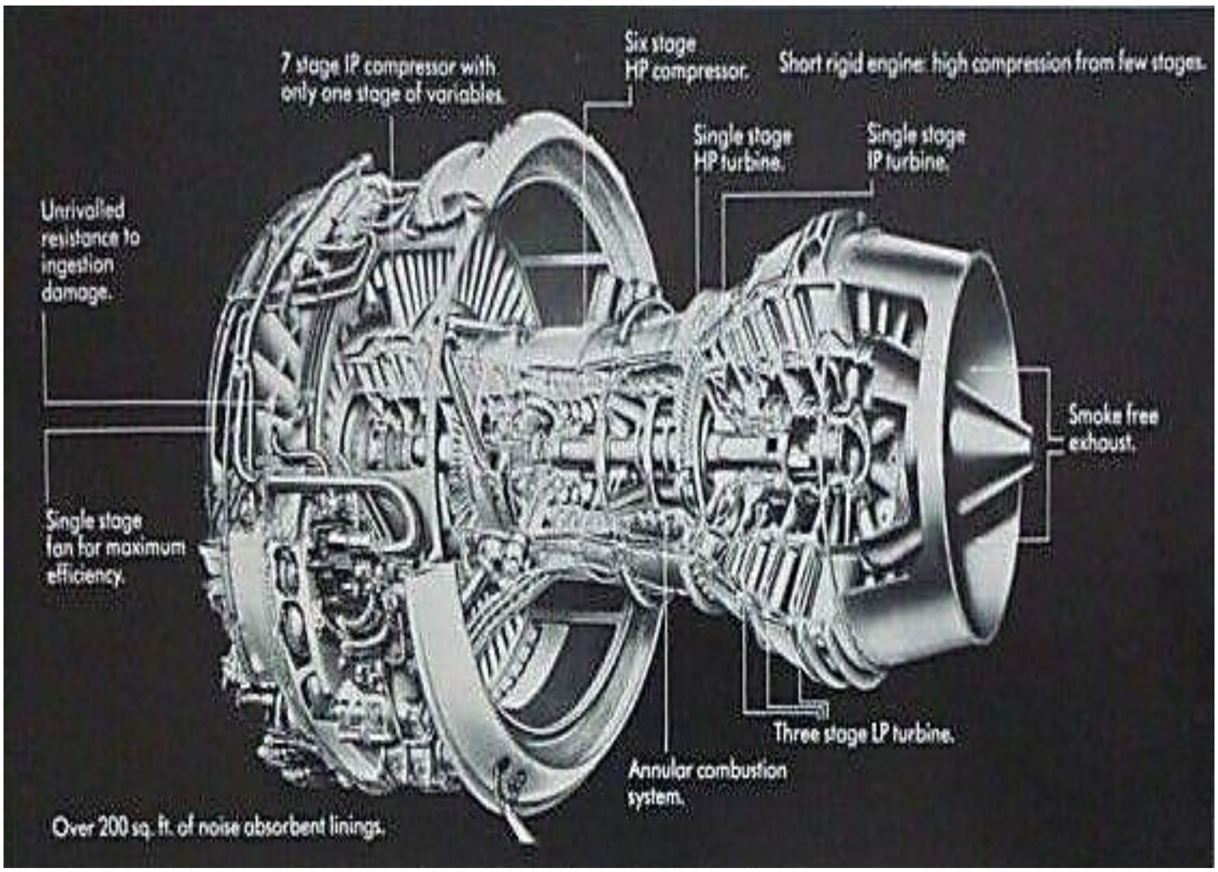
Six stage
HP compressor.
7 stage IP compressor with
only one stage of variables.
Short rigid engine: high compression from few stages.
Single stage
HP turbine.
Single stage
IP turbine.
Unrivalled
resistance to
ingestion
damage.
Smoke free
exhaust.
Single stage
fan for maximum
efficiency.
Three stage LP turbine.
Annular combustion
system.
Over 200 sq. ft. of noise absorbent linings.

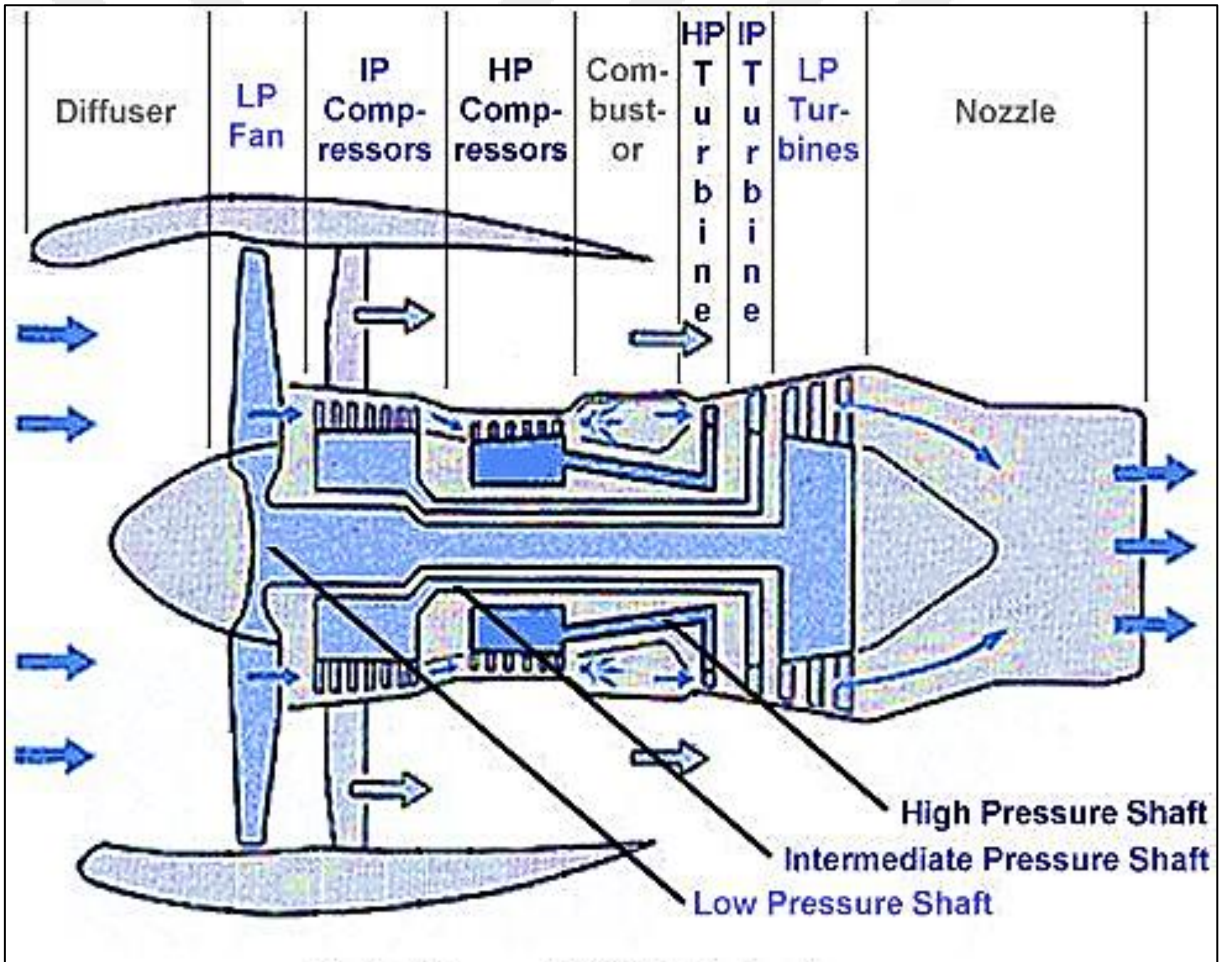

Rolls-Royce RB211 Turbofan